University of Windsor

Scholarship at UWindsor

2014

Failure mechanism of coated biomaterials under high impact-sliding contact stresses

Ying Chen
University of Windsor

Follow this and additional works at: https://scholar.uwindsor.ca/etd

FAILURE MECHANISM OF COATED BIOMATERIALS UNDER HIGH

IMPACT-SLIDING CONTACT STRESSES

By

Ying Chen

A Dissertation
Submitted to the Faculty of Graduate Studies
through the Department of **Mechanical, Automotive & Materials Engineering**
in Partial Fulfillment of the Requirements for
the Degree of **Doctor of Philosophy**
at the University of Windsor

Windsor, Ontario, Canada

2014

Failure Mechanism of Coated Biomaterials under High Impact-Sliding

Contact Stresses

by

Ying Chen

APPROVED BY:

_____
X. Wu, External Examiner
Mechanical Engineering/Engineering

_____
H. Hu
Department of Mechanical, Automotive & Materials Engineering

_____
V. Stoilov
Department of Mechanical, Automotive & Materials Engineering

_____
G. Zhang
Department of Mechanical, Automotive & Materials Engineering

_____
X. Nie, Advisor
Department of Mechanical, Automotive & Materials Engineering

May 2, 2014

DECLARATION OF ORIGINALITY

I. CO- AUTHORSHIP DECLARATION

I hereby declare that this dissertation does not incorporate material that is result of joint research. In all cases, the key ideas, primary contributions, experimental designs, data analysis and interpretation, were performed by the author and Dr. X. Nie as advisor.

I certify that, with the above qualification, this dissertation, and the research to which it refers, is the product of my own work.

II. DECLARATION OF PREVIOUS PUBLICATION

This dissertation includes 5 original papers that have been previously published/submitted for publication in peer reviewed journals/conference proceedings, as follows:

Thesis Chapter	Publication title	Publication status
Chapter 2	**Ying Chen** and Xueyuan Nie, Study on Fatigue and Wear Behaviors of a TiN Coating using an Inclined Impact-sliding Test, Surface & Coatings Technology 206（2011）1977	Published
Chapter 3	**Ying Chen**, Tse Cheng and Xueyuan Nie, Wear failure behavior of titanium-based oxide coatings on a titanium alloy under impact and sliding forces, Journal of Alloys and Compounds 578（2013）336	Published
Chapter 4	**Ying Chen** and Xueyuan Nie, Study of the fatigue wear behaviors of a WC DLC coating on 316L stainless steel, Journal of Vacuum Science and Technology A, 30 (2012) 051506	Published
Chapter 5	**Ying Chen,** Xueyuan Nie, Jonathan Housden, Adrian Leyland and Allan Matthews, Substrate and bonding layer effects on performance of DLC and TiN biomedical coatings in Hank's solutions under cyclic impact-sliding loads, Surface & Coatings Technology 237（2013）219	Published
Chapter 6	**Ying Chen** and Xueyuan Nie, Failure mechanisms of DLC coated Ti-6Al-4V and CoCr biomedical materials under cyclic high combined contact stresses	To be Submitted

I hereby certify that I am the sole author of this thesis and that no part of this thesis has been published or submitted for publication.

I certify that, to the best of my knowledge, my thesis does not infringe upon anyone's copyright nor violate any proprietary rights and that any ideas, techniques, quotations, or any other material from the work of other people included in my thesis, published or otherwise, are fully acknowledged in accordance with the standard referencing practices. Furthermore, to the

extent that I have included copyrighted material that surpasses the bounds of fair dealing within the meaning of the Canada Copyright Act, I certify that I have obtained a written permission from the copyright owner(s) to include such material(s) in my thesis and have included copies of such copyright clearances to my appendix.

I declare that this is a true copy of my thesis, including any final revisions, as approved by my thesis committee and the Graduate Studies office, and that this thesis has not been submitted for a higher degree to any other University or Institution.

ABSTRACT

This study uses a newly developed testing method— inclined cyclic impact-sliding test to investigate the failure behaviors of different types of biomaterials, (SS316L, Ti6Al4V and CoCr) coated by different coatings (TiN, DLC and PEO), under extremely high dynamic contact stress conditions. This test method can simulate the combined impact and sliding/rolling loading conditions, which is very practical in many aspects of commercial usages. During the tests, fatigue cracking, chipping, peeling and material transferring were observed in damaged area. This research is mainly focused on the failure behaviors of load-bearing materials which cyclic impacting and sliding are always involved. This purpose was accomplished in the three stages:

First, impact-sliding test was carried out on TiN coated unhardened M2. It was found that soft substrate can cause early failure of coating due to the considerable plastic deformation in the substrate. In this case, stronger substrate is required to support coating better when tested under high contact stresses.

Second, PEO coated Ti-6Al-4V was tested under pure sliding and impact-sliding wear conditions. PEO coating was found not strong enough to afford the high contact pressure under cyclic impact-sliding wear test due to its porous surface structure. However, the wear performance of PEO coating was enhanced due to the sub-stoichiometric oxide. To sum up, for load-bearing biomedical implants involved in high impacting movement, PEO coating may not be a promising surface protection.

Third, the dense, smooth PVD/CVD bio-inert coatings were reconsidered. DLC and TiN coatings, combined by different substrates together with different interface

materials were tested under the cyclic impact-sliding test using a set of proper loading. The results show that to choose a proper combination of coating, interface and substrate based on their mechanical properties is of great importance under the test condition. Hard substrates provide support to coating better and a ductile and adhesive interface layer can delay the cracked coating from peeled-off.

DEDICATION

I would like to dedicate this dissertation to my parents for their unconditional love, support and encouragement.

ACKNOWLEDGEMENTS

TABLE OF CONTENTS

LIST OF TABLES

LIST OF FIGURES

CHAPTER 1 INTRODUCTION

1. GENERAL OVERVIEW

1.1 What is biomaterial and its properties

A biomaterial is any synthetic material that is used to replace or restore function to a body tissue and is continuously or intermittently in contact with body fluids [1-3]. Exposure to body fluids places several strict restrictions on materials that can be used as biomaterial [1-3]. First and foremost, a biomaterial must be biocompatible—it should not elicit an adverse response from the body, and vice versa. Additionally, it should be nontoxic and noncarcinogenic. These requirements eliminate many engineering materials that are cost-effectively available. Next, the biomaterial should possess adequate physical and mechanical properties to serve as augmentation or replacement of body tissues.

The most common classes of materials used as biomedical materials are polymers, metals, and ceramics [4, 5]. These three classes are used singly and in combination to form most of the implantation devices available today.

The ideal material or material combination should exhibit the following properties [5-10]:

- A biocompatible chemical composition to avoid adverse tissue reactions.

- Excellent resistance to degradation (e.g., corrosion resistance for metals).

- Acceptable strength to sustain cyclic loading endured by joint.

- A low modulus to minimize bone resorption.

- High wear resistance to minimize wear debris generation.

Metals have been used as implants since more than 100 years ago when Lane first introduced metal plate for bone fracture fixation in 1895 [5]. In the early development,

1

metal implants faced corrosion and insufficient strength problems. Shortly after the introduction of the 18-8 stainless steel in 1920s, which has had far-superior corrosion resistance to other metals available in that time, it immediately attracted the interest of the clinicians. Thereafter, metal implants experienced vast development and clinical use. The high strength and resistance to fracture that this class of material can provide assuming proper processing, gives reliable long-term implant performance in major load-bearing situations. Coupled with a relative ease of fabrication of both simple and complex shapes using well-established and widely available fabrication techniques (e.g., casting, forging, machining), this has promoted metal use in the field of orthopedics and dentistry primarily, the two fields in which highly loaded devices are most common.

The advantage of metal is their strength and therefore their resistance to damage in comparison with ceramic and polymer materials. The ceramics is poor in toughness, particularly with regards to its notch toughness; therefore, ceramics often result in a sudden fracture. Consequently, they are unsuitable for use in regions that are subject to heavy loads and repeated impact loads, or as parts (for example, screws) where pressure is concentrated. The weakness of polymeric materials makes the polymers inapplicable in locations where a large load is applied, and their inability to withstand heat limits sterilization methods.

Up to now, the three most used metals for implants are stainless steel, CoCr alloys and Ti alloys [5-8]. The first stainless steel used for implants contains ~18wt% Cr and ~8wt% Ni, and it is more resistant to corrosion than a carbon steel. Further addition of molybdenum Mo) has improved its corrosion resistance further, known as type 316 stainless steel. Afterwards, the carbon (C) content has been reduced from 0.08 to 0.03

wt.% which improved its corrosion resistance to chloride solution, and named as 316L.

Table 1-1 summarized the type of metals generally used for different implants division.

Some of the metal implants are illustrated in Fig. 1-1.

Table 1- 1 Implants division and type of metals used [10]

Division	Example of implants	Type of metal
Cardiovascular	Stent	316L SS; CoCrMo; Ti
	Artificial valve	Ti6Al4V
Orthopedic	Bone fixation (plate, screw, pin)	316L SS; Ti; Ti6Al4V
	Artificial joints	CoCrMo; Ti6Al4V; Ti6Al7Nb
Dentistry	Orthodontic wire	316L SS; CoCrMo; TiNi; TiMo
	Filling	AgSn(Cu) amalgam, Au
Craniofacial	Plate and screw	316L SS; CoCrMo; Ti; Ti6Al4V
Otorhinology	Artificial eardrum	316L SS

As shown in Fig. 1-1, a typical hip prosthesis consists of the femoral stem, a femoral ball, and a polymeric (ultrahigh molecular weight polyethylene, or UHMWPE) socket (cup) with or without a metallic backing [1-3]. Femoral components usually are manufactured from Co-Cr based alloys or titanium alloys. The ball (articulating portion of the femoral component) is made either of highly polished Co-Cr alloys or of a ceramic. Modular designs, where the stem and ball are of two different materials, are common [5].
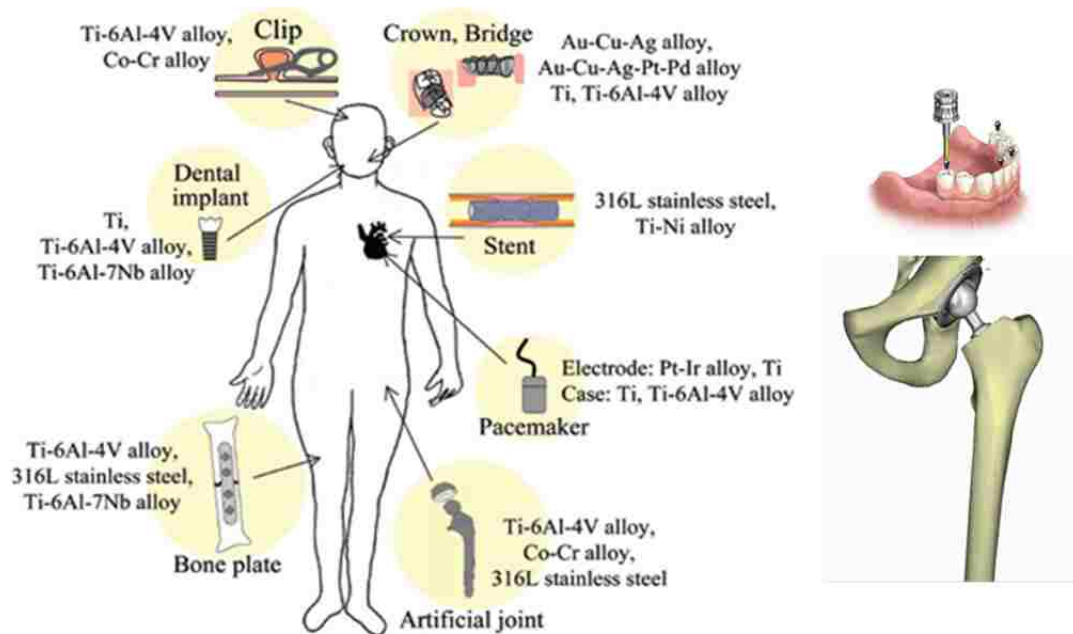
Figure 1- 1 Metallic devices and metallic biomaterials' applications [11].

1.2 Typical connection of joints in the body

The articulations are divided into three classes: synarthroses or immovable, amhiarthroses or slightly movable, and diarthroses or freely movable joints [12].

Synarthroses (immovable articulations) include all those articulations in which the surfaces of the bones are in almost direct contact, fastened together by intervening connective tissue or hyaline cartilage, and in which there is no appreciable motion, as in the joints between the bones of the skull, dental implants and stem-femur connection in the total hip replacements (THPs).

Amphiarthroses (slightly movable articulations) locate between the contiguous bony surfaces which are either connected by broad flattened discs of fibrocartilage or are united by an interosseous ligament.

Diarthroses (freely movable articulations) include the greater number of the joints in the body. In such a joint, the contiguous bony surfaces are covered with articular cartilage and enclosed by a synovial cavity with synovial fluid. This kind of body fluid is a viscous, which contains proteinases and lubricin, some salt and other ingredients. The principal role of synovial fluid is to reduce friction between the articular cartilage of synovial joints during movement [13].

1.3 The usage of biomaterials

One of the primary reasons that biomaterials are used is to physically replace hard or soft tissues that have become damaged or destroyed through some pathological process [1-7, 9]. Although the tissues and structures of the body perform for an extended period of time in most people, they do suffer from a variety of destructive processes, including fracture, infection, and cancer that cause pain, disfigurement, or loss of function. Under

such circumstances, it may be possible to remove the diseased tissue and replace it with a more suitable synthetic material.

Almost all interactions between cells/tissues and a metal implant occur at the implant surface – As such, the surface properties of metals implant materials are of great importance.

1.4 Challenges for using artificial bio-implants

Loosening is one of the most common complications resulting from a faulty device. This occurs when components of an implant begin to separate from the bone. Four principal causes of implantation loosening are [14]:

- Mechanical failure of the implant or cement;

- Introduction of wear debris into the interface region;

- Relative motion across the interface;

- Stress shielding in the bone.

Each of these phenomena can initiate a biological response in the bone leading to resorption and the eventual loosening of the implant.

1.5. Stress analysis of hip and knee implants

Fig. 1-2 shows schematic representation of the load transfer in the proximal femur before and after hip replacement [15, 16]. In the natural state, the stress is distributed over the entire cross section of the femur. Bending and axial compression are the major modes of loading. The post-surgery stress state is significantly different mainly due to the manner in which the load is transferred to the femur. In this case, the load is partially transferred through shear across the bone/cement/prostheses interfaces. This altered load transfer leads to increased stresses at the interface and unloading of the bone away from

6

the prosthesis. The interface shear stresses are further increased due to the stiffness ratio

between the prosthesis and the bone, typically of the order of 10 : 1 and higher.
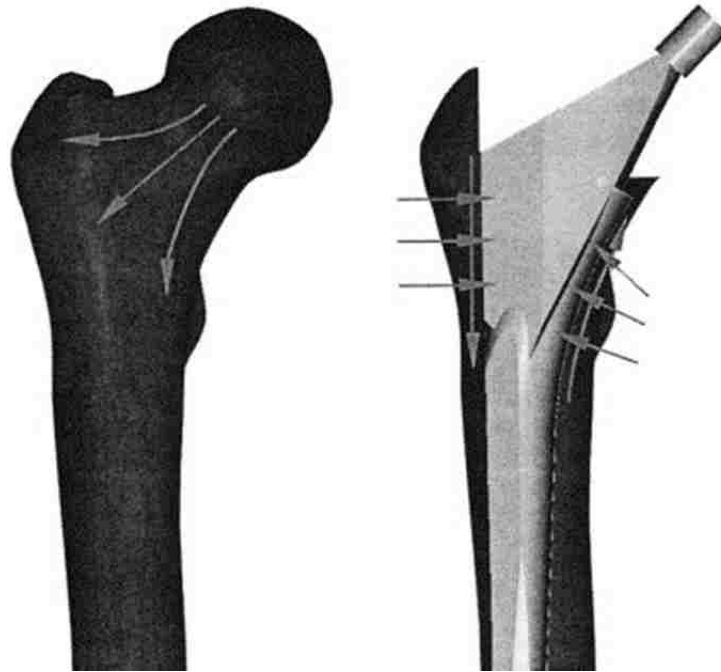
Figure 1- 2 Schematic representation of the load transfer before and after total hip

arthroplasty (THA) [15, 16].

In addition, the bending displacements in the bone surrounding the stem are

reduced because of the relatively high flexural stiffness of the prosthesis. This reduced

bending unloads the outer fibers of femur leading to a state of stress shielding. The

change in the load distribution increases stresses in some regions and reduces them in

others. If these changes are large enough, they can lead to adaptive bone remodeling.

Areas that see higher loads, may experience an increase in bone mass, while areas that

see a reduction in load may experience a decrease. The other factors mentioned earlier

might also play a role in this remodeling but stress shielding is often implicated.

The natural stress distribution in the femur is significantly altered after total hip

arthroplasty (THA). When an implant is introduced, it will carry a portion of the load,

7

causing a reduction of stress in some regions of the remaining bone. This phenomenon is commonly known as stress shielding. In response to the changed mechanical environment the shielded bone will remodel according to Wolff's law, resulting in a loss of bone mass through the biological process called resorption. Resorption can, in turn, cause or contribute to loosening of the prosthesis. The problem is particularly common among younger THA recipients.

Most synthetic biomaterials used for implants are commonly-used materials that are familiar to an average materials engineer or scientist [17]. Fig. 1-3 highlights the extraordinary mechanical properties of bone in contrast to technical bulk materials used for medical purpose.
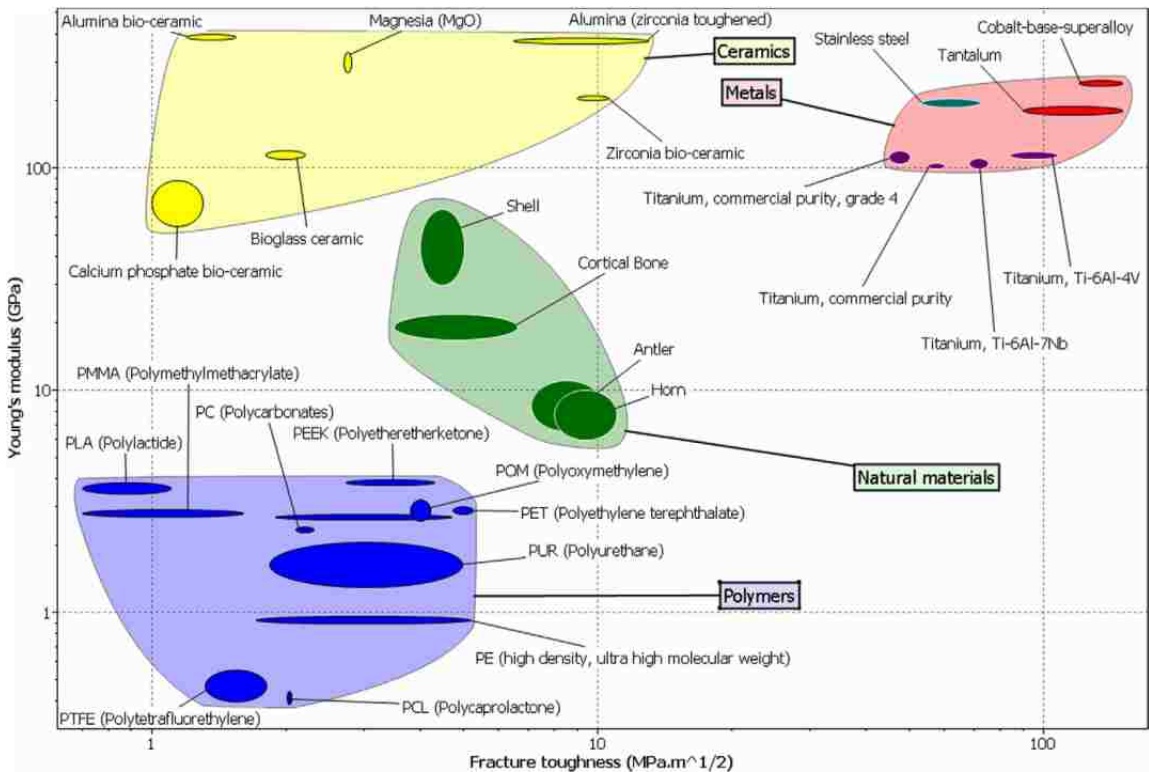
Figure 1- 3 Mechanical properties of natural materials in comparison with bulk materials for medical purpose. [17].

In some situations, such as in total hip and knee replacement, the high strength of the metal in the implant induces it to assume more than its share of responsibility for the load in that region. This decreases the load born by the surrounding tissue and therefore shields it from experiencing stress. The mechanical properties of bone and three metal biomaterials are summarized in Table 1-2. However, those are just general data of the materials, the value of which may vary largely due to the fabrication processes. For example, the UTS for as-case CoCrMo alloy is around 725 MPa, but the hot forged one has a value of 1205 MPa.

Table 1- 2 Mechanical properties of bone and metal biomaterials [6, 7, 10]

Materials	Young's Modulus (GPa)	Yield Stress (MPa)	Tensile Strength (MPa)
Cortical bone	15-30	30-70	70-150
Co-Cr	210-250	448-1606	793
Ti-6Al-4V	110	485	760-860
316L SS	190	220-1213	586-1351

2. TESTING METALLIC BIOMATERIALS IN THIS DISSERTATION

Three types of metallic biomaterials were used as substrates in this study, the detailed composition of each material were summarized in Table 1-3 as follows.

Table 1- 3 Chemical compositions of ASTM F-75 CoCr alloy, Ti6Al4V and 316L [6]

ASTM F-75	Composition (wt.%)	Ti-6Al-4V	Composition (wt.%)	AISI 316L	Composition (wt.%)
Chromium (Cr)	27.0% to 30.0%	Carbon (C)	0.1% max	Carbon (C)	0.03% max
Molybdenum (Mo)	5.0% to 7.0%	Iron (Fe)	0.3% max	Silicon (Si)	1% max
Nickel (Ni)	0.50% max	Nitrogen (N)	0.05% max	Manganese (Mn)	2% max
Iron (Fe)	0.75% max	Oxygen (O)	0.2% max	Phosphorous (P)	0.045% max
Carbon (C)	0.20% to 0.35%	Aluminium (Al)	5.5-6.76%	Sulphur (S)	0.03% max

Silicon (Si)	1.00% max	Vanadium (V)	3.5-4.5%	Chromium (Cr)	18% max
Manganese (Mn)	1.00% max	Hydrogen (H)	0.015% max	Nickel (Ni)	14% max
Tungsten (W)	0.20% max	Titanium (Ti)	Balance	Molybdenum (Mo)	3% max
Phosphorous (P)	0.020% max			Nitrogen (N)	0.1% max
Sulphur (S)	0.010% max			Iron (Fe)	Balance
Nitrogen (N)	0.125% to 0.250%				
Aluminium (Al)	0.10% max				
Titanium (Ti)	0.10% max				
Cobalt (Co)	Balance				

I. Stainless steel

The first metal alloy developed specifically for human use was the "Vanadium steel" which was used to manufacture bone fracture plates and screws [5-7]. It is no longer used in implant application, because its corrosion resistance in vivo is inadequate. The 316L stainless steel materials are resistant to a wide range of corrosive agents due to their high Cr content (more than 12 wt.%), which allows the formation of a strongly adherent, self-healing and corrosion resistant coating oxide of Cr_2O_3. Several types of stainless steel are available and the most widely used for implant manufacture is austenitic stainless steel. In order to be austenitic at room temperature, stainless steel needs to contain a certain amount of austenite stabilizing elements such as Ni or Mn. The stainless steel most widely used in clinical applications is AISI 316L that contains 0.03 wt.% C, 17–20 wt.% Cr, 12–14 wt.% Ni, 2–3 wt.% Mo and minor amounts of nitrogen, manganese, phosphorus, silicon and sulphur.

Stainless steel is widely used in temporary devices such as fracture plates, screws and hip nails among others, owing to their relatively low cost, availability and easy

processing [5, 6, 17]. Their use in orthopedic joint prosthesis is restricted because other metallic alloys such as Ti-based and Co–Cr-based alloys exhibit superior mechanical and corrosion properties.

The wear resistance of austenitic stainless steel is rather poor and this is the reason why the metal-on-metal pairs in joints such as the hip (femoral head and acetabular cup) were discarded, because of high friction and the large number of wear debris particles that were produced, which led to a rapid loosening. This is one of the main reasons why the Co–Cr–Mo alloy (ASTM F75) was introduced in hip prostheses. Co–Cr-based alloys exhibit an excellent corrosion resistance, even in chloride environments, that they combine with a good wear resistance [19]. Their mechanical properties are also superior, most significantly their fatigue strength. These materials have a high elastic modulus (220–230GPa) similar to that of stainless steel (approx. 200GPa), and an order of magnitude higher than that of cortical bone (20–30GPa). On contact with bone, the metallic devices will take most of the load due to their high modulus, producing stress shielding in the adjacent bone. The lack of mechanical stimuli on the bone may induce its resorption that will lead to the eventual failure and loosening of the implant [20-22]. It is necessary to make a good design of the geometric shape of the implants to minimize the disadvantage of stress-shielding.

II. Titanium and its alloys

The use of titanium as implant material goes back to 1930s. it is primarily due to its lightness and good mechano-chemical properties [6, 18]. Titanium is featured by its light weight. Its density is only 4.5g/cm^3 compared to 7.9g/cm^3 for 316 stainless steel and 8.3g/cm^3 for cast CoCrMo alloys [4, 6]. Ti and its alloys, e.g. Ti6Al4V are known for

their excellent tensile strength and pitting corrosion resistance which make it most widely used for implant applications [6]. Titanium alloyed with Ni, i.e. Nitinol, forms alloys having shape memory effect which makes them suitable in various applications such as dental restoration wiring.

Young's modulus of Ti and Ti alloys is valued as it is half that of stainless steel or Co-Cr alloy, and is relatively close to that of cortical bones and therefore create less risk of stress protection of bone. The excellence of Ti in mechanical biocompatibility has led to its widespread use in the area of biomaterial such as in fixtures of dental implants, fracture fixation materials and artificial joints. In addition, from past experience, it has become clear that its compatibility with both hard and soft tissues surpasses that of all other metal materials [23]. Its compatibility with blood is not yet clear, however, its safety for application within the human body has been well established, and it lacks toxicity. Its safety and tissue compatibility are a result of the chemical characteristic of Ti, or more specifically, its surface properties, and knowledge of these properties is thus of extreme importance.

Ti is an extremely active element, and its standard electrode potential for the reaction, Ti $\rightarrow$ Ti + 2 e$^-$ with regards to the standard hydrogen electrode is as low as -1.63V, indicating its high activity. According to Pourbaix [24], of the metal elements that are in practical use, Ti is the most thermodynamically active (easily-ionized) metallic element. This active property forms a basis for the chemical characteristics of Ti, such as the difficulty encountered in working the metal, its resistance to corrosion, and its low thermal conductivity. Although Ti as an element is extremely active, Ti as a metallic material is highly resistant to corrosion. This is because of the highly reactive nature of

Ti. It reacts readily with water molecules in solution, or moisture in the atmosphere to form a thin layer (≈5 nm thick) of titanium oxide on the metal surface. Even when the surface is scratched, the newly exposed sub-layer rapidly becomes coated with oxide, appearing inert. For this reason, its resistance to corrosion is much higher than that of stainless steel or Co-Cr alloy. This nature not only provides resistance to corrosion, but also explains its ready incorporation into the body, and its lack of toxicity [25].

Many Ti alloys have been developed for biomedical purposes [26-28]. Ti-6AI-4V alloy, a typical Ti alloy is an α+β-type, and used commonly in biological materials. This alloy has several properties that are superior to those of other Ti alloys, including processability, thermal processability, and weldability, in addition to its resistance to corrosion, strength, and biocompatibility. A notable characteristic of Ti-6AI-4V alloy is its 0.2% proof stress of 895 MPa, a value that is much higher than even that of stainless steel or Co-Cr-Mo alloys. This indicates that even under a high load, it is not easily plastically deformed. However, titanium alloys are insufficient in tribological performances [29, 30], characterized by high coefficient of friction, severe adhesive wear with high tendency to seizing and low abrasion resistance. There are two widely accepted reasons for the inferior tribological properties: the first is its low resistance to plastic shearing and the low work hardening; and the second reason is due to the low protection exerted by the surface oxide. The oxide is formed by high flash temperatures caused by friction during sliding. The stationary or dynamic contact loads between Ti-alloy components and other metals or itself can cause damage to the thin oxide film and thus lose the protection.

a. The surface of titanium

Biomaterials function by interacting with biological tissues; therefore the reaction between the material surface and biological tissues needs to be fully understood [31]. It is self-evident that reactions are determined by the properties of the material surface, including resistance to corrosion and tissue biocompatibility. The metal surface under atmospheric conditions or in solutions always forms a layer of reactive film. The film that is formed in solution displays low solubility, and provided it has been formed without pores and is highly adhesive, it becomes resistant to corrosion (an inert/passive film). The passive film that is formed is transparent and is as thin as 1-5 nm. Metals such as Ti, Zr and Ta, that are essential as metal biomaterials, are easily oxidized (these are also known as valve metals). As this layer envelops the metal surface, it stops the progress of corrosion passed this point, therefore resulting in an apparently inert metal [32]. With regards to Ti, the reaction below occurs in solution at room temperature, resulting in its inert properties.

$Ti + 2H_2O \rightarrow TiO_2 + 4H^+ + 4e^-$ (anode reaction) (1)

$2H+ + 2e^- \rightarrow H_2$ (cathode reaction, in acidic solution) (2)

$O_2 + H_2O + 4e^- \rightarrow 4OH^-$ (cathode reaction, in neutral or alkaline solution) (3)
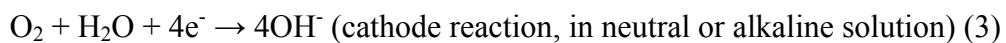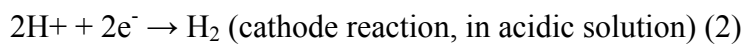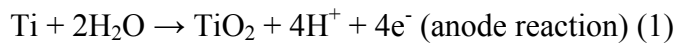
The reaction described by equation (1) does not occur in one step, but in steps from Ti ,Ti^{2+}, Ti^{3+} to Ti^{4+}.

The same reaction (1) can occur with atmospheric moisture; Ti as a biomaterial generally exists as an inert metal covered by an oxidative layer.

The passive film of Ti is made up of amorphous or low crystalline stoichiometric TiO_2. However, this is not completely amorphous, and includes lower oxide and crystalline grains.

14

Any damage to the surface can be self-repaired rapidly. As shown in Fig. 1-4 when the passive film is damaged, outflow of Ti ions and the anodic current that accompany regeneration of the film can be detected, however, the current declines within a short period, once the film has regenerated. This is why the corrosion resistance of these materials is high.

Even though an inert film is formed on the titanium surface, the surface remains active. It reacts with the moisture in air, forming hydroxyl groups on the surface. Due to the passive surface layer of Ti as shown in Fig. 1-4, an inert film is formed in solution as well as on reaction with moisture in the atmosphere, resulting in the formation of hydroxyl groups.
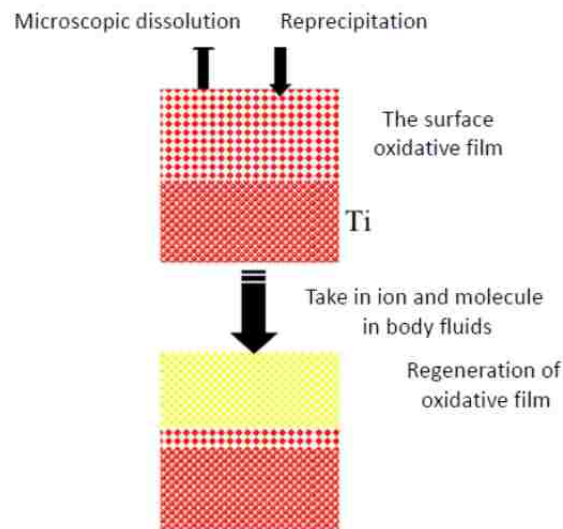
Figure 1- 4 Reconstruction of surface oxide (inert) layer in the biological environment

b. Reconstruction of the oxide passivation film

The passive film appears to be in a stable state, however, a cycle of repetitive partial solubilization and re-deposition can be detected at the microscopic level. The structure is therefore constantly changing in accordance with its biological surroundings (Fig. 1-4)

[33,34]. Calcium phosphate is also formed on the surface of Ti-6Al-4V alloy when it is used for fracture fixation. In particular, calcium phosphate with a large [Ca/P] ratio can be detected on the surface of an intramedullary needle inserted into the medullary cavity. Furthermore, when Ti or Ti alloy is immersed in Hank's solution, calcium phosphate has been found to be deposited, and under conditions used for cell culture, formation of sulfite or sulfide has also been found. These findings show that the physiological processes that occur in the body are well reflected by in vitro experiments.

    c. Corrosion-resistant properties of titanium

Metal Ti itself does not exhibit toxicity, but this can arise from the metal ions or derivatives of the metal including oxides, hydroxides, salts, or complexes that result as a product of rust or corrosion. These can subsequently bind biological molecules or cellular organelles, inhibiting their biological functions. The passive state maintaining current density is lower for Ti and Ti-6Al-4V than for other materials, suggesting relatively high resistance to corrosion.

Ti-6Al-4V, reported by [31], showed charge stabilization after five days of being immersed in biological saline, but in Hank's solution, the charge continued to show a gradual increase. This suggests that the passive film of Ti is stable in saline, but the film grows in Hank's solution. As noted above, the reason for this is formation of a calcium phosphate film on the Ti surface in Hank's solution.

On investigation of the effect of uric acid and amino acids, immersion charges measured for a period of 150 days did not change, suggesting that these biological molecules had no effect on the corrosion of Ti alloys. Proteins are generally known to accelerate metal corrosion, especially for the long-term crevice corrosion, but have no

effect on Ti or Ti alloys.

III. Cobalt-Chrome alloys

CoCr alloys have been utilized for many decades in making artificial joints [35]. They are generally known for their excellent wear resistance. Especially the wrought CoNiCrMo alloy has been used for making heavily loaded joints such as ankle implants.

Amongst all the above discussed alloys, the CoCrMo is most corrosion resistant. However, it is not preferred for bearing surfaces of implants as bare material due to its poor frictional properties (debris and ion-release). The superior mechanical properties (particularly fatigue strength) make it useful for implants which require long service life.

The chloride content of the environment is an important factor to consider when looking at the corrosion of an alloy. Chloride ions are aggressive species which can lead to localized corrosion processes in the form of pitting and crevice corrosion. If the chloride ions are present in an aerated solution, this is believed to increase the corrosion rate of CoCrMo, Ti6Al4V and 316L stainless steel in aqueous environment. When tested under a HBSS solution, the corrosion resistance (Rc) measured by potentiodynamic polarization test in our lab showed that CoCrMo had greatest resistance, Ti6Al4V showed moderate resistance while 316L, although it show good corrosion resistance under many circumstances, was not good enough when chloride took place.

a. General mechanical properties of CoCr alloy

Good mechanical properties of CoCr based alloys are a result of a multiphase structure, age hardening among alloy components and precipitation of carbides, which substantially increase their hardness (refer to Table 1-2 for the details). High mechanical properties should assure technical and functional durability (long-life) of the implant

applications. Although CoCrMo alloys are the strongest, hardest, and most fatigue resistant of the metals used for joint replacement components, care must be taken to concern about wear debris and metal ion release from orthopedic implants into the body fluids, such as Co and Cr ions [36, 37]. These metal ions and wear debris, concentrated at the implant-tissue interface, may migrate through the tissue. Over time the level of metal ions may become clinically significant, resulting in implant failure, osteolysis and allergic reactions.

The elastic modulus of CoCr alloys are very high, comparing to that of strongest bones inside body, and, cobalt alloys are generally cast into their final shape because they are susceptible to work-hardening at room temperature. That is, the improvements in strength and hardness gained by cold working are not worth the loss in fracture toughness. More considerable design on the geometric size of the implants is required to obtain a near-net shape casting.

b. Resistance to Corrosion – The Passivation of CoCrMo

Due to the formation of a chromium rich passive oxide film (Cr_2O_3) on CoCrMo alloys, they show a high resistance to corrosion. When a metal is in a passive state it will still corrode in a slow and uniform mode, but it will resist the thermodynamic tendency to rapidly dissolve. This condition is achieved when a passive oxide film is formed at the metal surface. Passive oxide films can vary in thickness, chemical composition as well as in oxidation states and are affected by a number of factors, including pH, electrode potential and composition of the electrolyte [38]. When an alloy is placed in an electrolyte, the oxide film undergoes continual dissolution /depassivation and growth /repassivation processes. However, if the dissolution rate is high then active dissolution

of the metal ions will occur accelerating the rate of corrosion [36].

c. Types of Corrosion for CoCr alloy

Corrosion may be general or localized. General corrosion involves the uniform dissolution of the metal surface. In contrast, localized corrosion can take place on a passive metal surface in the presence of aggressive ions. Here, localized attack occurs in specific sites where there are high local dissolution rates, which lead to high rates of penetration [36]. Chloride ions will enhance the localized corrosion process and occur at local sites caused by imperfections where there are pits or inclusions. There are several forms of localized corrosion [39], but pitting, crevice corrosion, fretting, and tribocorrosion are the most relevant types for artificial hip joints. Pitting corrosion is confined to a point or small hole within the metal. Pitting can initiate at sites where there are small surface defects such as a scratch or a dent, a small change in chemical composition of the alloy or damage to the oxide film. In the pit there is a rapid depletion of oxygen, and the pit becomes a net anode, undergoing rapid dissolution. This anodic reaction produces electrons that are used in oxygen reduction reactions at the external surface. The generation of metal ions in the pit cavity leads to a net positive charge in the pit, resulting in an influx of chloride ions to maintain the charge balance. Hydrolysis of metal cations causes a decrease in pH. These factors promote pit growth, as high concentrations of chloride and hydrogen ions promote metal dissolution.

Crevice corrosion is associated with the formation of stagnant solution in crevices or occluded areas such as those formed under washers, fastener heads, lap joints and clamps. The mechanism of crevice corrosion is similar to that of pitting corrosion: depletion of oxygen, more acidic conditions and build-up of aggressive ionic species such as chloride

enhance metal dissolution and produce accelerated attack within the crevice. However, the difference is that an external crevice former is required to initiate corrosion on the surface.

Fretting corrosion can also occur where micro-motion between two surfaces causes depassivation leading to localized corrosion. These small amplitude displacements occur when the total amplitude of movement is smaller than the contact width of the prosthetic joint [40]. The micromotion between the faying surfaces, which can often happen over a crevice, causes depassivation followed by a period of active dissolution during the repassivation process, increasing the concentration of metal ions in the cavity leading to acidification through hydrolysis and ingress of chloride ions for charge balance. Minor movements of the hip joint frequently occur when people adjust or change position and so fretting corrosion can accelerate wear.

3. COATING & SURFACE TREATMENT OF THE BIOMATERIALS

The application of coatings is one of the approaches that are available to modify the surface of materials. Various coating techniques and materials have been used with the objective of improving surface properties. There are various surface treatments which may increase the wear resistance and prevent and/or reduce the release of potentially harmful metal ions from implant materials. One is to thicken the protective oxide layer already present on the surface of metallic biomaterials via a process known as passivation [41]. Anodizing and Plasma Electrolytic Oxidation (PEO) are both the way to promote the growth of passivation layer that mainly contain the oxides to grow. However, the type of material is limited to be light material. Another method is to apply coatings or protective layers to increase the wear resistance and reduce the possibility of implant

20

failure and osteolysis [42, 43]. PVD and CVD are very effective process to make dense and smooth protective coatings on many types of substrates. However, some problems with coatings have arisen, mainly the delamination or wear of the coating. Nonetheless, investigations continue to find suitable materials and techniques to improve the properties of metallic biomaterials. To date, this approach has been used mainly in vitro to further evaluate coating behavior, biological properties of coated substrates, and mechanical characteristics of both coatings and substrates. Fig. 1-5 summarizes the classification of coating techniques for industrial use, some of which have been implemented in orthodontics to improve the surface properties of such materials.
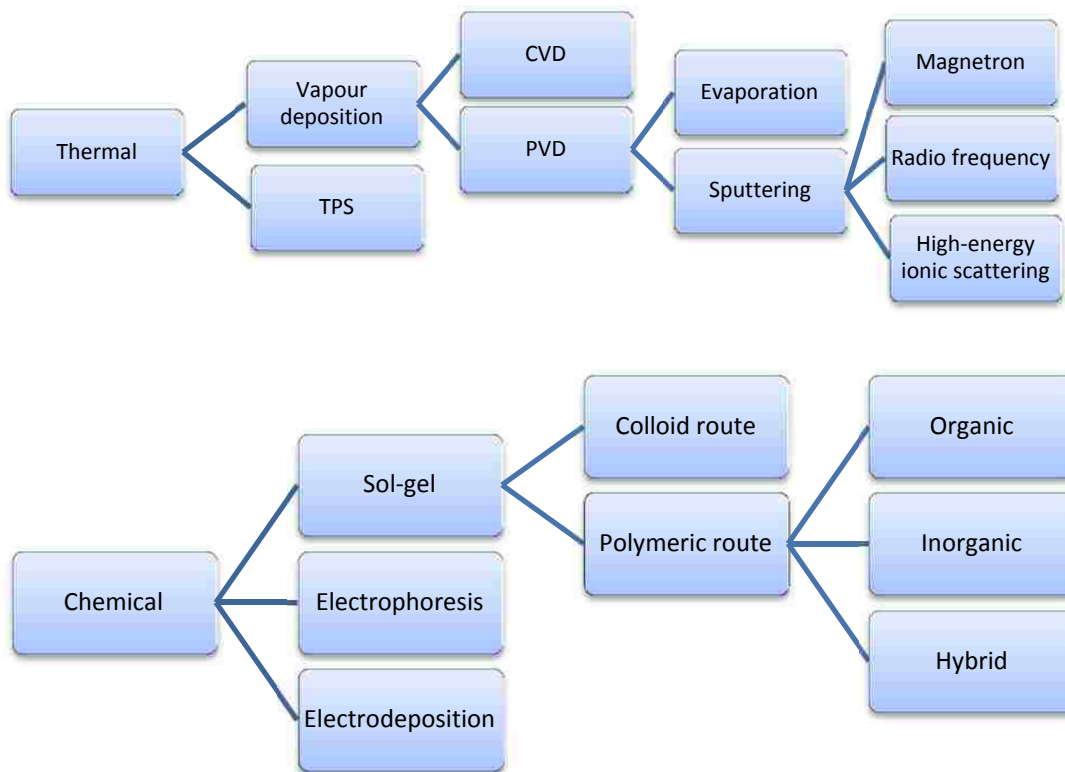
Figure 1- 5 Classification of processes used for coating at the industrial level [44]

There are three types of coatings deposited by different routes in this dissertation, which are Plasma Enhanced Chemical Vapor Deposition (PECVD) [45, 46], Plasma

21

Assisted Physical Vapor Deposition (PAPVD)[47] and Plasma Electrolytic Oxidation (PEO) [48]. In this study, the coatings made by first two methods were provided by Tevac Ltd. UK [49].

I. Chemical Vapor Deposition (CVD)

This technique involves the flowing of a precursor gas into a chamber that contains one or more heated objects to be coated. Some chemical reactions take place on and near the hot surfaces, which results in the deposition of a thin film on the surface. The production of chemical by-products and their further exhaustion out of the chamber along with unreacted precursor gases accompanies the process. CVD has distinctive advantages: the films obtained with this technique are conformal (film thickness on the sidewalls is comparable to thickness on the top), a wide variety of materials can be applied and they can be deposited with a high level of purity, and it also presents high deposition rates. Its main disadvantage lies in the properties of the precursors, since they need to be volatile at near-room temperatures, which is non-trivial for a great number of elements. Other drawbacks include the fact that precursors can be toxic, explosive, expensive, corrosive, the by-products can be hazardous, and films need to be deposited at elevated temperatures, which restricts the types of materials that can be coated [50].

Diamond-like carbon (DLC) coatings is a kind of amorphous carbon materials (i.e. have no dominant crystalline lattice structure) that display some of the typical properties of diamond. Two main phases of carbon atoms coexist in the DLC coatings, which are sp3 (diamond) and sp2 (graphite) phases.

As is well known, carbon –carbon interatomic bonds can be of two types: the near-planar trigonal or sp2 form found in graphite, or the tetragonal sp 3 variety that

22

occurs in diamond. It is the three-dimensional character of sp3 bonding, together with the strength of the short C–C covalent bond that give diamond its great strength. [51].

Traditionally, the largest inherent problem with DLC coatings has been issues of adhesion: typically the higher the sp3 percentage in a DLC film, the harder the DLC film but the higher the compressive stress within that film. In extreme cases, such stresses can create unstable interfaces (i.e. adhesion and/or cohesion issues) and the film may become prone to delamination. So modern techniques usually alleviate the problem by priming the substrate surface prior to coating through shallow metal ion implantation and thus increase interface strength. In this study, two types of DLC coatings with different interface materials were chosen. One is a tungsten-based interlayer and the other is a silicon-based interlayer.

The DLC coatings were prepared by PACVD using a standard commercial process at Tecvac Ltd. Samples were sputtering-cleaned in an Ar-H_2 discharge prior to DLC coating and a thin Si bond layer was first deposited at a thickness of 0.4-0.5 μm. A total pressure of 0.8 Pa was used during the deposition and the substrates were R.F. biased to a total power of 500-550 W. the maximum coating temperature did not exceed 300 ° C.

II. Physical Vapor Deposition (PVD)

This process consists of atomic deposition procedures in which a material is vaporized from solid or liquid sources in the form of atoms or molecules and transported in the form of vapor through a vacuum or low-pressure gaseous (plasma) environment to a substrate, where it finally condenses. This technique is suitable for depositing films in the range of a few nanometers to thousands of nanometers, for multilayer coating, graded

composition deposits, very thick deposits, and freestanding structures.

Titanium nitride coating on the metallic implant has been a popular method to improve corrosion resistance of metallic implant such as Ti alloy and Co based alloy by physical vapor deposition, plasma spray process, etc. [52, 53]. Modification of metallic implant surface by electropolishing, sand blasting or shot peening method were also reported to improve the corrosion resistance of the implant. It is known that a significant improvement of corrosion resistance can be achieved for the electropolished surfaces and sand blasted surfaces, where the former surfaces are corroded most slowly. The modification of corrosion resistance properties by the two methods are considered due to the increasing surface area and the introduction of compressive stress on the surface [54]. In addition, chemical composition modification is also possible by sand blasting process with the introduction of sand particle that form certain layer on the surface being blasted.

TiN coatings were deposited by electron beam PAPVD using a Tecvac IP70 coater. The coating temperature did not exceed 450° C.

Detailed information can be found in Table 1-3, the testing PVD/CVD coated specimens were provided by Tevac. Ltd. UK [49].

Table 1- 4 Elastic modulus and hardness of TiN and DLC coatings manufactured by Tecvac. Ltd [49].

Coating type	Substrate material	Thickness (μm)	Bonding layer material (0.3-0.5 μm)	Elastic modulus of coating (GPa)	Hardness of coating (GPa)	Surface roughness Ra (μm)
TiN	Ti6Al4V	2.3	Ti	345	22.5	0.133
	M2	2.3	Ti	345	24	0.036
a:H-DLC	Ti6Al4V	2.7-2.9	Si	190	18	0.046
	M2	2.7-2.9	Si	190	20	0.030

	CoCrMo	2.7-2.9	Si	190	18	0.226
W-DLC	**316L SS**	2.7	W	180	15	0.026
	M2	2.7	W	180	18	0.020

The ideal bearing surface should also be resistant to yielding (plastic or permanent deformation), also known as resilience. The hardness of many materials is approximately three times its yield strength. The load required to cause plastic deformation (P_{yield}) can be estimated from contact mechanics theory and is proportional to the ratio of the surface's material properties, hardness (H) and elastic modulus (E):

$$P_{yield} \propto H^3/E^2$$

Thus, coatings with a high hardness and a low elastic modulus, and therefore a high plastic resistance ratio H^3/E^2, will be more likely to resist plastic deformation during low load contact events and exhibit a higher yield strength.

The mechanical properties of the substrate become increasingly important with higher load contact stresses and larger deformations, where the depth of indentation is greater than one-tenth of the coating thickness. In such situations the mechanical response of a coated system is generally controlled by the plastic rather than the elastic response of the substrate: as substrate hardness increases the resistance to penetration increases. Finally, to minimize interfacial stresses and allow the coating and substrate to elastically deform as one unit the elastic modulus of the coating and substrate should be similar.

III. Plasma electrolytic oxidation (PEO)

In this research, bio-ceramic composite coatings were produced on Ti-6Al-4V alloy by PEO. This technique is based on the interaction between oxide film growing on the metal surface and spark micro-discharges, which are initiated at potentials above the

dielectric breakdown voltage of the film in an aqueous electrolyte [55-58]. Since it normally involves at least some conversion (oxidation) of the substrate, the interfacial adhesion tends to be superior to that of most deposited coatings. PEO coatings also contain significant levels of surface-connected, fine-scale porosity and, partly as a consequence of this, have a relatively low global stiffness and making them strain-tolerant.

The combination of good interfacial adhesion, high hardness, surface-connected porosity (giving good lubricant retention and providing spaces for the skeletogenous cells to grow after implantation) and excellent tribological performance of PEO coatings make it a good choice for many applications, including biomedical implants. In general, the wear performance is inferior under corrosive or impact loadings. Of course, this is expected with ceramic coatings, which tend to fracture under such conditions, whereas a metallic coating (such as TiN) or substrate tends to undergo plastic deformation.

4. REVIEW OF IN VITRO TEST OF BIOMATERIALS

I. General overview of testing methodologies

Most manufacturers of materials operate an extensive quality assurance program and materials are thoroughly tested before being released to the general practitioner.

1- Standard Specifications: Many standard specification tests of both national and international standards organizations (ISO) are now available.

2- Laboratory Evaluation: Laboratory tests, some of which are used in standard specification, can be used to indicate the suitability of certain materials. It is important that methods used to evaluate materials in laboratory give results, which can be correlated with clinical experience.

3- Clinical Trials: Although laboratory tests can provide many important and useful data on materials, the ultimate test is the controlled clinical trial and verdict of practitioners after a period of use in general practice. Many materials produce good results in the laboratory, only to be found lacking when subjected to clinical use.

II. Fatigue wear evaluation methodologies

An important aspect in hip and knee implants is their tribological and fatigue failure performances, particularly in terms of wear of the articulating load-bearing surfaces. This is considered the main drawback of metal on metal devices.

Fatigue fracture and wear have been identified as some of the major problems associated with implant loosening, stress-shielding and ultimate implant failure of medical devices [59,60]. The selection of biomaterials for wear resistance unfortunately cannot rely only on conventional thinking of using hard ceramics because of their low coefficient of friction and high modulus of elasticity. This is because ceramics are generally prone to brittle fracture and need absolute quality control to avoid fatigue fracture for medical device applications.

The actual in vivo mechanisms are complex and involve the hostile body environment and take too long time to achieve and hard to repeat. The development of tools using new methodologies involving in vitro tests to predict the fatigue fracture/wear of those biomaterials is the major tendency of the industry. It is impossible to fully avoid failure of biomaterials, but to predict the failure time and to identify the mechanisms using these methods [61]. In the laboratory, accelerated tests are always used by choosing appropriate testing conditions and evaluating models.

The current fatigue tests used to evaluate biomaterials can be categorized as

follows (see Type I-III in Fig. 1-6) [59]:

1. Stress/life (S/N) or COF/distance approach,

2. Fracture mechanics approach, and

3. Fatigue-wear approach using simulated physiologic multi-axial loading

The first two methods are used primarily for the materials screening process and are useful for the initial process of materials selection of implant materials that will be subjected to high cyclic loading conditions (for example, for orthopedic implant applications). The third method is considered to be an in vitro evaluation to determine the fatigue performance close to a physiologic environment and is normally a precursor to animal experiments (in-vivo tests). The first two approaches are seen to be less expensive. The third approach is costly as dedicated custom-made simulators need to be used. As simulators vary in design, comparisons of results can be difficult.
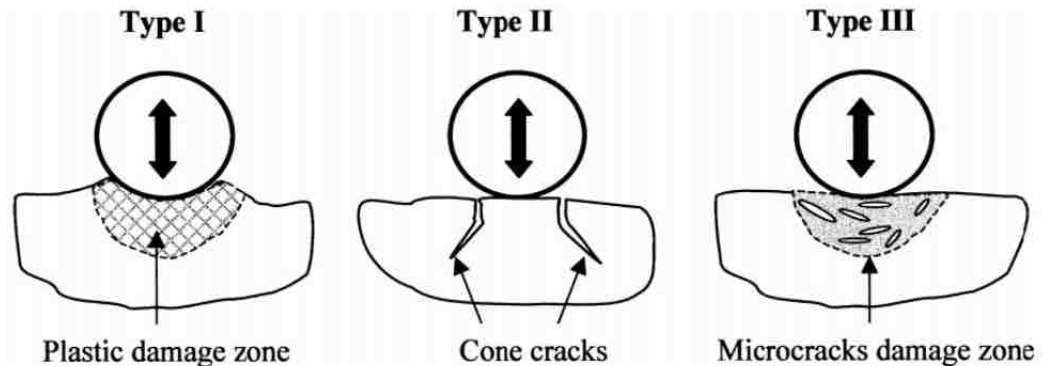
Figure 1- 6 Schematic illustration of the various types of surface and subsurface damage arising from a spherical indenter [59].

The S/N approach (see Type I in Fig. 1-6) is normally done using smooth specimens in a physiologic environment (inside body simulation) either in (a) cyclic dynamic loading (especially for metal biomaterials) or (b) static loading (especially for

polymers). The advantage of this approach is that it represents both initiation and propagation of cracks in the aggressive environment. In the case of metallic implant biomaterials, it allows the electrochemical effects to be considered together with an applied stress–strain field (especially in fretting corrosion fatigue experiments) in the assessment of the durability of the biomaterial. The design stresses rely on the accuracy of the endurance stresses, which need large safety factors and good failure models for prediction. Pin-on-disc (POD) testing is a cost effective preliminary screening method that yields valuable information regarding material wear characteristics and durability. Pin-on-disc testing can be used for screening candidate biomaterial couples and for optimizing design performance prior to cost-intensive joint simulator wears tests. Understanding the tribological performance of the materials helps the estimation of the failure behaviors when complex loads are involved.

In the fracture mechanics approach (see Type II in Fig. 1-6), the fatigue-crack propagation of the biomaterials are studied by (a) long cracks ($\leq$ 0.3 mm) using compact-tension specimens or (b) small cracks (1–250 nm) using micro indentation methods in a servo-hydraulic machine [62.]. This approach, often done in a physiologic environment, is good for studying brittle implant materials like ceramics [63, 64] and dental composites [65], where sensitivity to initial flaw sizes and crack propagation rates determine the lifetime of the implant.

The fatigue-wear approach (see Type III in Fig. 1-6) on smooth specimens is an important contribution as the rate of removal of a passive oxide or molecular absorbed layer between the two articulating surfaces often determines the accuracy of the lifetime prediction and provides cytotoxicity and morphology data of wear debris for evaluating

29

the host tissue response to the debris. Physiologic loading using a multi-axial load profile is normally applied throughout the fatigue tests. These are more realistic comparative tests than basic wear screening tests, such as pin-on-disk (ASTM F732) or ISO 6474. Over the years, numerous dedicated machines such as the hip wear simulator [66]. A hip simulator can replicate motions associated with activities such as walking, running, stair climbing, deep knee bends, etc. as shown in Fig. 1-7) and issues related to wear testing of metal–metal implants and the accelerated heart valve tester [67] have been used. However, as always the case, these testing methods are often very hard to approach and expensive to operate.
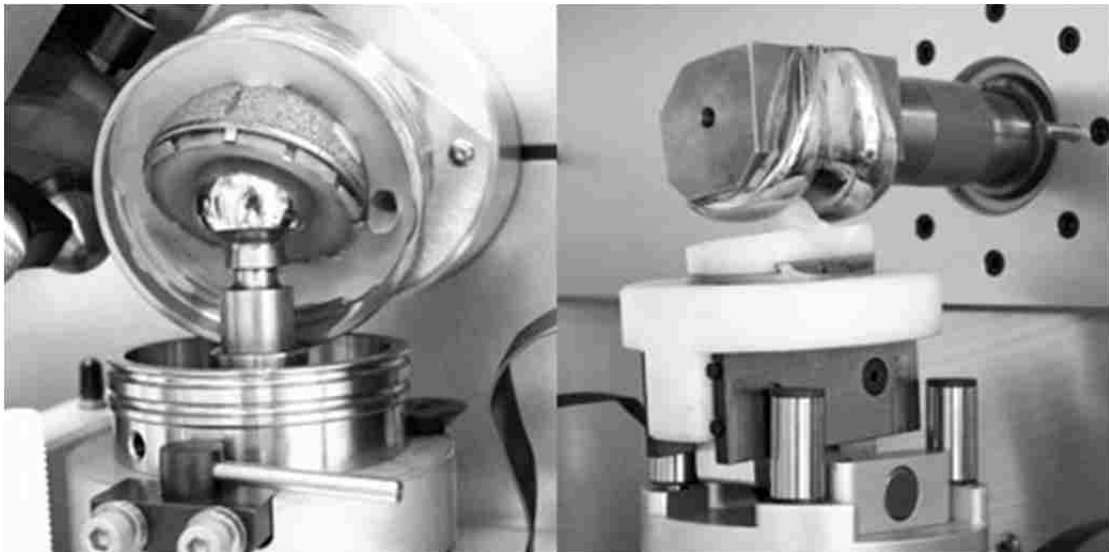
Figure 1- 7 Hip and knee implant wear simulators.

If the actual in vivo wear characteristics can be reproduced in the in vitro experiments in terms of the environment and mode of deformation, then in vitro experiments can prove to be very useful in cost and also in elucidating the actual wear mechanisms.

There has long been concern that metal-on-metal hip arthroplasties may develop

problems associated with metal sensitivity. The disadvantage of metal-to-metal bearings is that they shed many more wear particles which is thought to produce local tissue concentrations that can be ten times higher than those found in metal-on-polymer joints. It is thought that this sensitivity can lead to loosening of the joint, as well as groin pain and pain in and around the soft tissues of the joint, which can ultimately lead to revision surgery.

5. IMPACT TESTS FOR COATED & UNCOATED BIOMATERIALS

I. Perpendicular impact test

There are many service conditions in which impact loads are encountered by its counterface. In engineering practice, notched bar impact toughness, obtained in a standard impact testing machine (e.g., Charpy impact test), has long been considered as a measure of relative resistance of a material against rupture due to high-rate impact loading. This is generally true when the impact energy is so large that a single blow will cause rupture. But in the study of biomedical implant applications, such a high loading is under no circumstance. In most cases rupture takes place under repeated impact of comparatively low energy. Prediction of the expected life of the biomaterial implants can best be accomplished by testing the material under repeated impact loads, termed as impact fatigue.

The early study of dynamic repetitive impact testing method, which was known as the perpendicular impact tester or ball-on-plate test, was introduced by O. Knotek, et al. [68]. At that moment, there was a need in the biomedical industries, to develop an evaluation method on hard coatings, since well-established testing methods such as the pin-on-disc, scratch adhesion, or the abrasive wheel test did not induce these kinds of

31

contact conditions. The impact tester is applied as a convenient method for the characterization of coating fatigue properties, both cohesive and adhesive. It can be used on brittle and hard ceramic coatings [69] and ductile metals. Formation of the impact crater: the loss of the material's ability to undergo plastic deformation results in various forms of degradation (cracks, work-hardened areas).

The main origin of the failure of hard coatings under cyclic loading is the excessive plastic strain of the substrate after too many impacts. With a high Young's modulus, the fragile coatings are subjected to high stresses due to the substrate strain. The comparison of impact tests with scratch tests or Rockwell C adhesion tests7J8 aids in understanding the surface fatigue failure mechanisms [70]. Formation of the impact crater occurs in approximately three stages:

• Initially, massive plastic deformation occurs,

• The growth of the crater ceased mainly due to greater contact area of the crater and the ball. Areas in the vicinity of the crater walls exhibit loss of plasticity,

• Crack initiation and chipping of work-hardened regions occur. This mechanism leads to further growth of the crater.

There have been a number of studies on the wear behavior of thin coatings subjected to repetitive impact in which a flat, coated sample is periodically hammered by a ball normal to the sample surface [71-73] (see Fig. 1-8). In these tests, the balls are typically ~6 mm in diameter and consist of hard materials (e.g. WC), the impact loads are high (≥200 N) and the contact surfaces are dry. Using such test conditions, Bantel and Matthews [72] and Lugscheider et al. [74] differentiated the impact-wear behavior of various coatings deposited on identical substrates. Knotek et al. [73] revealed differences

in the impact-induced wear of varying coating/substrate systems. In addition, Knotel et al. [73] and Bouzakis et al. [75, 76] showed that the impact-induced degradation of the coating is a fatigue behavior yielding 'S-N' curve when load is plotted against the number of impacts to failure. Failure of the coating is evidenced by occurrence of annular fractures and the chemical manifestation of substrate exposure in the worn area.
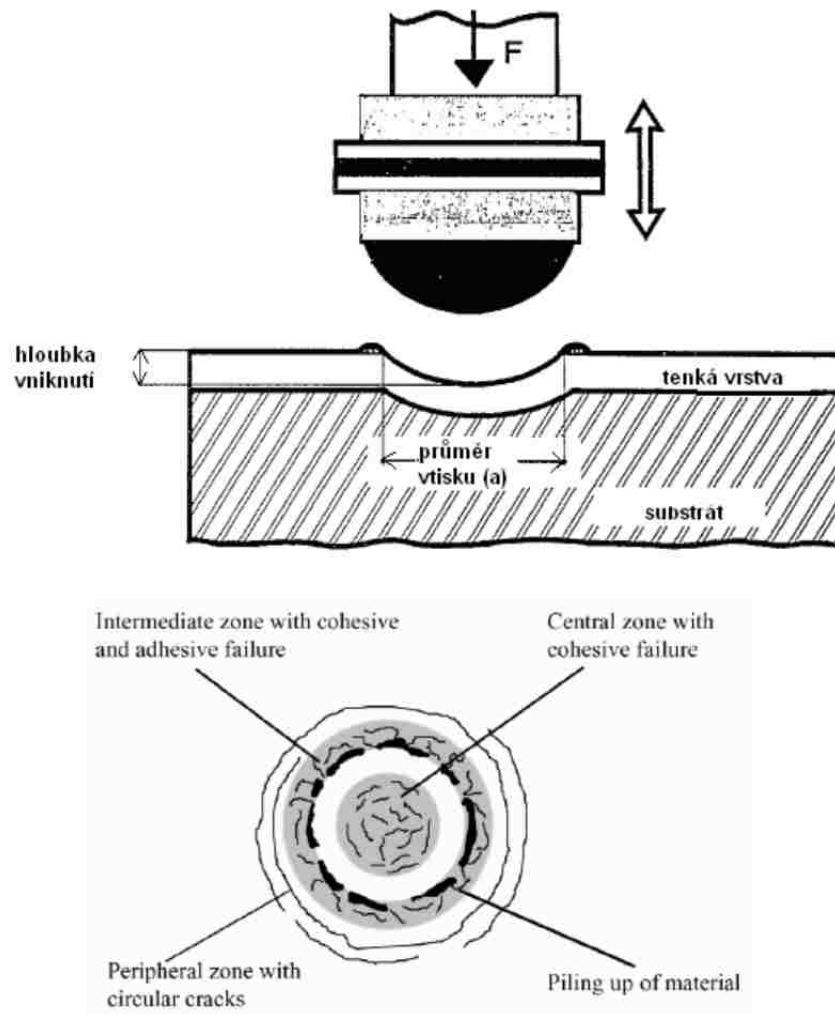
Figure 1- 8 Ball-on-plate repetitive impact testing

Furthermore, with such an impact tester, it is possible to determine combinations of bulk materials, interlayers and coatings which are best suited for applications, such as for impact forming or repetitive impact wear of machine parts in stamping, die casting.

However, those repetitive impact tests used in the above studies involve only normal loading, while the in-service artificial hip and knee joints experience a combination of normal and tangential loadings, as well as rolling and pure sliding in some circumstances.

Ball-on-plate repetitive impact testing was used to evaluate the resistance of coatings to dynamic loading and also to assess the effect of triode-plasma diffusion pretreatments on coating adhesion and substrate load-support.

II Inclined cyclic impact-sliding wear test

However, in many applications, mechanical components are often subjected to combined attacks of impact and sliding leading then to surface damage. In this case, there is still a need for a testing method that can study wear caused by repetitive impact-sliding motions at high contact stress conditions. Only a few studies have been done using different technologies. A. Ramalho et al. used a dual cylinder-on-plane instrument (see Fig. 1-9) to simulate the valve-seat contact of internal combustion engines [77]. K.-D. Bouzakis et al. [75, 76] used a similar test setup using only one plane impacted. The inclined impact tests, supported by a finite elements method (FEM) simulation, used to characterize the fatigue performance of coatings. Stress field during the impact test in coatings with various adhesion strength properties, versus the inclination angle, was built. Bouzakis concluded that a more intense stress field was occurred during inclined impact test, compared to that on perpendicular impact test. To the low adhesive coatings, the coating removal propagation became much faster at high inclination angles.
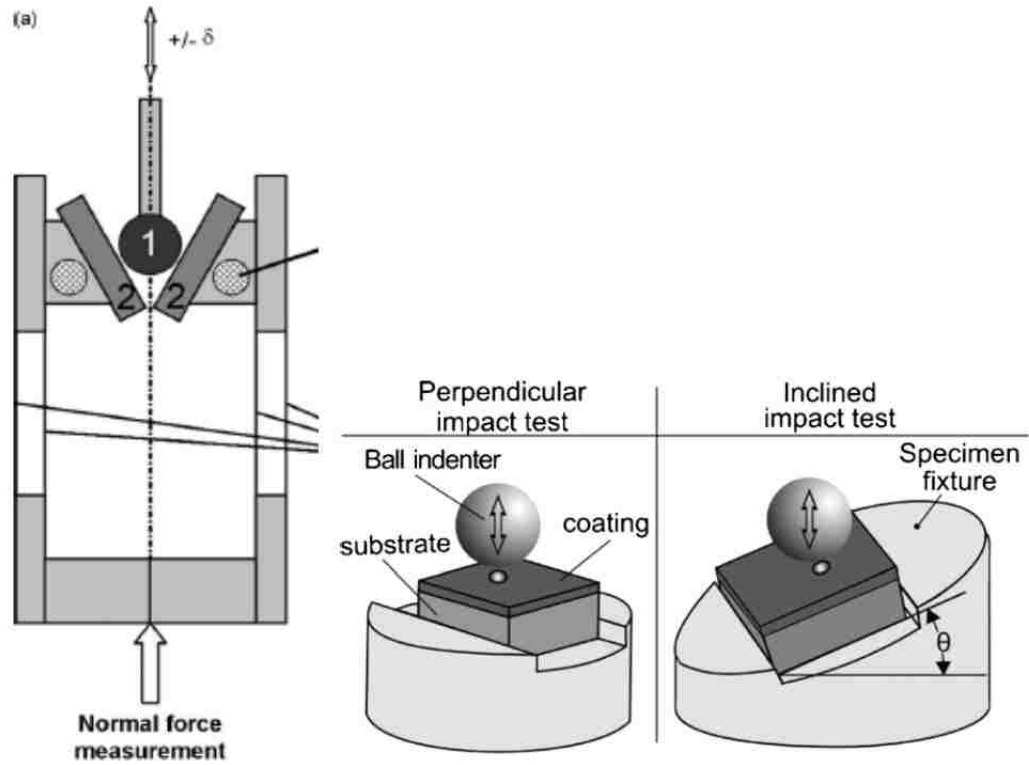
Figure 1- 9 (a) A dual cylinder-on-plane instrument by Ramalho [77] and (b) An inclined impact test by Bouzakis [76].

This cyclic inclined impact-sliding wear test, was developed, which constitutes a new reference to the prediction of the coatings' impact failures under inclined impact forces. However, in these studies the inclined angle, θ, was kept constant during the impact tests.

In our laboratory, we have developed a new test method—the inclined impact-sliding test was introduced and found to be effective as a model test to simulate wear and fatigue in either bulk materials or coatings subjected to a high local dynamic impact and sliding contact stress on the surface. During the test, repetitive impact and sliding interactions were applied on an inclined coated surface by a 10-mm-diameter steel ball, which caused normal and tangential forces simultaneously. With the up-and-down

vertical movements of the steel ball, the sample was first impacted and then pushed downward after full contact due to the sample holder rotating around the fixed roller bearing before returning back to the original location, where the loading re-zeroed at the end of each cycle. The inclined impact-sliding wear test caused an impact crater, which was named as "head part," and a relatively long sliding track, which was named "tail part." Different fatigue behaviors and types of cracks were observed in the head and tail parts of the impact-sliding track. Fig 1-10. shows an illustration of the inclined impact-sliding wear test machine with a typical shape of a tested track. The inclination angle, θ, equals 20° in the static situation and changes in a range of 10°–20° during the test. Due to the existence of the inclination angle, the loading forces consist of a normal component, F_n, and a tangential one, F_t, whose values depend on the instantaneous value of inclination angel θ in each cycle (Fig 1-10 (b)). The contact dynamic load varies during the contact period in each test cycle. The value of the impact force, F_i, can be adjusted by changing the gap distance between the steel ball and the sample surface and the pressure of the compressed air on the piston in the air cylinder. The pressing force, F_p, is determined by the air pressure for the given diameter of the piston and the value of which keeps increasing with the downward pressing of the counterface ball till the ball stops and withdraw from the test surface at the end of sliding track (the end of tail), where the maximum $F_{p_{max}}$ is approached. When tested in our lab, the value of F_i can vary from 80 N to 600 N and F_p can be adjusted in a range of 200 N to 800 N, depending on the required test conditions. The real-time measurement of F_i and F_p is collected by a pressure transducer and shown as a load (N) vs time (s) by a Kyowa PCD-300A for the data acquisition setup using a 10,000 Hz sample frequency to ensure a high accurate

loading curve.
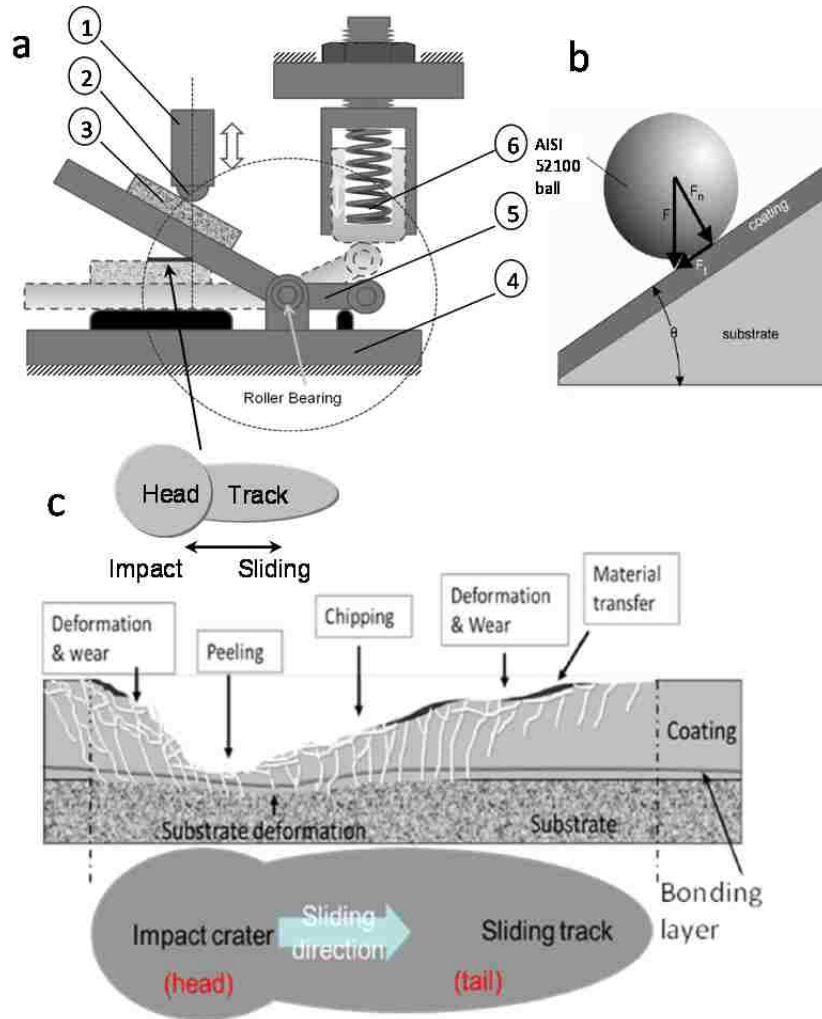
Figure 1- 10 (a) Schematic illustration of cyclic inclined impact-sliding wear tester, (b) normal and tangential forces applied by impact ball to the inclined coating surface, and (c) schematic illustration of the tested track from cross-sectional way.

Fig 1-11. shows one of the loading curves, using F_i=200 N, Fp_{max}=400 N, testing frequency=2.5 Hz. From the curve, F_i is an instant force which shows a tiny peak with following few vibrations while F_p is a long-term force which keep increasing till the end of sliding motion.
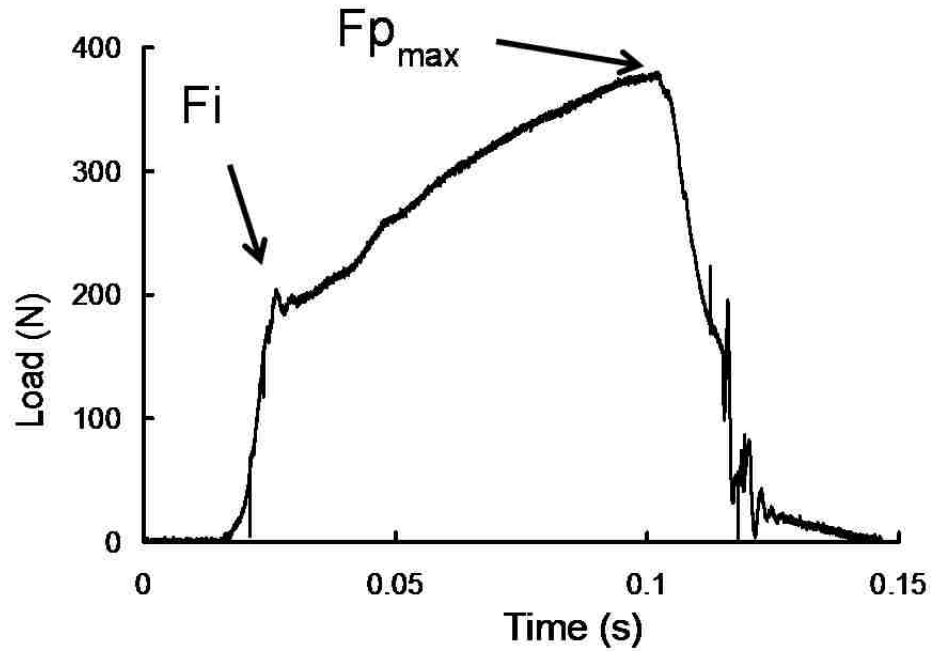
Figure 1- 11 Dynamic loading variations during one test cycle with Fi=200N and

Fpmax=400N.

To make this inclined impact-sliding wear test standard and the results to be comparable and repeatable, a precise evaluation of the test result is required. In this case, we developed a classification of coating failure based on the percentage of substrate exposure. Fig. 1-12 shows the 6 degree of test results with degree 5 to be lightest and degree 0 to be worst, in this case, the coating is fully failed.
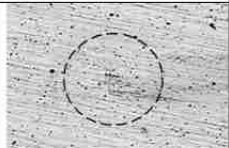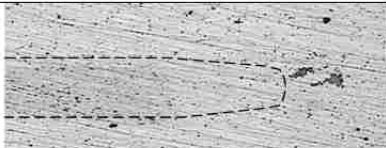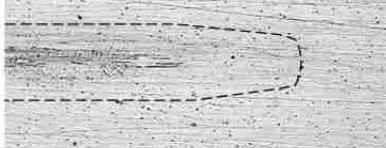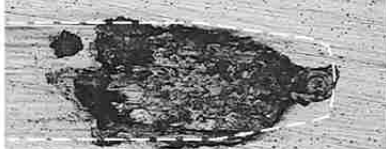
Classification (C)	Impact (I)	Sliding (S)	Overall (O)	
5			I5+S5	5
4			I4+S5	4.5
			I4+S4	4
			I3+S4	3.5
3			I3+S3	3
			I2+S4	3
			I2+S3	2.5
2			I2+S2	2
			I1+S3	2
			I1+S2	1.5
1			I1+S1	1
			I0+S2	1
			I0+S1	0.5
0			I0+S0	0

Figure 1- 12 Classification of failure based on percentage of exposure area of the

substrate.

Based on massive tests, typical wear and fatigue events that lead to failure of the coating, characterized by exposure of the substrate, are:

1. Formation of partial annular cracks at the trailing edge of the impact crater (head),

2. Thinning of the top coating due to sliding wear,

3. Formation of through-thickness shear cracks in the top layer,

4. Delamination of the top layer from the interlayer,

5. Formation of through-thickness cracks in the interlayer

6. Delamination of the interlayer from the substrate.

7. Plastic deformation in the near-surface-area substrate.

The main testing equipment used in this study is the impact-sliding contact fatigue wear tester. A pin-on-disc tribometer was also used for friction and wear tests. Nanoindention (Hysitron) was used for measurement of hardness and elastic modules of the biomaterials studied. A surface profiler, optical microscope and scanning electron microscope were utilized for surface observations and characterizations. The detailed conditions of the usages were described in the subsequent chapters.

6. OBJECTIVES OF THIS RESEARCH

- 1. Better understanding of the failure behaviors of various biomaterial surface under high contact stresses, including:

- A. Different substrates of biomaterials including CoCr, Ti-6Al-4V and 316L stainless steel

- B. Failure behaviors with or without coatings (TiN and DLC);

- C. Effects of interface bonding layers on coating failure behavior

- D. Effect of biological fluids (HBSS) in respect of corrosion or lubrication;

- 2. Use of the accelerated testing methods to investigate performance of the hard biocoatings on the commonly-used metallic biomaterials. In simulating high contact loading conditions when joint transmitting high dynamic loads.

- 3. Providing clues for the selection of coating and substrate pairing system for

various medical applications.

7. THE LAYOUT OF THE DISSERTATION

The layout of the dissertation is described as follows.

Chapter 1 – Introduction and background information about the metallic biomaterial and the potential deformation it concerns during service. Proper surface protection methods are also included and a brief introduce is made of the testing instruments used in this research.

Chapter 2 – A try out test was carried out using cyclic impact-sliding test method on hard TiN coating (H ≈ 34 GPa) on unhardened M2 steel (soft substrate) to study the substrate effects on coatings when the substrate has insufficient mechanical properties.

Chapter 3 - Another type of biomedical coating—PEO coating was made on Ti-6Al-4V substrate and tested under pure sliding and impact-sliding wear conditions. It was found that, for load-bearing biomedical implants, PEO coating is not a promising surface protection due to its low cohesive strength.

Chapter 4 – Mechanism concerning studies was carried out using a W-DLC coated 316L stainless steel. Results show that when soft coating combined with soft substrate, higher resistance against dynamic loadings is formed, because the coating and substrate deform simultaneously.

Chapter 5 – Failure behaviors of a combination of hard coating and hard (or soft) substrate as well as the effects interface layer were investigated by using

different coating, interlayer and substrate materials. The results showed the substrate with high hardness provided better support to the coating and a corrosion-resistant bonding layer and its ability to block extension of cracking under cyclic dynamic loads can have a critical influence on the coating failure behaviors in a corrosive environment.

Chapter 6 – The studies on combined effect of coating and substrate was continued in this chapter. A comprehensive study was carried out on the last commercially used metallic biomaterial—CoCr. Ti6Al4V was studied as well as a comparison.

Chapter 7 – Conclusion the critical parameters during the tests to the failure mechanisms of the coated metallic biomaterials and the summary of the testing results.

Chapter 8 – General conclusions and future works.

REFERENCES

[1]   M. Zhang, C. Ruan, S. Dou, X. Tu, Y. Ma, Y. Wang, Materials Letters, 93 (2013) 282.

[2]   E. Mázl Chánová, F. Rypáček, A volume in Woodhead Publishing Series in Biomaterials 2013, pp. 91.

[3]   J. Czernuszka, Materials World, 4 (1996) 452.

[4]   P. Parida, A. Behera, S.C. Mishra, International Journal of Advances in Applied Sciences (IJAAS) 1(3) (2012) 31.

[5]   H. Hermawan, D. Ramdan, J.R.P. Djuansjahy (2011), Prof. Reza Fazel (Ed.), ISBN: 978-953-307-637-9.

[6]   A. Srivastav, Published: January 8, 2011 under CC BY-NC-SA 3.0 license, DOI: 10.5772/13488.

[7]   R. Narayan (ed.) Biomedical Materials, DOI 10.1007/948-0-387-84872-3_2. pp. 41.

[8]   Y. Okazaki, E. Gotoh, Materials Transactions, 43(12) (2002) 2949.

[9]   J. Breme, V. Biehl, Handbook of Biomaterial Properties, published by Chapman & Hall, London, UK, pp.135.

[10]   J. Ejiofor, T.J. Webster, Dekker Encyclopedia of Nanoscience and Nanotechnology, Second Edition DOI: 10.1081/E-ENN2-120009390, pp.327.

[11]   Sachiko Hiromoto, Corrosion of Metallic Biomaterials in Cell Culture Environments Handbook of Materials for Medical Devices, Chapter 1

[12]   http://www.mananatomy.com/basic-anatomy/types-joints (March 25th, 2014)

[13]   http://en.wikipedia.org/wiki/Synovial_fluid#Composition (March 25th, 2014)

[14]   R.W. Carwford, D.W. Murrary, Annals of Rheumatic Diseases, 56 (1997) 455 doi:10.1136/ard.56.8.455

[15]   M.G. Joshi, S.G. Advani, F. Miller, M.H. Santare, Journal of Biomechanics, 33 (2000) 1655.

[16]   I. Oh, W. Harris,.Journal of Bone and Joint Surgery 60A (1978) 75.

[17]   A. Butscher , M. Bohner, S. Hofmann, L. Gauckler, R. Müller, Acta Biomaterialia 7 (2011) 907.

[18] K. Mediaswanti, C. Wen, E.P. Ivanova, C.C. Berndt, F. Malherbe, V.T. Hong Pham, J. Wang,   J Biomim Biomater Tissue Eng 18: 104. doi: 10.4172/1662-100X.1000104

[19] D.C. Hansen, The Electrochemical Society Interface, 2008 pp.31-34

[20] R. Huiskes, Acta Orthop. Belgica, 59 (1993)118-129.

[21] T.W. Bauer, J. Schils, Skeletal Radiology. 28 (1999)423-432and 483-497.

[22] R. Huiskes, H. Weinans, B. Rietbergen, Stress Shielding and Bone Resorption, 274 (1992) 124-134.

[23] M. Geetha, A.K. Singh, R. Asokamani, A.K. Gogia, Progress in Materials Science 54 (2009) 397–425.

[24] M. Pourbaix, Atlas of electrochemical equilibria in aqueous solution, Houston, Texas: National Association of Chemical Engineers; 1974.

[25] http://www.aqb.jp/english/file/TheBasicsPart3-7.pdf (March 20th.2014)

[26] C.N. Elias, J.H.C. Lima, R. Valiev, and M.A. Meyers, Biological Materials Science, (2008) pp 46-49.

[27] B.P. Bannon, E.E. Mild, Titanium Alloys in Surgical Implants, ASTM STP 796. H.A. Luckey, F. Kubli, Jr., Eds., American Society for Testing and Materials, 1983, pp 7.

[28] L. De Nardo, L. Altomare, B. Del Curto, A. Cigada, L. Draghi, Surface Engineering of Light Alloys, (2010) 568.

[29] K.G. Budinski, Wear, 151 (1991) 203;

[30] J. Qua, P.J. Blau, T.R. Watkins, O.B. Cavin, N.S. Kulkarni, Wear 258 (2005) 1348;

[31] N. Adya, M. Alam, T. Ravindranath, A. Mubeen, B. Saluja, The Journal of Indian Prosthodontic Society, 5 (2005) 126.

[32] F. E. Heakal, K.A. Awad, Int. J. Electrochem. Sci., 6 (2011) 6483.

[33] D. J. Blackwood, L. M. Peter, Electrochemical Acta., 33(8) (1988) 1143.

[34] K.E. Healy, P. Ducheyne, J. Biomed Mater. Res. 26(3) (1992) 319.

[35] J.A. Disegi, R.L. Kennedy, R. Pilliar (eds.), West Conshohocken, US.ASTM STP 1365.

[36] M.J. Runa, L.A. Rocha, M.T. Mathew, 1st Portuguese Meeting in Bioengineering, 2011 Instituto Superior Técnico, Technical University of Lisbon.

[37] S. Kurz, A.W.E Hodgson, S. Virtanen, V. Fervel, S. Mischler, European Cells and Materials 3. (2002) 26.

[38] G. Bellefontaine, The corrosion of CoCrMo alloys for biomedical applications, Ms.c thesis. Univ. of Birmingham, 2010.

[39] L. Reclaru, R. Lerf, P.-Y. Eschler, J.-M. Meyer, European Cells and Materials 1. Suppl. 1 (2001) 29.

[40] http://www.fda.gov/downloads/AdvisoryCommittees/CommitteesMeetingMaterials /MedicalDevices/MedicalDevicesAdvisoryCommittee/OrthopaedicandRehabilitatio nDevicesPanel/UCM310281.pdf (March 15th, 2014)

[41] O. Ä OztÄurk, U. TÄurkan and A.E. Ero·gu: Surface & Coatings Technology, 200 (2006) 5687.

[42] J.R. Goldberg, J.L. Glibert, Biomaterials, 25 (2004) 851.

[43] U. Tiirkan, O. Oztilrk, A.E. Eroglu, Surf. Coat. Technol., 200(2006) 5020.

[44] S. Arango, A. P. Vargas, C. Garcia, Coatings, 3 (2013) 1-15. Doi: 10.3390/coatings300001.

[45] J.C. Avelar-Batista, E. Spain, G.G. Fuentes, A. Sola, R. Rodriguez, J. Housden, Surf. Coat. Technol.201 (2006) 4335.

[46] G. Cassar, S. Banfield, J.C.A. Wilson, J. Housden, A. Matthews, A. Leyland, Surf. Coat. Technol.206 (2012) 2645.

[47] L. Wang, D.O. Northwood, X. Nie, J. Housden, E. Spain, A. Leyland, A. Matthews, Journal of Power Sources 195 (2010) 3814.

[48] I. Apachitei, A. Leoni, A.C. Riemslag, L.E. Fratila-Apachitei, J. Duszczyk, Applied Surface Science 257 (2011) 6941.

[49] www.tecvac.com (March 30th, 2014)

[50] J. Grabarczyk, I. Kotela, 37 (2009) 277.

[51] G. Dearnaley, J.H. Arps, Surf. Coat. Technol., 200 (2005) 2518.

[52] A. Paschoal, E.Vanâncio, L. Canale, O.Silva, D. Huerta-Vilca, A. Motheo, Artificial Organs, 06/2003; 27(5) (2003) 461.

[53] U. Turkan, O. Ozturk, A.E. Eroglu, Surf. Coat. Technol., 200 (2006) 5020 – 5027.

[54] Y.L. Jeyachandran, Sa.K. Narayandass, Trends Biomater. Artif. Organs, 24(1) (2010) 90.

[55] A. Yerokhin, X. Nie, A. Leyland and A. Matthews, Surf. & Coat. Technol., 122 (1999) 73.

[56] X. Nie, A. Leyland, A. Matthews, Surf. coat. Technol. 133 (2000) 331.

[57] A. Yerokhin, X. Nie, A. Leyland and A. Matthews, Surf. & Coat Technol., 130 (2000) 195.

[58] X. Nie, A. Leyland and A. Matthews, Surf. & Coat. Technol., 125 (2000) 407.

[59] S.H. Teoh, International Journal of Fatigue 22 (2000) 825.

[60] St John KR, editor. ASTM STP 1144: Particulate debris from medical implants: mechanisms of formation and biological consequences. Philadelphia: American Society of Testing and Materials, 1992.

[61] Handbook of biomaterials evaluation: scientific technical and clinical testing of implant materials, editor, Andreas F.von Recum 2nd ed. ISBN 1-56032-479-1

[62] "Milligan High Cycle Fatigue of Structural Materials" edited by W.O. Soboyejo and T.S. Srivatsan, TMS, Warrendale PA, 1997, pp. 305.

[63] R.O. Ritchie, R.H. Dauskardt, J. Ceram. Soc. Japan 99 (1991) 1047.

[64] R.O. Ritchie, J. Heart Valve Dis., 5S (suppl. I) (1996) 9.

[65] C.H. Lloyd, L. Mitchell, J. Oral Rehabilitation 11 (1984) 257.

[66] J.B. Medley, J.J. Krygier, J.D. Bobyn, F.W. Chan, A. Lippincott, M. Tanzer. Proc. Inst. Mech. Eng., Part H: J. Eng. Med., 211 (1997) 89.

[67] H. Reul, M. Eichler, K. Potthast, C. Schmitz, G. Rau, J Heart Valve Dis; 5(Suppl.I) (1996) S97.

[68] O. Knotek, B. Bosserhoff, A. Schrey, T. Leyendecker, O. Lemmer, S. Esser, Surf. Coat. Technol., 54-55 (1992) 102.

[69] R. Bantle, A. Matthews, Surf. Coat. Technol., 74-75 (1995), 857.

[70] G. Berg, C. Friedrich, E. Broszeit, C. Berger, Fresenius J Anal Chem 358 (1997) 281.

[71] F. Ledrappier, Y. Gachon, Tribotest Journal 11-4 (2005) 333.

[72] R. Bantle, A. Matthews, Surf. Coat. Technol., 74-75 (1995) 857.

[73] O. Knotek, B. Bosserhoff, A. Schrey, T. Leyendecker, O. Lemmer, S. Esser, Surf. Coat. Technol., 54-55 (1992) 102.

[74]   E. Lugscheider, O. Knotek, C. Wolff, S. Bärwulf, Surf. Coat. Technol., 116–119 (1999) 141.

[75]   K.-D. Bouzakis, A. Asimakopoulos, G. Skordaris, E. Pavlidou, G. Erkens, Wear 262 (2007) 1471.

[76]   K.-D. Bouzakis, A. Asimakopoulos, N. Michailidis, S. Kompogiannis, G. Maliaris, G. Giannopoulos, E. Pavlidou, G. Erkens, Thin Solid Films 469–470 (2004) 254.

[77]   A. Ramalho, Ph. Kapsa, G. Bouvard, J.-C. Abry, T. Yoshida, M. Charpentier, M. Bourgeois, Wear 267 (2009) 777.

CHAPTER 2 STUDY ON FATIGUE AND WEAR BEHAVIORS OF A TIN

COATING USING AN INCLINED IMPACT-SLIDING TEST

1. INTRODUCTION

The Titanium nitride (TiN) was widely used as the coating material for cutting tools punching or forming and injection molding due to its outstanding mechanical properties. TiN can extends the service time of tools working at high speeds by modifying surface properties such as decreasing the coefficient of friction, increase hardness and improving wear resistance [1-3]. M2 high-speed steel is widely used for production of cutting tool due to its high thermostability in the presence of high hardness, fatigue strength and is suitable when abrasive/adhesive wear resistance is required [4, 5]. It is necessary for the tool steel, as in stamping dies, or whether the tool has to withstand impact loading, to maintain a keen cutting edge. In this case, some methods in order to enhance its surface hardness and wear resistance are used such as nitriding and PVD/CVD coating, in which, TiN is the most common PVD hard coating in use today for its ideal combination of hardness, toughness, adhesion and inertness.

The exact determination of the mechanical properties and fatigue strength of metal coatings subjected to varying dynamic loads is an important aspect of many engineering problems. There are many well-established testing methods have been utilized to simulating the coating failures on various substrates for different applications, such as pin-on-disc wear test and scratch test. Due to the lack of methods to evaluate the durability of coatings, repeated impact testing was developed and found to be an effective method in 1990 [6]. The impact tests was utilized as a convenient method for characterization of coatings, especially hard coatings such as physical vapour deposition

(PVD) and plasma-assisted chemical vapour deposition (PACVD) or plasma electrolytic oxidation (PEO) coatings [7-12]. Adhesive and cohesive failure modes of those coatings as well as the creep behavior of Plasma and HVOF coatings can be elucidated through this test. However, in many applications, mechanical components are often subjected to combined attacks of impact and sliding leading then to surface damage. In this case, there is still a need for a testing method that can study wear caused by repetitive impact-sliding motions at high contact stress conditions. In this paper, a new inclined impact-sliding wear testing method was introduced first, and then it was used to reveal the fatigue behavior of TiN coated unhardened M2 steel. This substrate is relatively soft and is not strong enough to support the thin hard coating under high repeated loading conditions. However, it provides an ideal case for us to observe the deformation effect of an unhardened substrate on the bending and cracking of coating, the formation of cracks on the coating and the evolution of fatigue failures under the repetitive impact-sliding forces.

2. EXPERIMENTAL DETAILS

2.1 TiN coating characterizations.

In this paper, a TiN coated M2 steel disc (25.4 mm in diameter) was used as the impacted sample coupon. The coating has a hardness of 26.2 GPa, which is more than 8 times higher than that of the uncoated M2 steel (3.1 GPa). The thickness of the TiN coating is about 1.8 μm, which was measured according to its cross-sectional SEM micrographs and the surface roughness Ra is around 0.03 μm.

2.2 Impact-sliding wear test machine

The schematic of repeated inclined impact-sliding test fixture in our laboratory is shown in Fig. 2-1 with a typical impact-sliding scar. To start an impact-sliding test, the flat specimen is secured on the sample holder. The sample holder functions as a rocker which can rotate around a fixed roller bearing due to the pressing of the indenter ball when the piston moves up and down. The ball first impacts and then pushes downward against the flat coating specimen, causing sliding between the ball and the flat specimen in the first half of each test cycle. The ball slides reversely on the surface of the flat specimen and is then disengaged from the surface in the second half of the test cycle. The sample holder has an angle of 20º to the horizontal direction in the static state. A hard copper spring, which acts as a drive device, is fixed on the other end of rocker arm. During the impact test it can rotates the rocker back to its initial position when the indenter moves upward (Fig.2-1). A 10 *mm*-diameter bearing steel ball was used as the impact indenter that can moves in reciprocate mode in the vertical direction driven by a piston in the air cylinder.
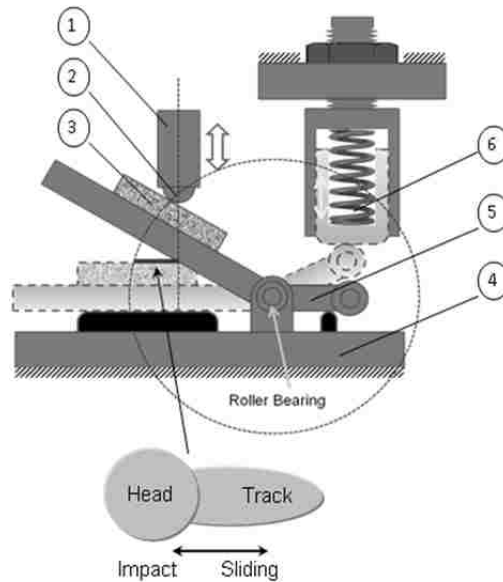
Figure 2- 1 Schematic of Impact-Sliding Wear Test Fixture. 1 - Ball indenter

drive (e.g., air cylinder), 2 - ball indenter, 3 - flat specimen (i.e., coating), 4 - rigid

frame, 5 - rotatable rocker, 6 - return drive (e.g., spring).

The test allows the simulation of the combination of impact fatigue failure and

sliding wear failure under repetitive high local loads, as encountered by machine parts

subjected to impact or tools used in interrupted cutting or cold forming. The impact force

and frequency are variable to adjust the test conditions for different applications, by

varying the dynamic force and the impact speed of the ball. Each cycle of impact can be

monitored during the test. A piezo-force transdeucer was used to record the impact force

from the indenter and the signal was received by a PCD30A signal collector

(oscillographv) with a high sampling frequency--10000Hz. There was a 2 *mm*

accelerating displacement before and after the ball indenter contact the impacted surface

in each cycle. The impact frequency is 5*Hz* in this study, which means the whole impact

period, with the up and down motion, is 200 *ms*. The ball was changed and the coating

surface cleaned with acetone before starting each tests with a fresh area in dry wear condition.

The distributions and evolution of fatigue failures in different areas of the impact-affected zone were observed by means of scanning microscopy (SEM). The energy-dispersive X-ray spectroscopy (EDX) was used to analysis the chemical composition on the scratch scars.

2.3 The experiment parameters

Fig. 2-2 shows the load curve during one impact cycle. Based on some previous tests, 96 MPa air pressure in our system provides a *Fi/Fp=520 N/400 N*. The load curve depicts that there is three stages in each impact cycle, i.e. impact loading stage, vibrating stage and static loading stage. When the indenter contact the impacted sample surface for the first time, the first peak of the load arise, which is the effective impact load—*Fi*. After the indenter ball completed the first full contact with the coating surface and formed a deep impact crater, a few times of rebounding and impacting occurred. From Fig. 2-2, we can find that a series of vibrating signal in the impact load vs. time curve, in which, each rebound process is actually an impact process with decreasing impact energy between two contact surfaces. Since there was no compression that was pre-set on the spring of the spring-driven device, more than one impact crater (head part) formed during the vibrating stage for the lack of rigidity. It should be noted that the vibration and rebound can reduced or eliminated by applying a pre-compression to the spring. After the vibration, the load continues to rise gradually until the pre-setup pressing load (*Fp*), and then the ball started to move up. This is named as the pressing load stage, in which a long tail with sliding failures was formed.

52

In order to study the evolution of the coating failures, 520N impact and 400N pressing forces were applied at a frequency of 5Hz with three different impact cycles (i.e., 250, 500 and 750 cycles). The impact-sliding force curve was recorded, and the force curve of one cycle is shown in Fig. 2-2.
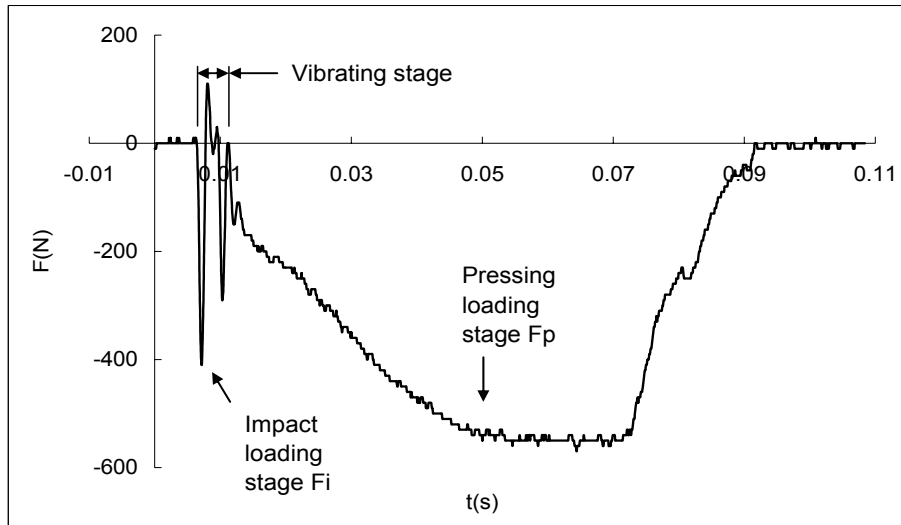
Figure 2- 2 The force curve in one impact cycle under Fi/Fp=520 N/400 N.

3. RESULTS AND ANALYSIS

3.1 Crack observation

Fig. 2-3 shows the distribution of fatigue cracks on the coating surface after 250 cycles' impacts. According to the load curve in Fig. 2-2, there are two peaks of signal monitored in the vibrating stage, which means there are two distinct impacts before the sliding wear takes place. This is due to the lack of the pre-compression of the spring-driven device (Fig. 2-1) which allows the sample holding arm bounded away by some degree. In this case, after the first full contact between two surfaces was completed, the specimen was accelerated downward and lost part of contact with the indenter ball. However, with the continuous downward motion of the indenter, a second impact crater

was formed, with a smaller diameter in size comparing to the first one for the decrease of impact energy.
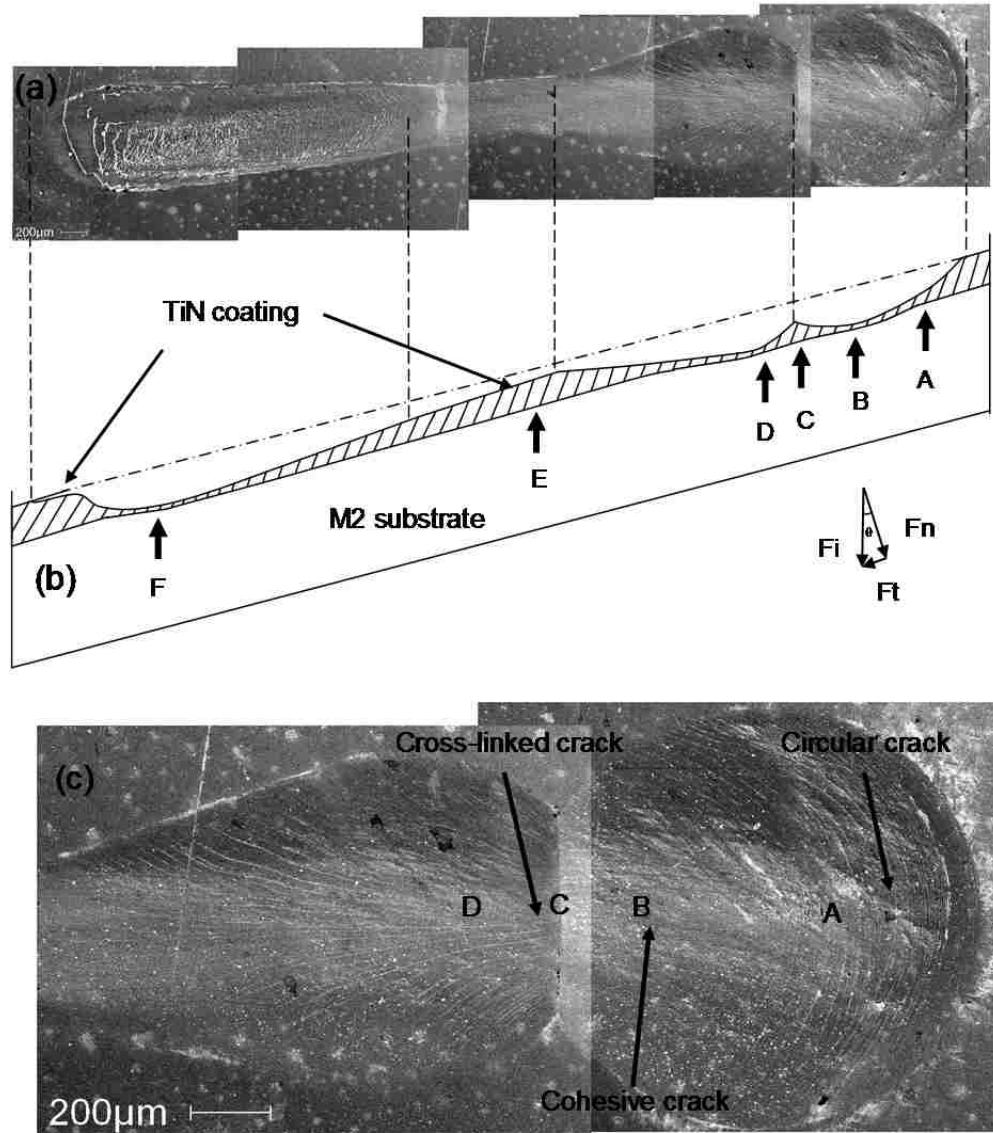
Figure 2- 3 SEM micrographs on impact scar of 250 cycles coating and its schematic view from the cross-sectional direction.
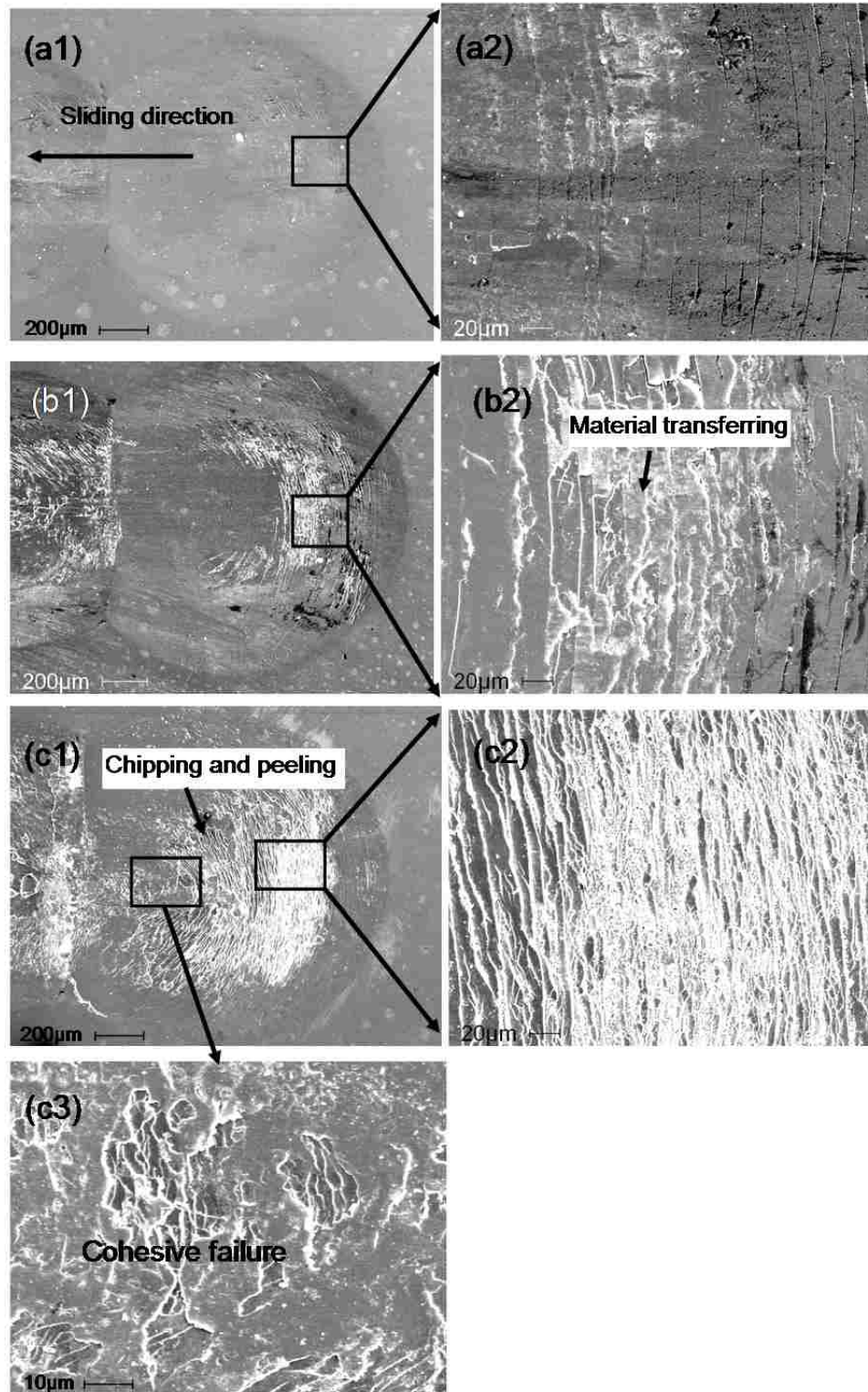
Figure 2- 4 The radial cracks on head part of each impact scars. (a) 250 cycle sample, (b)

500 cycle sample and (c) 750 cycle sample.

The cross-sectional schematic of the impact scar is also illustrated in Fig. 2-3. Due to the inclined angle of the specimen, the area where exerted by the highest impact force was not in the center point of the first impact crater but shift slightly to the upside from the center area (at Point A in Fig. 2-3). This has been discussed in detail by Bouzakis et al. in [11]. The impacting force, during the inclined impact test, is analyzed into the normal component Fn and the tangential one Ft, with their absolute values depending on the inclination angle θ (see the inset in Fig. 2-3). The normal component of impact force Fn caused bending stress in the coating in the rim of head part where a series of radical cracks were observed (Point A in Fig. 2-3 and Fig. 2-4). In the area slightly behind center of first impact crater (Point B), cohesive failures with a network of cracks could be observed due to the elastic deformation of the indenter ball and the combined results of static friction force and the normal impact force Fn. Between the two impact craters, there is a ridge boundary (Point C in Fig. 2-3) with less failures comparing to the adjacent areas B and D because it has less bending deformation due to the 'jump' of the indenter ball. From Fig. 2-5, it is can be observed that there are two types of cracks, which intersected with each other, occurred in the area D. The hyprebola-shaped crack distributed symmetrically in both sides of the axis. It was supposed to be formed by the two-direction bending deformations in the area of overlapped impact craters. The other type occurred in the second impact crater was also radical cracks, which was divided into several sections by the hyprebola-shaped cracks.

After the vibrating stage, sliding wear occurs under the tangential force Ft and formed a long sliding tail part. In the beginning of sliding wear, Fn was small for the inclined angle θ and the loss of impact energy in the vibrating stage. The deformation in

56

the initial part of the tail is not distinct (Point E in Fig. 2-3). However, with the downward motion of the indenter ball the increasing normal component Fn kept increasing following the loading curve in the pressing load stage until reached its maximum value (Point F in Fig. 2-3) which equaled to the maximum pressing force Fp (Fig. 2-2). In this case, the deformation was much distinct in the later part of the sliding scar. This increasing loading linear sliding wear is very similar to the scratch tests [12]. Scratch testing is a local forming operation of the coating-substrate compound, leading to compressive stresses in front of the indenter and tensile stresses behind the indenter. Shearing strain caused by friction between the indenter and coating appears in the contact area. At the rim of the less affected area to the deformed region bending stress appears. Due to the mechanism introduced above, a series of paralleled cracks were observed on the edges of the tail caused by the combination of tensile stress behind the indenter and the bending stress. Material transfer could be detected mainly in the center of the tail part after several hundred cycles of sliding impact.

3.2 The evolution of fatigue failures in the impact tests

For a given impact force, the durability of a coating is characterized by the number of impacts to failure, this being when the substrate material appears. After 250/500/750 cycle impact tests, the fatigue cracks were studied based on SEM observation.
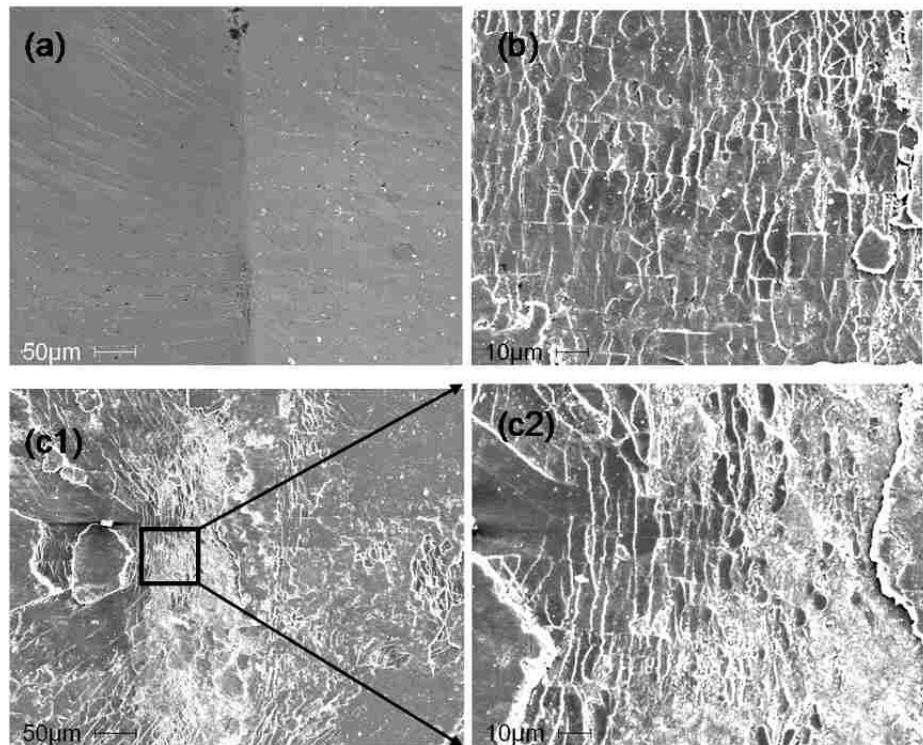
Figure 2- 5 Cohesive cracks at the center of the contact zone. (a) 250 cycle

sample, (b) 500 cycle sample and (c) 750 cycle sample.

Fig. 2-5 shows the impact crater (head part) of the scars under different impact cycles. A series of radical cracks were formed in 250 cycle coating surface (Fig.2-4a). With the increasing of the impact cycles to 500, material transferring was observed firstly on the areas of fatigue cracks due to the increased roughness (Fig. 2-4b). After 750 cycle impact, a great amount of micro-cracks were observed there. Chipping and peeling of the coating material firstly occurred in the center of contact area (Fig. 2-4 c3) and then expanded to the rim areas. At an early stage of the test, cohesive cracks appear around the contact area (Point B in Fig. 2-3). When the test was continued, the size of the impact crater became bigger, causing large degree of coating chipping. EDX analysis indicates

that inside those chipping area, the substrate material was exposed which means some of the fatigue cracks has penetrated the coating area and reached the substrate.

Fig.2-5 shows the network of cross-linked/intersectional cracks formed in the area D in Fig. 2-3. SEM micrographs show that this type of fatigue failures caused very severe deformation in the impact test even though the impact load was not very high. The bending deformation along with both the axial and normal-to-axial directions resulted in two-directional cracking. This type of cracks can form a network after certain cycles of impact which made the thin hard coating easily to chip and peel-off, especially in the very center of the contact zone, where the density of the cracks was greatest (Fig. 2-5c).

In the tail parts, another type of fatigue cracks (peripheral crack) was observed due to the bending deformation and tensile force during the sliding (similar to the scratch test) which are shown in Fig. 2-6.
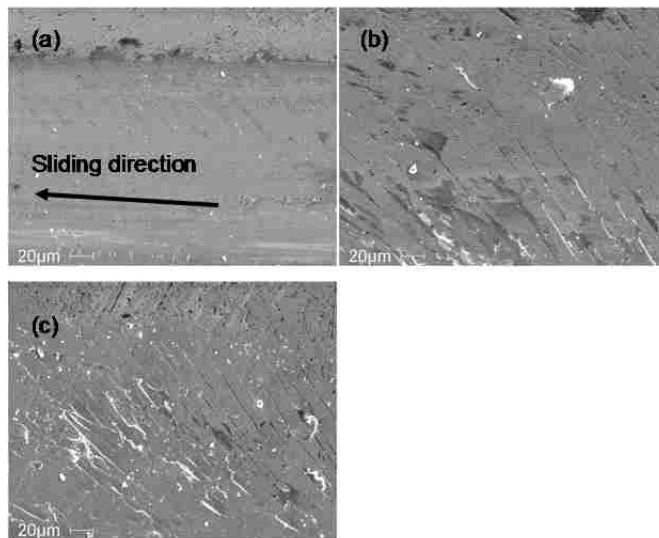
Figure 2- 6 Peripheral crack which parallel to each other distributed on both edges of the tail part. (a) 250 cycle sample, (b) 500 cycle sample and (c) 750 cycle sample.

59

From Fig. 2-6, it is clearly to find that this type of cracks were firstly formed on the edges of the tail where the tensile stress and bending forces made the decisive effect during the sliding movement. After several hundreds' sliding cycles, the length of these cracks increased and expanded to the center of the tail. At the same time, more and more cracks formed between the initial cracks due to the increasing deformation inside the coating. Peeling, chipping and material transferring could also be observed in some parts of this area after 750 cycle impacting.

4. CONCLUSIONS AND DISCUSSION

This paper firstly introduced a new coating evaluation method—inclined impact-sliding test, which can simulate the combined deformations of impact and sliding under high repetitive loading force conditions. This method was used to reveal the fatigue behavior of TiN coated unhardened M2 steel. This substrate-coating combination provided us a clear look at the deformation effect of a relative soft substrate on the bending and cracking of coating and the formation and evolution of the fatigue cracks under the repetitive impact-sliding loading. The results and observations can be concluded as follow:

1. There were four types of fatigue cracks were observed inside the impact-sliding scars, which were: radical cracks, cohesive cracks, intersectional cracks and peripheral crack.

2. Due to the inclined angle of the specimen during the impact-sliding test. The area with the highest impact force was no longer in the center of impact crater but shifted slightly upward from the center, where chipping, peeling of the coating easily happens.

3. Fatigue cracking observation:

a. The radial cracks occurred in the impact craters, the density of which increased greatly with the increase of impact cycles and expanded both inward—around the area exerted by the greatest impact force (Point A in Fig. 2-3), and outward—increased the size of impact crater.

 b. The cross-linked cracks were formed due to the bending deformations from axial and normal-to-axial directions. Coating failure always takes place in the center area of this type of crack, where the highest crack density was observed after a critical number of impact cycle.

c. The peripheral crack formed along the edges of tail part was very similar to the ones in the scratch testing. Its length and density increased with the increase of impact cycle.

4. According to this test, we can make a conclusion that a relative soft substrate allowed quick formation of fatigue cracking and failure under high load condition. So, it is necessary of the industry to increase the hardness of the substrate for the tools working in the environment like stamping. Use a hard substrate or hard interface layer with certain thickness can greatly reduce the cracking formation.

REFERENCES

[1]   P. Hedenqvist, M. Olsson, P. Wallen, A. Kassman, S. Hogmark and S. Jacobson. Surf. Coat. Technol., 41(1990)243.

[2]   J .Ghani, I.A. Choudhury, and H.H. Masjuki, Journal of Materials Processing Technology, 153(2004)1067.

[3]   J. Gu, G. barber, S. Tung and R.J. Gu, Wear, 225(1999)273.

[4]   F. Jährling, D. M. Rück and H. Fuess. Surf. Coat. Technol.111(1999)111.

[5]   Knotek, O., Bosserhoff, B., Schrey, A., Leyendecker, T., Lemmer, O., and Esser, S, Surf. Coat. Technol., 54-55 (1992) 102.

[6]   R. Bantle, A. Matthews, Surface and Coatings Techology 74-75 (1995) 857.

[7]   K.-D. Bouzakis, N. Michailidis, S. Hadjiyiannis, K. Efstathiou, E. Pavlidou, G. Erkens, S. Rambadt, I. Wirth, Surf. Coat. Technol.146–147 (2001) 443.

[8]   S. Hadjiyiannis, K.-D. Bouzakis, A. Asimakopoulos, E. Psimolophitis, P. Philimis, K. Michaelides, N. Charalampous. Coatings in Manufacturing Engineering, 1-3 (2008) 247.

[9]   K.-D. Bouzakis, A. Asimakopoulos, N. Michailidis, S. Kompogiannis, G. Maliaris, G. Giannopoulos, E. Pavlidou, G. Erkens. Thin Solid Films 469–470 (2004) 254.

[10]   E. Ledrappier and Y. Gachon. Tribotest Journal 114(2005) 333.

[11]   K.-D. Bouzakis, A. Siganos, Surf. Coat. Technol. 185 (2004) 150.

[12]   G. Berg, C. Friedrich, E. Broszeit, C. Berger, Fresenius J Anal Chem 358 (1997) 281.

CHAPTER 3 WEAR FAILURE BEHAVIOR OF TITANIUM-BASED OXIDE

COATINGS ON A TITANIUM ALLOY UNDER IMPACT AND SLIDING FORCES

1. INTRODUCTION

Titanium alloys, due to their excellent combination of low density, high strength to weight ratio, corrosion resistance and biocompatibility, are widely used in the aerospace, automotive, chemical and biomedical industries [1]. The typical examples of applications in aerospace are the landing gears of the Boeing 777, Boeing 787 and the Airbus A380 aircrafts in replacement of high-strength low alloy steels, 4340M and 4330M [1-3] and in automotive industry currently racing engine use Ti-6Al-4V for intake valves, valve retainers, connecting rods, clutch discs, transmission pressure plate and suspension coil springs [4]. Titanium and its alloys have excellent corrosion resistance towards many of the highly corrosive environments, particularly, oxidizing and chloride containing process streams [5, 6]. The great corrosion resistance of titanium alloys results from the formation of highly stable, continuous, adherent and protective oxide films on the metal surface. The nature, composition and thickness of the surface oxides are depend on environmental conditions [7, 8]. Corrosion may not be an issue for titanium in an aerospace environment [9, 10]. However, these alloys are insufficient in tribological performances [11], characterized by high coefficients of friction, severe adhesive wear with a high tendency to seizing and low abrasion resistance, when Ti alloys slide against other engineering materials. Budinski [11] realized extensive research on tribological properties of titanium alloys and reported that Ti6Al4V has poor abrasion resistance. Masmoudi et al. [12] studied the influence of environment on friction coefficient values of Ti6Al4V alloy. There are two reasons for the inferior tribological properties [13, 14]:

the first is its low resistance to plastic shearing and the low work hardening; and the second reason is due to the low protection exerted by the surface oxide. The oxide is formed by high flash temperatures caused by friction during sliding. The stationary or dynamic contact loads between Ti-alloy components and other metals can cause damage to the thin oxide film and thus lose the protection.

Accelerated laboratory wear tests using test machinery are popular within the surface engineering research community. Different machinery can be used to understand the tribological behavior of material couples. The commonly used techniques include pin-on-disc, block-on-ring, micro-abrasion and ball-on-plate impact tests [15]. Straffelini et al. [16] studied the mechanisms responsible for the wear resistance under different load and sliding speed conditions in self-mated Ti-6Al-4V disk on disk sliding test. The researchers found that in dry sliding wear the Ti-6Al-4V alloy underwent forms of oxidative wear and plastic shearing [13, 17]. This is certainly a disadvantage when employing titanium alloys in kinematic linkage and dynamic load bearing applications, to the point that significant research and design efforts have been dedicated in recent years to developing coatings and surface engineering process to mitigate war and reduce friction in systems containing these materials. So far several well-developed methods have been utilized to enhance the surface properties of titanium alloys, such as coatings, carburizing and plasma nitriding [18]. Oxidation treatment is the most popular and effective technique to produce a relatively thick coating for the surface protection of Ti alloys [19, 20]. For example, electrolytic anodizing [21] and high temperature heat treatment [22] as well as other techniques such as PVD/CVD coatings are widely used by surface engineers [23] Plasma electrolytic oxidation (PEO) has been successfully used to

prepare oxide coatings on Ti-6Al-4V [24-27]. This technique is based on the interaction between oxide film growing on the metal surface and spark micro-discharges, which are initiated at potentials above the dielectric breakdown voltage of the film in an aqueous electrolyte [24-26]. The use of this hard nano-structured coating is regarded as an effective practice in reducing titanium component wear [28-30]. A number of researches have been done in wear and corrosion aspects [23-26]. However, there is lack of research in wear properties of the coatings under extremely high contact stress and dynamic loading conditions.

This paper mainly focuses on studying the impact and friction wear behaviors of various PEO coatings on a Ti-6Al-4V alloy under severe testing conditions. Different current modes and treatment time were utilized during the PEO process to produce coatings of different thicknesses. An inclined impact-sliding test method was used to simulate extremely high dynamic loading conditions [31, 32]. Those conditions may appear when the coated Ti-6Al-4V alloy, used for such as sliders of aircraft landing gears, accidentally suffer the combined attacks of impact and sliding forces during abnormal landing operation conditions. Although the extreme load conditions rarely exist in normal operations of, for instance, aircrafts, it is worth investigating how the coatings respond to such instances.

2. EXPERIMENTAL DETAILS

2.1 Sample coupon

In this study, a Ti-6Al-4V rectangular bar with a cross-sectional size of 25 mm × 25 mm was cut into pieces along its cross-sectional direction with a thickness of 7 *mm* each and used as substrate materials. All the sample coupons were polished progressively

up to 2500 grade SiC abrasive sandpapers to obtain an average roughness $R_a \approx 1.0$ μm and then degreased in acetone ultrasonically and distilled water before dried in ambient condition (20°C, 65% humidity). The chemical composition of the Ti-6Al-4V alloy is shown in Table 3-1.

Table 3- 1 Chemical composition of Ti-6Al-4V in weight percent.

Element	Al	V	Fe (Maximum)	C	O (Maximum)	N	H (Maximum)	Ti
Average	5.50-6.75	3.50-4.50	0.40	0.1	0.02	0.05	0.015	Balance

2.2 PEO procedure

During the PEO treatment, the sample was connected to the power source unit as the anode by a Ti wire and a stainless steel plate as the counter cathode electrode. 18 g Na_2HPO_4 was dissolved in 3 litres of distilled water to make a 6 g/l electrolyte with a pH value around 12 [24]. 6 g/l Na_2SiO_3 was added into the electrolyte before the treatment of sample 2 (S2) and sample 3 (S3). The parameters during the PEO treatments were summarized in Table 3-2. Sample 1 (S1) was treated by a pulsed unipolar power source while the other two (S2 and S3) were made by a pulsed bipolar power source. All the coatings were made at the same pulse frequency, 2000 Hz.

Table 3- 2 Parameters of PEO procedure and thickness and roughness of coatings

No.	PEO treatment time (min)	Power supply mode	Current density (A/cm^2)	Thickness (μm)	Thickness-after polish (thickness decrease) (μm)	Surface Roughness R_a	Surface Roughness-after polish R_a	Skewness R_{sk}
1	20	Unipolar	0.08 0.06/-	10.8	8.8(-2.0)	1.22	0.96	-0.67338
2	25	Bipolar	0.05	17.8	9.7(-8.1)	2.22	0.8	-1.32368
3	43	Bipolar	0.06/-0.05	26.9	10.6(-13.3)	3.8	0.81	-2.23051

After the PEO process, coated samples were washed carefully by soft soap solution and flushed by tap water to clean the remaining alkaline. The coating thickness was

measured by a PosiTector 6000 coating thickness gauge. 8 data were collected on each coating surface to obtain an average result. The average coating thickness of each sample was listed in the 5th column of Table 3-2.

A Mitutoyo surface profiler SJ201P was used to measure the average roughness R_a and skewness R_{sk} on the surfaces of as-formed and polished PEO coatings. The values of R_a and R_{sk} have been reported to have significant influences on tribological properties [33, 34]. Skewness R_{sk} describes the asymmetry of the height distribution histogram. If $R_{sk} = 0$, height distributions on the surface is symmetric, for example, a Gaussian like. If $R_{sk} < 0$, the surface is featured with holes and if $R_{sk} > 0$ the surface is flat one with peaks. Because all the R_{sk} values in this study were negative, a schematic of surfaces with negative skewness is shown in Fig. 3-1 [33, 34]. In this case, the lower R_{sk} value, the more contacting areas existed between the coating and counterface steel ball.
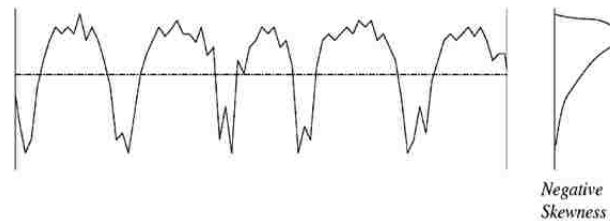
Negative Skewness

Figure 3- 1 Schematic of surface (cross-sectional) with a negative skewness R$_{sk}$

[33, 34].

In order to study the sliding behavior and wear resistant of PEO-deposited TiO$_2$ coatings, a pin-on-disc (POD) test was carried on all of the coated samples. The test was carried out using a steel ball pin as the counterface material (AISI 52100, HRC 58-60, and 5.5 mm in diameter) in the ambient condition (40% humidity and 20 ºC) under a 2 N normal load. The diameter of the circles of wear scars was 4 mm and the sliding speed

was 0.075 *m/s*. A pure sliding was obtained by keeping the sample rotating and the counterface ball fixed. The coefficient of friction (COF) (dynamic) was automatically recorded during each test using a data acquisition system. The POD tests were firstly carried out on 3 freshly-made PEO coatings and uncoated substrate under a 100 m sliding distance. In order to minimize the effect of surface roughness to the coating performance in the tests, the outer surfaces of as-formed coatings were polished carefully to the same level of roughness to remove prominent ceramic particles. And then, the POD tests were used again under the same loading condition on the polished sample surfaces for a 300 m sliding distance. The sliding distances of as-made and polished coatings were based on the several trial tests to obtain typical failure behaviors on coating surfaces without fully worn-out of surface layer. Polished coatings have an even lower coefficient of friction comparing to as-made and uncoated ones, thus they could sustain longer sliding distance. Before the POD tests all the testing pins were degreased in acetone ultrasonically and then ethanol to remove any possible contaminations.

An inclined impact-sliding test method [31, 32], which has been regarded as an effective way to study coating failures under extremely high dynamic loading conditions, was used to investigate wear behavior of the PEO coatings under attacks of impact and sliding forces. The detailed information about the test instrument can be found from the literature [31]. With the up-and-down vertical movement of a pin driven by air cylinder, the pin first impacts the sample and then slides on the sample surface in each cycle. The impact force, F_i, and pressing force, F_p, are implemented subsequently when the pin ball contacts the coating surface through impact and then sliding. During the tests, the repetitive impact and sliding forces were applied on the coating surface by a 10-mm

68

diameter AISI 52100 steel pin ball. In each impact-sliding cycle, the forces comprised a dynamic impact load, F_i (80 and 200 N), and a "pressing" load, F_p (with the maximum values of 200 and 400 N). The "pressing" load signifies that force which acts at the end of the sliding motion where the maximum normal load of 200 and 400N are reached. The values of F_i and F_p were pre-determined based on trial test results, different test cycles were used to study different extents of damage, i.e., 1000 test cycles for the lowest loading condition (F_i= 80 N, F_{pmax}=200 N), and 100 cycles for the other two loading conditions. The frequency of the test was 2.5 Hz [31].

After the tests, the sliding wear tracks and impact-sliding wear scars were observed using optical microscopy (OM) and scanning electron microscopy (SEM) with an energy dispersive X-ray (EDX) analysis for better understanding of coating wear behavior under the sliding and impact-sliding motions.

3. RESULTS AND DISCUSSION

3.1 Characteristics of PEO coatings on Ti-6Al-V

SEM micrographs on polished PEO coatings are shown in Fig. 3-2. PEO process bases on conventional anodic oxidation but the applied voltage of PEO process exceeds the critical breakdown voltage of the insulated film [26]. A typical PEO coating has a dense, thin inner layer and a porous, thick out layer. From the SEM observations, although polished to obtain a similar surface roughness, the size of remained pores on S3 were found to be largest, at an average value of around 5 μm. The pores on S1 and S2 were measured to be around 2 μm after polishing.
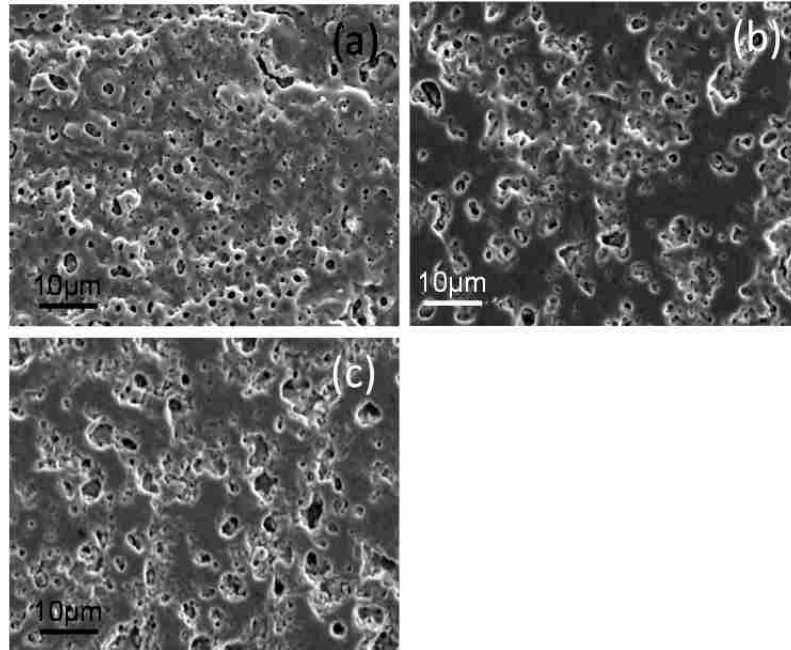
Figure 3-2 SEM micrographs of surface morphologies of polished sample
surfaces (a) S1 (b) S2 and (c) S3.

3.2 Wear behaviors of as-made and polished coatings and uncoated substrate.

As-prepared PEO coatings (thickness: S1:10.8 μm; S2:17.8 μm; S3:26.9 μm)
were tested by POD under a 2 N normal load for a 100 m sliding distance in an ambient
condition. The coefficient vs. sliding distance of S1, S2 and S3 are shown in Fig. 3-3 (a)
by curves 1, 2 and 3, respectively. The COF of all the PEO coatings quickly reached to a
value of 0.8~0.9 at the first 10 m sliding. S1 and S2 had a constant COF value while S3
exhibited some fluctuations which may due to the chipped. The COF of the Ti substrate
was also measured for a 100-meter sliding, which (in a range of 0.2~0.7) was lower than
that of the coatings, but quite unstable (oscillation of COF values) and had sharp
transitions indicating significant changes in the contact area during the test. As reported
by previous literatures [26, 32], the sliding mechanism of a PEO coating is governed by

abrasive wear which leads to production of wear debris. The rough outer layers of the PEO S1-S3 coatings were polished to be slightly smoother and the counterface pin balls were flattened. The wear debris came from the polished coatings and the counterface balls. The transferred materials from the balls to the coating surfaces were oxidized during the sliding tests and stuck and departed from the coating surfaces. The dynamic material transferring may be the reason of the COF fluctuation of S3.
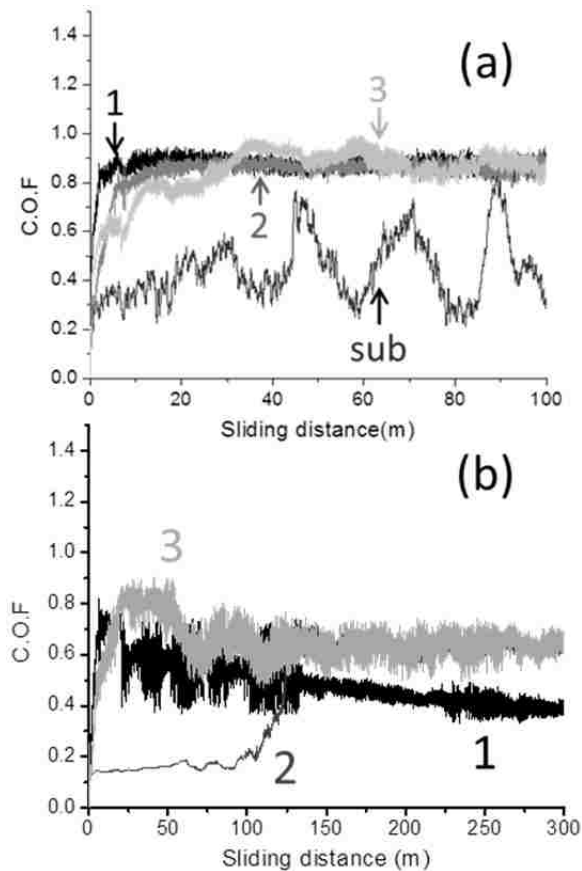
Figure 3- 3 COF vs. sliding distance in POD wear tests for coatings 1-3 and Ti-6Al-4V substrate. (a) Before polishing, 2N, 100m; (b) After polishing, 2N, 300m.

The sliding wear mechanism of the Ti-6Al-4V substrate is complex. The frictional behavior of selected orthopedic Ti alloys was studied by Long and Rack [35] who found

that their performance were a function of contact stress, sliding velocity, cyclic count and alloy phase structure. The COF oscillation of the uncoated Ti substrate in this study may be explained by the adhesive wear mechanism and a large quantity of substrate material deformation and delamination due to periodic localized fracture of the surface materials. An oxide surface layer easily forms as well and this layer readily adheres and transfers to counterface surface [36]. Severe wear of the Ti substrate was the result of the sliding.

The tribotest results indicated that abrasive wear had dominated the wear behavior during the whole sliding process for all of 3 coated samples with a constant value of COF in the range of around 0.8 regardless of coating thickness and surface roughness. Compared with the uncoated substrate, all of the PEO coatings provided the improved wear protection since none of the coating was failed after the 100 m sliding.

In order to investigate the effect of surface roughness, S2 and S3 were polished to the same roughness level of S1. After the polishing, POD tests were carried out again on the three coatings under the same load for a 300 m sliding. In this case, significant differences in COF were found for the coated samples, which are shown in Fig. 3-3 (b). The COF curve of the polished S2 exhibits a 3-stage sliding behavior: (1) from the beginning→60 m, COF has a very constant low value (≈ 0.15); (2) from 60 m→130 m, COF shows an increasing value from 0.15→0.65 with some fluctuation and finally reaches to (3) 130 m→300 m (the end), a constant high value (≈ 0.65). S1 and S3 showed a high COF value at the beginning of the test to be around 0.7-0.8, and decreased gradually to lower values (S1: 0.4 and S3: 0.65). This different sliding behavior comparing to S2 may be explained by the different chemical compositions in the coatings as discussed later on.

72

3.3 OM and SEM observations on POD wear tracks

The optical and SEM micrographs taken from wear tracks on the coatings (hereafter, testing coated samples were polished) are shown in Fig. 3-4, where EDX spectra were collected from the center areas of the wear tracks (marked by capital letters on SEM micrographs in Fig. 3-4) and shown in Fig. 3-5. From the atomic percentage summarized in the table insert in Fig. 3-5, Ti, Al and V of the substrate composite elements had a low percentage in both S2 and S3 coatings while Fe had a very high percentage on S2 and S3, comparing to that on S1. This means the material transfer from the counterface steel pin covered the surface of the contact area during the sliding motion. As a result, the sliding couple was changed from steel vs. TiO_2 to steel vs. steel. This is the reason why the COF curves of S2 and S3 almost overlapped (COF≈0.65) during the second half (after 150 m) of the 300 m sliding (see Fig. 3-3 (b)). Furthermore, the SEM images shown in Fig. 3-4 (d) and (f) indicate that S2 had a much less damage than S3 and COF curves in Fig. 3-3 (b) also suggest that the coating on S3 was quickly covered by transferred material (in the first 25 m sliding) in the contact zone, while only slight wear took place on S2 in the first 100 m sliding until small patches of transferred materials began to occupy the wear track on S2 but hadn't reached to 100% area up to the end of the POD test (see Fig. 3-4 (d)). One of the possible reasons to explain the low value of COF in the first 100 m sliding of S2 is the existence of lubricious oxide [37, 38]. The sub-stoichiometric titanium oxide, which can be expressed as Ti_nO_{2n-1}, leads to the low friction coefficient during the sliding wear tests. As a result, less *Fe* was picked up as indicated by EDX analysis result. An abrasive wear was the wear mechanism of S1, showing a high COF value. The COF

decreased at the late stage (after 150 m) should be due to the surface polishing effect, as shown by the SEM image, Fig. 3-4 (b).
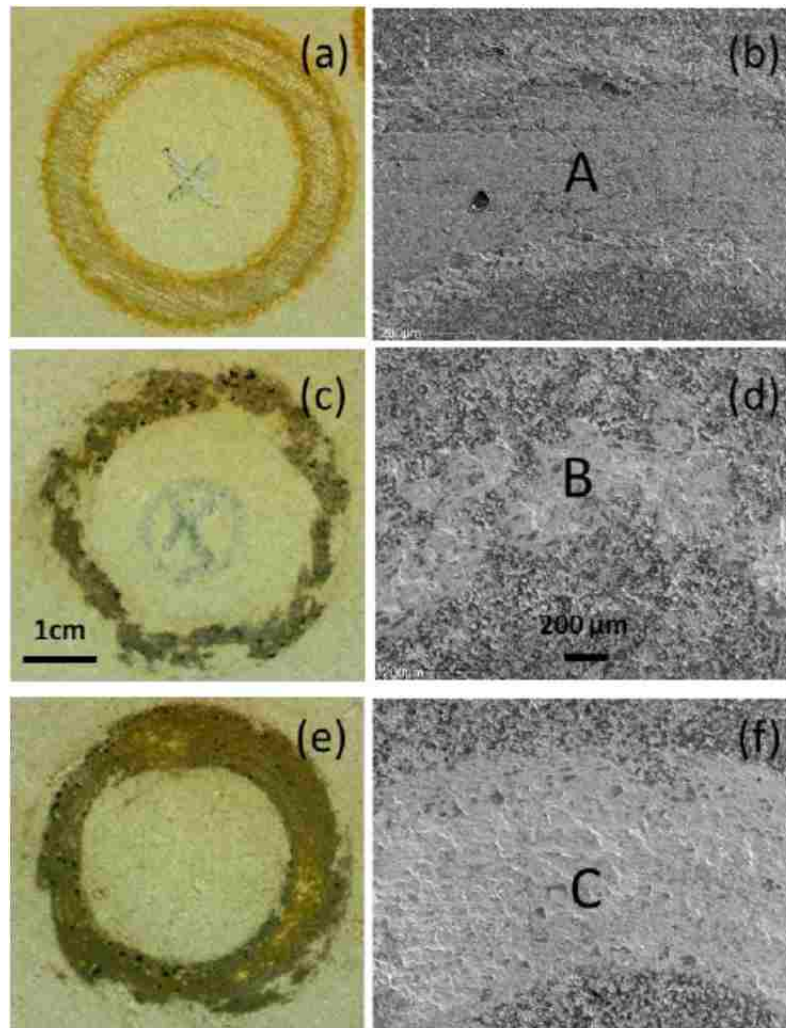
Figure 3- 4 OM and SEM micrographs on POD wear tracks under 2N, 300m condition (after polishing work): (a, b) S1, (c, d) S2 and (e, f) S3. EDX spectra taken from some typical areas in the SEM micrographs are shown in Fig. 3-5.

	S1	S2	S3
O	57.49	56.56	58.2
Al	2.4	1.85	2.33
Si	0	12.7	11.1
P	8.37	3.54	2.92
Ti	22.12	14.81	16.26
V	0.16	0.3	0.1
Fe	9.57	20.57	19.61
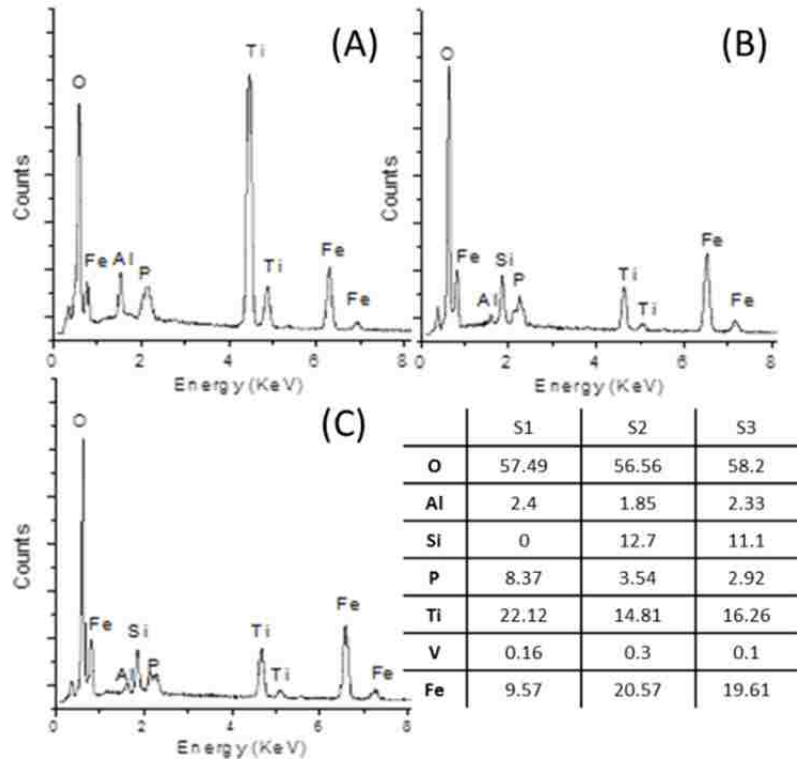
Figure 3- 5 EDX spectra collected on related areas in Fig. 3-4 and atomic percentage

of main elements in the center of wear tracks.

To prove this possible explanation of a sub-stoichiometric Ti oxide, it is necessary

to calculate the oxygen vs. cation ratio from coating surface, which are summarized in

Table 3-3. The stable state of oxides for the elements Ti, Si and P are TiO_2, SiO_2 and

P_2O_5 (neglect Al since its minimal concentration), respectively. So, the O/cation ratio of

those elements should be 2, 2, and 2.5, correspondingly. However, the O/All (Ti+Si+P)

values are in a range of 1.72~1.78, which is lower than 2. This suggests that there are

certain amount of sub-stoichiometric Ti oxide existed in the PEO coatings. Due to the

lowest O/All value of S2, this lubricant effect showed most significantly on S2.

Table 3- 3 Atomic ratio of oxygen vs. cations in the polished coatings and wear tracks.

No.	Atomic ratio on coating O/All	Stoichiometric expression	Atomic ratio on wear track O/Fe
1	1.75	$(Ti_{0.67}Al_{0.073}Si_0P_{0.25})O_{1.75}$	5.68
2	1.72	$(Ti_{0.45}Al_{0.056}Si_{0.39}P_{0.11})O_{1.72}$	2.43
3	1.78	$(Ti_{0.5}Al_{0.071}Si_{0.35}P_{0.09})O_{1.78}$	2.66

It should be noted that study on lubricity of oxides is a very complicated issue [39] and more comprehensive characterization instruments such as XPS (X-ray photoelectron spectroscopy), XAS (X-ray absorption spectroscopy) and TEM (transmission electron microscopy) are needed, which are out of the scope of this study. The purpose of the tribotest study was to determine the COFs of the PEO coatings, because different COFs would cause different friction and shear forces with a coating during an impact-sliding wear test and may have a significant effect on impact-sliding test results.

3.4 OM and SEM observations on impact tracks

As introduced in our previous studies [31], a typical inclined impact-sliding track is composed of two parts: a head crater, which is mainly caused by impact force, F_i, and a long tail part, which is the sliding damage under pressing force, F_p. Fig. 3-6 gives a schematic cross-sectional illustration of a typical impact-sliding track on a PEO-coated Ti alloy where the PEO coating usually has a three-layered structure [24]. In this study, peeling means the coating is fully removed from the coating/substrate interface and the underlying metal substrate is exposed. Chipping is another type of damage where a part of the upper layer of the coating is gone, and some of the inner layer is adherent to the metal substrate [32].
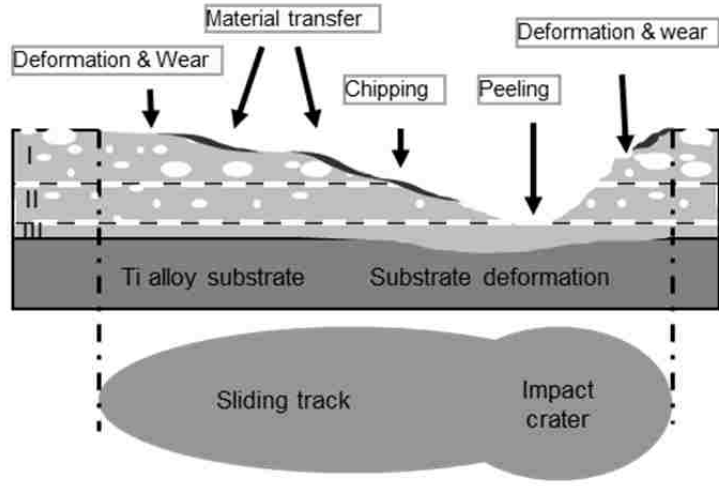
Figure 3- 6 Schematic illustration of coating failure behavior in the inclined impact-sliding tests. Area I, porous top layer; area II, dense inner layer; area III, diffusion layer.

Fig. 3-7 shows the OM images of impacted tracks tested on polished coating surfaces under combined loadings: F_i =200 N, F_{pmax}=400 N (Fig. 3-7 (a1-c1)) and F_i =80 N, F_{pmax}=200 N (Fig. 3-7 (a2-c2)). According to Herztian's theory [40], the contact pressures were calculated for the ball-to-plate cases and are listed in Table 3-4.

Table 3- 4 Estimated contact pressures during the impact and pressing according to Herztian's theory.

Fi	80 N	140 N	200 N	300N	400N
Mean pressure	1.08 GPa	1.30 GPa	1.47 GPa	1.72 GPa	1.89 GPa
Maximum pressure	1.62 GPa	1.95 GPa	2.2 GPa	2.58 GPa	2.83 GPa

A compressive yield strength for a typical annealed Ti-6Al-4V is in the range of 825-895 MPa [41], which is much lower than the requirement to withstand the above maximum contact stresses. As a result, the substrate deformation could be observed after several cycles of the test. The observations indicate that the test load (F_i= 200 N, F_{pmax}=400 N), is too high. On the other hand, the F_i= 80 N, F_{pmax}=200 N used seems

reasonable, and only a small amount of the coating top layer has been damaged in the tests. S1 showed the greatest (F_i= 80 N, F_{pmax}=200 N) endurance to either highest (F_i= 200 N, F_{pmax}=400 N),) or lowest impact-sliding loads while S3 showed the worst. Specified data to evaluate the failure levels of impact-sliding tracks are listed in Table 3-5, in which, failed area percentage means the damaged coating area vs. the whole coating contacted area.
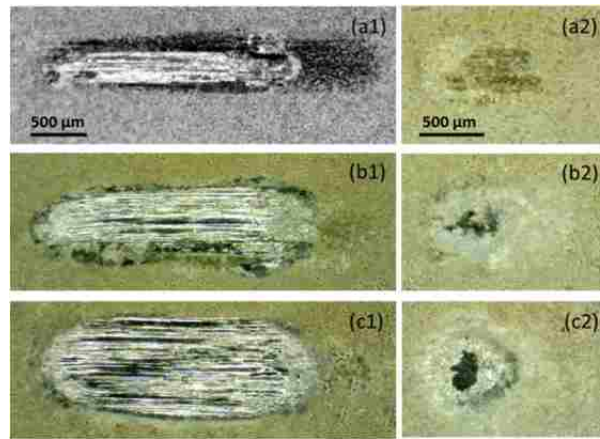
Figure 3- 7 Optical micrographs on impact-sliding tracks under (a1-c1) Fi =200 N, Fpmax =400 N and (a2-c2) Fi =80 N, Fpmax =200 N. The head crater is in the left for all OM and SEM micrographs.

Table 3- 5 Evaluation on failure levels of the PEO under different loading conditions.

Fi and Fpmax	80 N and 200 N		140 N and 300 N		200 N and 400 N	
No.	Failed area (%)	Track width (μm)	Failed area (%)	Track width (μm)	Failed area (%)	Track width (μm)
S1	0	567	25	654	50	606
S2	4	726	40	563	85	944
S3	8	991	90	704	95	1070

It is clear that the width of the tracks increased gradually with the increase of the force level and the coating thickness for the F_i= 80 N, F_{pmax}=200 N and F_i= 200 N, F_{pmax}=400 N cases. Usually, the load bearing capacity increases with the increase of coating thickness. However, in this case, the roughness of the coatings may play a very

important role when the COFs are at the same level. S3 has a very rough surface—R_a=3.8 µm. The outer surface of the PEO coating with such a high roughness likely has a detrimental effect in this impact-sliding test, especially the sliding wear part, since it can cause significant abrasive wear on the counterface steel pin at the very beginning of the wear test. This would cause the third-body wear damage and quickly damage the coating surface. In order to minimize the effect of coating roughness to the coating performance in the tests, S2 and S3 were polished to the same level of roughness of S1 (refer to Table 3-2). The impact-sliding tests were repeated under a middle loading condition of F_i= 130 N, F_{pmax}=300 N. The OM and SEM micrographs of the tested samples are shown in Fig. 3-8. All the tracks have their impact crater (head) shown in the left side of the images with the same magnification. Typical points A-D are studied by EDX as shown in Fig. 3-9.
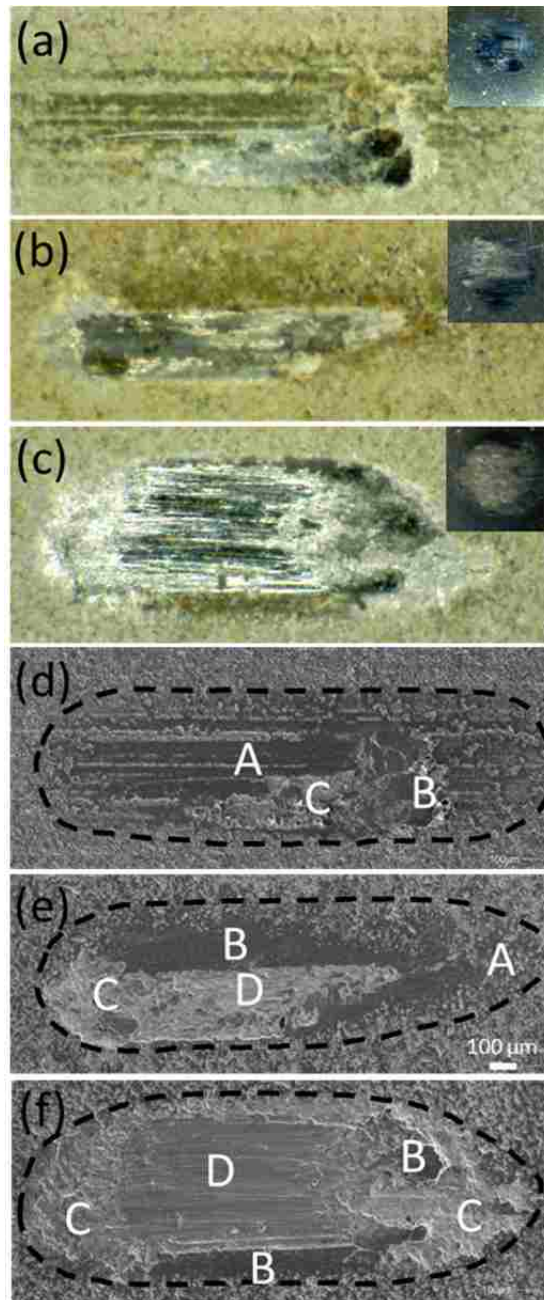
Figure 3- 8 OM and SEM micrographs on 100 cycles' impact tracks under 140 N/300 N loading condition, in which (a-c) are OM images, (d-f) are SEM images. The damages on pin balls were inserted in the OM micrographs. EDX spectra on the typical areas are shown in Fig. 3-8. All the images are at a same magnification, the scale bar is shown in (e).
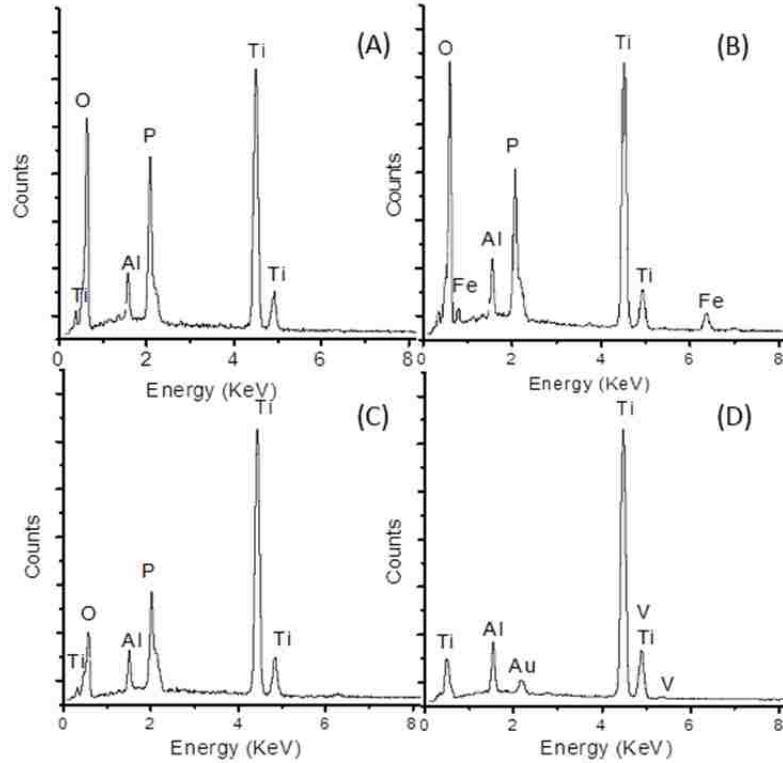
Figure 3- 9 EDX spectra taken on related areas which shown in Fig. 3-8.

Fig. 3-9 is the EDX spectra collected from the typical areas A-D on impact tracks.

Area A, which occupied most of impact-affected area on S1 showed a similar chemical

composition as the untested coating surface, which means area A was only slightly

polished by abrasive wear. S1 could also sustain the cycled impact force F_i during the test

due to the compensation of metal substrate. The material transfer from the steel ball

could be found on all impact tracks. Some of them were rubbed on the coating surface

(area B in Fig. 3-7 (e)), while others were pushed away by the movement of the steel ball

and piled up in the tail part of the tracks (area B in Fig. 3-7 (d and f)). Chipping could be

observed in area C distributed in both head and tail parts. Large area (<80%) of fully

failed coating (peeling) was observed on S3 (area D) since there was no oxygen that

could be detected by EDX (see Fig. 3-9 (D)).

In the latest tests, S1 again showed the best impact-sliding wear resistance after 100 test cycles. This result agreed well with the observation in the previous tribotest part. The 100 cycles' impact-sliding made the performances of all three coatings similar to their behavior shown at the late stage of COF curves (after 150 m sliding, refer to Fig. 3-3 (b)), in which, S1 exhibited the best sliding wear resistance and lowest COF value ($\approx$ 0.4). Only few amount of Fe was found in the tail part on the track of S1 and a less damage was observed on the counterface ball surface (see the inserted OM image of steel ball in Fig. 3-8 (a-c)). Large areas on the tracks of S2 and S3 were covered by Fe oxide during the tests and some Fe oxides were pressed into the coating surface by the extremely high loading forces. What's worse, some Fe oxides stuck with the coating material and then peeled-off and pushed away together by the following sliding motions of the steel ball. Finally, the relatively soft substrate was exposed (area D in Fig. 3-8 (e and f)). Around 30% and 90% areas of the impact-sliding wear tracks were failed on S2 and S3, respectively. The fact that the failed area percentage was less on S2 than on S3 might be due to the lubricity existed in the early stage of the test providing protection to S2 as shown in Fig. 3-3 (b). The middle low R_{sk} value of the S2 coating surface may also benefit the contact stress distribution (Table 3-2).

From Table 3-5, the track on S1 was wider than that on S2 (see Table 3-5) and had a less impact damage in the head area. The improved performance of S1 may be attributed to its thinner thickness and more porous surface than the polished S2, During the tests, the pores in the top layer of the coating might cushion the impact force during the test to some degree, that's the reason why the S1 deformed less in the head crater which was mainly caused by the impact load Fi. The wider impact track on S1 resulted from the

effect of the relatively soft substrate due to the thinner coating. On the other hand, the hard and dense inner layer of the coating S2 after the polishing can protect substrate [24] better from deformations under the pressing load due to its high loading support capability. Thus, the polished S2 exhibited a better wear resistance than S1 in the middle and tail parts of the wear tracks where the 300 N pressing force was applied. Therefore, the soft substrate effect would be beneficial to cushion impact energy for the coating but would not be good for a sliding wear case where the pressing force is so high to cause the underlying substrate deformation. Such phenomena have been observed by Su [32]. As a result of the extremely high loading condition, the dense, hard PEO coatings might fail quicker than the less dense ones. Furthermore, the hard layer may be brittle under the dynamic impact force attack and cause an accelerated damage after the layer is broken and forms wear debris as seen in the crater part (Fig. 3-8 (d-f)).

4. CONCLUSIONS

Three PEO coatings with thickness in the range of *10-27 μm* were formed on Ti-6Al-4V alloy using unipolar and bipolar current modes in alkaline solutions. The PEO coatings were firstly tested using a POD tribometer and then using an inclined impact-sliding wear tester to study coating failure behavior under extremely high contact stress conditions. The POD tribotest on the PEO coatings show that the surface roughness of the coatings had a very significant effect to the sliding behaviors of the wear couples. The high surface roughness of thick coatings may result in no advantage that is otherwise brought from the increasing of coating thickness. Reversely, the rough coating cause early failure and a large mass-loss on the counterface ball. All the coating had a relatively

high but constant COF comparing to the substrate. After polishing the coatings, the COF decreased greatly. But the mechanisms on three coated samples were very different:

For the coatings having similar coating thickness and surface roughness R_a, the coating surface profile characteristics such as skewness R_{sk} seemly played a significant role in the transferring and wear mechanism of the counterface material. Close-to-zero value of R_{sk} caused less counterface material transfer to the coating S1, which exhibited a decreased COF after the running-in process. The reduced COF would lead to a less shear stress in the coating during the impact-sliding test. As a result, S1 had the best performance among the three coatings. The sub-stoichiometric Ti oxide in S2 showed a high lubricity and less intendancy of picking up materials from a counterface steel pin ball. As a result, the material transferred from the steel ball was less for S2 than for S3, Fig. 3-4 (d and f). However, with the increase of the sliding distance, more amount of patchy Fe oxide covered the wear track, causing the COF increase. At the final stage of the tests, S2 and S3 had the same high COF values. The Fe oxides show no lubricity in this test, although some Fe (*FeO*, known as Wuestite [42], or *Fe_2O_3* and *Fe_3O_4* [43]) oxides may exhibit a low COF.

The results of POD tests agreed well with the failure behaviors of coatings during the inclined impact-sliding tests. S1 had the lowest COF value after the steady stage was reached and it also showed the best performance during the impact-sliding test.

For a thin and relatively smooth coating, the porous structure may help in resilience of the impact force compared to the exposed dense inner layer of the thick coatings that were ground to have a similar surface finish. Therefore, the wear failure behavior can be

altered by changing surface profiles and by doping different chemical elements, the latter can change wear mechanisms by changing surface affinity behavior and stoichiometry.

Beside the effects of the coating thickness and pores as previously discussed for the polished coating, the lubricant sub-oxide in the coating was supposed to facilitate the decreasing of COF but the benefit may exist only at the beginning of the test of S2. With the increase in impact-sliding test cycles, a large amount of counterface material transfer occurred and the COF of S2 would increase significantly, like that in the late stage of its POD test. On the contrast, S1 had less counterface material transfer and its COF reduced due to the polishing running-in effect. A low COF would introduce a less shearing force in the coating, which is very critical for the performance of a coating during the impact-sliding tests. Therefore, S1 showed a better result than S2. The S3 had a high COF from the beginning. As a result, S3 had the worst performance in both POD and impact-sliding tests.

REFERENCES

[1]   ASM Handbook, Vol. 2, ASM International, pp. 634-646, (1998) 11.
[2]   W.F. Brown, H. Mindlin, C.Y. Ho, in Aerospace Structural Metals Handbook, Vol. 4, CINDAS/USAF Perdue University, (1997) 12.
[3]   S.L. Chawla, R.K. Gupta, in Materials Selection for Corrosion Control, Chapter 18, ASM International, (1995) 275.
[4]   F. De Paolis, C.Caroselli, S. Riscifuli, Paper presented at the RTO AVT Specialists' Meeting on "Cost Effective Application of Titanium Alloys in Military Platforms", held in Loen, Norway, 7-11 May 2001, and published in RTO-MP-069(II).
[5]   R. W. Schutz, ASM Handbook Volume 13B, Corrosion: Materials (ASM International) Published: (2005) 252.

[6]   http://www.ticotitanium.com/wp-content/uploads/2009/11/paper02170.pdf.   (10 April, 2013)

[7]   ASM handbook, Mechanical testing, Surface Engg. Of Ti and Ti alloys, ASM Int., 8, (1997) 840.

[8]   ASM handbook, Corrosion, Specific alloy systems, ASM Int., 13, (1997) 671.

[9]   E.O. Ezugwu, Z.M. Wang, Titanium alloys and their machinability a review. J. Mater. Processing Tech. 68 (1997) 262.

[10]   J. Donachie, Titanium: A Technical Guide, second ed, ASM International, 2000, pp. 143.

[11]   K.G. Budinski, Wear. 151 (1991) 203.

[12]   M. Masmoudi, M. Assoul, M. Wery, R. Abdelhedi, F. El Halouani, G. Monteil, Applied Surface Science. 253(2006) 2237.

[13]   A. Molineri, G. Straffelini, B. Tesi, T. Baccai., Wear. 208 (1997)105.

[14]   S. Krol, W. Grzesik, Z. Zalisz, M. Hepner, , Tribology International. 37 (2004) 633.

[15]   G. Cassar, J.C. Avelar-Batista Wilson, S. Banfield, J. Housden, A. Matthews, A. Leyland, Wear. 269 (2010) 60.

[16]   G. Straffelini, A. Molinari, Wear. 236 (1999) 328.

[17]   Y. Liu, D.Z. Yang, S.Y. He, W.L. Wu, Trans. Nonferrous Met. Soc. 13(2003) 1137.

[18]   A. Bloyce, P.H. Morton, T. Bell. ASM handbook, vol. 5. Materials Park, OH: ASM International; 1994. pp. 835.

[19]   S.R.J. Saunders, M. Monteiro, F. Rizzo. The oxidation behavior of metals and alloys at high temperatures in atmospheres containing water vapour: A review, Progress in Materials Science. 53(2008) 775.

[20]   P. Kofstad, P.B. Anderson, O.J. Krudtaa, Journal of the Less Common Metals. 3 (1961) 89.

[21]   A. Afshar, M.R. Vaezi, SCIENTIA IRANICA; SUMMER 2003; 10(3) 361.

[22]   O.M. Ivasishin. Materials Science and Engineering, 168 (1993) 23.

[23]   B. Vijay, K. Arjun, H.A. Kumar, A. V. kumar, P. Chandrasekar and V. Balusamy. J. Surface Sci. Technol. 23(1-2) (2007) 49.

[24]   A. Yerokhin, X. Nie, A. Leyland, A. Matthews, Surf. Coat. Technol.130 (2000) 195.

[25]   X. Nie, A. Leyland, A. Matthews, Surf. Coat. Technol.133 (2000) 331.

[26] X. Nie, A. Leyland, A. Matthews, Surf. Coat. Technol.125 (2000) 407.

[27] H. Liang, B. Shi, A. Fairchild, T. Cale, Vacuum. 73 (2004) 317.

[28] S. Tsunekawa, Y. Aoki, H. Habazaki, Surf. Coat. Technol. 205(19) 4732.

[29] L. Ceschini, I. Boromei, E. Lanzoni, C. Martini G. Sambogna, Friction and wear behavior of PEO- and PVD- coated Ti6Al4V against hard Cr and PS- Al_2O_3/TiO_2 AITC-AIT 2006 International Conference on Tribology 20-22 September 2006, Parma, Italy.

[30] H.M. Nykyforchyn, V.S Agarwala, M.D. Klapkiv, V.M. Posuvailo, Simultaneous Reduction of Wear and Corrosion of Titanium, Magnesium and Zirconium Alloys by Surface Plasma Electrolytic Oxidation Treatment, Advanced Materials Research, 38 (2008) 27.

[31] Y. Chen and X. Nie, Study on fatigue and wear behaviors of a TiN coating using an inclined impact-sliding test, Surface & Coatings Technology. 206 (2011) 1977.

[32] J.F. Su, D. Yu, X. Nie andH. Hu, Inclined impact-sliding wear tests of $TiN/Al_2O_3/TiCN$ coatings on cemented carbide substrates, Surface & Coatings Technology. 206 (2011) 1998.

[33] J.F. Su, X. Nie, H. Hu, J. Tjong, Friction and counterface wear influenced by surface profiles of plasma electrolytic oxidation coatings on an aluminum A356 alloy, J. Vac. Sci. & Technol. A 30, 061402 (2012);

[34] C.A. Kotwal, B. Bhushan, Contact analysis of non-gaussian surfaces for minimum static and kinetic friction and wear, Tribology transactions, 39 (1996) 890.

[35] M. Long, H.J. Rack, Titanium alloys in total joint replacement-a review, Biomaterials. 19 (1998) 1621.

[36] J. Qu, P.J. Blau, T.R. Watkins, O.B. Cavin, N.S. Kulkarni, Wear. 258 (2005) 1348.

[37] M. N. Gardos, Tribology Letters. 8 (2000) 65.

[38] M. N. Gardos, Tribology Letters. 8 (2000) 79.

[39] A. Erdemir, Tribology Letters. 8 (2000) 97.

[40] http://www.tribology-abc.com/calculators/e2_1.htm, (12 April, 2012).

[41] R. Boyer, G. Welsch, E. W. Collings, eds. Titanium Alloys, ASM International, Materials Park, OH, 1994.

[42] K. Bobzin, F. Ernst, K. Richardt, T. Schlaefer, C. Verpoort, G. Flores, Surf. Coat. Technol. 202 (2008) 4438.

[43] A. Borisova, Y. Borisov, A. Tunik, L. Adeeva, E. Lugscheider, C. Herbst, Thermal Spray 1999: United Thermal Spray Conference (DVS-ASM), 1999, pp.174.

CHAPTER 4 STUDY OF THE FATIGUE WEAR BEHAVIORS OF A WC DLC

COATING ON 316L STAINLESS STEEL

1. INTRODUCTION

Nowadays, Physical Vapour Deposition (PVD) and Plasma Assisted Chemical Vapour Deposition (PACVD) coatings provide cost-effective solutions for a variety of manufacturing problems. PVD and PACVD coatings are used in applications where toughness, durability, corrosion and erosion resistance are required. DLC coatings have high hardness, high resistivity, good dielectric and optical properties, and offer a wear-resistant and chemical barrier for many materials along with a low friction coefficient and chemical inertness. Furthermore, DLC coatings are also expected to be the emerging biomaterials for load-bearing mechanical devices due to the excellent corrosion and wear protection properties.

In many industrial applications, the machinery and equipment are often subjected to combined attacks of repetitive impact and sliding forces leading then to surface damage. The determination of the properties of the coatings corresponding to the dynamic loads is an important aspect of many engineering problems. The design of an impact tester which simulates impact conditions has been reported by Knotek [1, 2] and Bantle with Matthews [3]. In this test, a dynamic load is applied vertically to a hardened steel ball which impacts the coating surface, which elucidates the cohesive and adhesive failure modes of the coatings. Three types of fatigue cracks were found in the impact craters; (a) cohesive failure in the central zone, (b) cohesive and adhesive failure in the intermediate zone and (c) circular cracks in the peripheral zone. However, this kind of test method can only indicate the pure impact failures under cycled impacts whereas coating fatigue

cracking behaviors observed either in the automotive manufacturing industry or in biomaterial implants are usually associated with the combined effects of impact and sliding motions.

An inclined impact test, was then developed, which constitutes a new reference to the prediction of the coatings' impact failure under inclined impact forces [4,5]. However, in these studies the inclined angle, θ, was kept constant during the impact tests. In our previous study[6-8], a newly-developed test method—the inclined impact-sliding test—was introduced and found to be effective in order to simulate coating failures under extremely high impact and sliding contact stress conditions. During the test, repetitive impact and sliding interactions were applied on an inclined coated surface by a 10-mm-diameter steel ball, which caused normal and tangential forces simultaneously. With the up-and-down vertical movements of the steel ball, the sample was first impacted and then pushed downward after full contact due to the sample holder rotating around the fixed roller bearing before returning back to the original location, where the loading re-zeroed at the end of each cycle. The inclined impact-sliding test caused an impact crater, which was named as "head part", and a relatively long sliding track, which was named "tail part"[6-8]. Different fatigue behaviors and types of cracks were observed in the head and tail parts of the impact-sliding track. The value of the impact force, Fi, can be adjusted by changing the gap distance between the steel ball and the sample surface and the pressure of the compressed air on the piston in the air cylinder. The pressing force, Fp, is determined by the air pressure for the given diameter of the piston and, finally, the inclination angle, θ, equals 20º in the static situation and changes in a range of 10º —20º during the test. Due to the existence of the inclination angle, the loading forces consist of

90

a normal component, *Fn*, and a tangential one, *Ft*, whose values depend on the instantaneous value of θ in each cycle. In this paper, we used the inclined impact-sliding test method under *Fi/Fp=200 N/400 N* (impact-pressing) forces to investigate the fatigue behaviors of a PACVD WC-DLC coating on a stainless steel substrate. The uncoated stainless steel was also tested using the same method.

2. EXPERIMENTAL DETAILS

2.1. The specimen

A 25 mm diameter WC-DLC coated 316L stainless steel disc was used as the test specimen whose coating was prepared using standard commercial processes at Tecvac Ltd, UK. The maximum coating temperature did not exceed 300 ºC [9, 10] and the WC-DLC coating deposited using PACVD had a thickness of 2.8 μm. The coating has a three-layer structure consisting of a top DLC coating layer with a thickness of around 2 μm, a tungsten-carbide (WC) transition layer with a thickness close to 1 μm, and a very thin W bonding layer. The Young's modulus and hardness of the coated sample were measured by a Hysitron Ubi 1 nano-indentation test machine.

2.2. Pin-on-disc wear test on the DLC coating

In order to study the long-sliding-distance wear-resistant property of the DLC coating, a pin-on-disc wear test was used. The test was carried out using a steel ball pin (AISI 52100, HRC 58-60, 5.5 mm in diameter) under ambient conditions (40% humidity and 20ºC) under a 5 N normal load and the coupons were rotated to give linear sliding speeds of about 75 mm/s. In this range, the sliding speed had no effect on wear rate. After the test by 5,000, 30,000, 60,000 and 275,000 revolutions, the wear tracks were observed

using scanning electron microscopy (SEM) and analyzed using energy dispersive X-ray (EDX). The dynamic friction coefficient during the long sliding distance (i.e. 275,000 revolutions) wear test was recorded and furthermore, the wear rate, K, was calculated according to the following expression:

Wear rate = Volume loss / (Sliding distance × Normal load).

A Mitutoyo SJ.201P surface roughness tester was used to measure the surface profile across the wear tracks with six points on each wear track measured in order to get average data. On the 30,000 revolutions' wear track the wear rate $K_1=1.318\times10^{-6}$ mm^3/Nm was calculated and on the 60,000 revolutions' track, the wear rate $K_2=1.423\times10^{-6}$ mm^3/Nm was calculated demonstrating that an increase in the testing revolutions did not obviously influence the wear rate and that the DLC coating has a very good solid lubrication property and wear resistance.

2.3. The sliding test and force curve of each test cycle

The inclined impact-sliding test was performed under repetitive high-impact and sliding-load conditions in an ambient environment (40% humidity and 20 ℃) with a test frequency of 2.5 Hz with 0.15 s on-time (time of the steel ball moving downwards) and 0.25 s off-time (time of the steel ball moving upwards and recess).

Fig. 4-1 (a) shows the force curve of the loading and unloading process in one test cycle, in which, there are two types of forces during each test cycle; the impact force, *Fi*, and pressing force, *Fp*. *Fi* was mainly determined by the pre-set gap between the coating surface and indenter ball (*0.2 mm* in this study) while *Fp* could be changed only by the air pressure driving the movement of piston. In this way the impact and pressing forces

could be changed separately to simulate different loading conditions of industrial or biomedical applications. In this paper, a combined load of *Fi/Fp=200 N/400 N* was used, as shown in Fig. 4-1. The surfaces of the contact areas on the coating surface and the steel ball were cleaned using 95% ethanol before each test and the ball was changed to a new one to obtain a fresh surface. A load cell was used to measure the forces and the signal was recorded using a PCD30A data acquisition system with a 10,000 *Hz* sampling frequency. After the tests, the coatings were observed using SEM with EDX in order to study surface morphology and analyze the chemical compositions of the impact tracks.
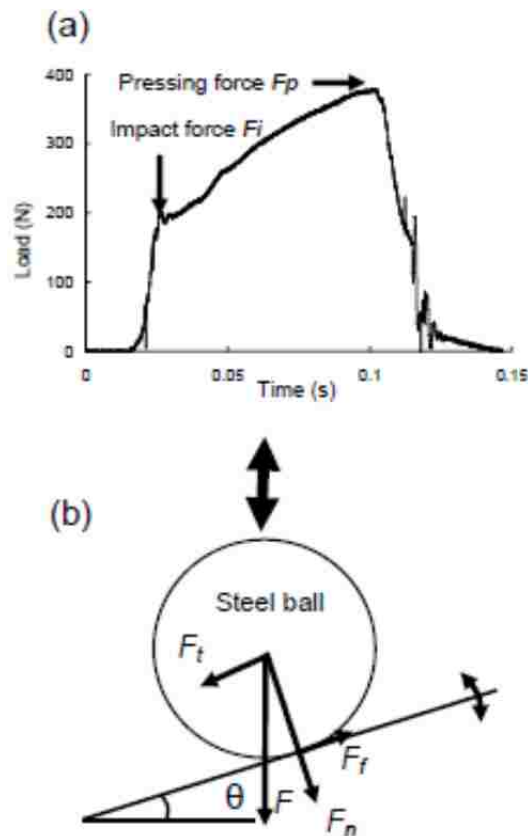
Figure 4- 1 The force curve of the loading and unloading process in each impact cycle under a Fi/Fp=200 N/400 N load condition.

Fig. 4-1 (b) simply illustrates the forces when the indenter ball and inclined coating surfaces contact each other (loading process). The applied vertical force was divided into two components; a tangential component, Ft, and a normal one, Fn, and both force components changed their values during each cycle of the test. Fn was measured using the load cell device and its force curve is shown in Fig. 4-1 (a). $Ft = Fn*tan\ \theta$, where θ was varied from 20º to about 10º. F_f is the friction force, which is very difficult to determine due to the changing degree of deformation in the contact area under the indenter ball and the possible change of friction coefficient of the DLC coating during the test.

3. RESULTS AND DISCUSSION

3.1. Nano-indentation test on the DLC coating

In this paper, a Hysitron nano-indentation machine was used to evaluate the mechanical properties of the DLC coating and the curve of the load-displacement data recorded for the DLC coating is shown in Fig.4-.2. Five indentations with a 500 μN load were created with a maximum contact depth of 92 nm. For the 2-μm-thick top DLC layer of the coating the indentation depth was less than 1/10 of the thickness of the DLC top layer, which has minimal underlying layer effects [11]. The DLC coating has a very smooth black surface with a surface roughness around $Ra \approx 500$ nm. The load-displacement curve (see Fig.2) shows almost complete elastic recovery [12] and the hardness and elastic modulus values were determined to be 20.5 GPa and 180 GPa, respectively.
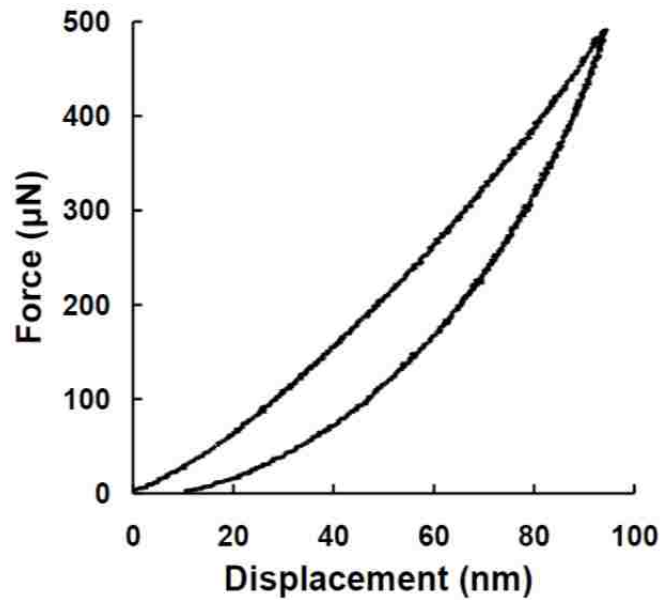
Figure 4- 2 Load—displacement curve of the DLC coating by nano indentation

test.

3.2. SEM observations on the pin-on-disc wear tracks

Fig. 4-3 shows the back scatter SEM micrographs taken of the wear tracks after 5,000, 30,000, 60,000 and 275,000 revolutions. According to SEM observations, in the early stages of the wear test (around 5,000 revolutions) the wear surface is very smooth and only some sliding grooves can be seen and the top layer of DLC coating is not worn through. After 30,000 revolutions, it can be observed that the DLC coating top layer is thinned at the center of the wear track since the brightness of the image increased due to the increased exposure of the underlying tungsten. A number of tiny, parallel fatigue cracks are formed and distributed asymmetrically inside the wear track and are found to be very similar to the tail part of the inclined impact-sliding test in appearance (see Fig.4-7 (D1-D4)). This is due to the compressive stress in the front of ball pin and tensile stress

behind the pin during the wear test, which is very similar to the situation occurring in the scratch test [13, 14]. When the wear distance was doubled to 60,000 revolutions, the wear track became much wider and a higher percentage of the W-C transition layer was exposed and a large amount of the worn DLC top layer became wear debris and piled up on both sides of wear track. Sliding grooves became distinct again on the W-C transition layer (Fig. 4-3 (c)) and a few fatigue cracks remained in some narrow bands between sliding grooves (Fig. 4-3 (c), pointed out by arrows). This indicates that the fatigue cracks observed in the 30,000 revolutions' sliding track (Fig. 4-3 (b)) were only formed in the top DLC coating layer and hadn't penetrated through the W-C transition layer to the substrate. After the DLC top layer was removed, fatigue cracks were produced and became distinct again in the brighter W-C transition layer. These laterally formed fatigue cracks could still be seen in the very-long-siding-distance (275,000 revolutions) wear track (see Fig. 4-3 (d)) and, after 275,000 revolutions, the coating has not yet worn through since the low friction coefficient was maintained, as shown in Fig. 4-4, and the cracked coating was still well adhered to the base. Very little pin material transfer took place since no Fe was detected by EDX (take point A in Fig. 4-3 (d) for example and its EDX spectrum is shown in Fig 4-3 (e)). Although the wear track surface seems to be very rough after such a long sliding distance, the dynamic COF curve shows that the friction coefficient kept decreasing all the way to the end of test. Two stages were found according to Fig. 4-4, which are an initial break-in period with a continuously decreasing friction coefficient, followed by a low friction (COF≈0.1) steady-state stage. Previous publications [15-17] indicated that the initial reduction in the friction coefficient during

the break-in stage has been attributed to the gradual release of hydrogen from the DLC structure at "hot spots", which produce a low shear strength layer [15].
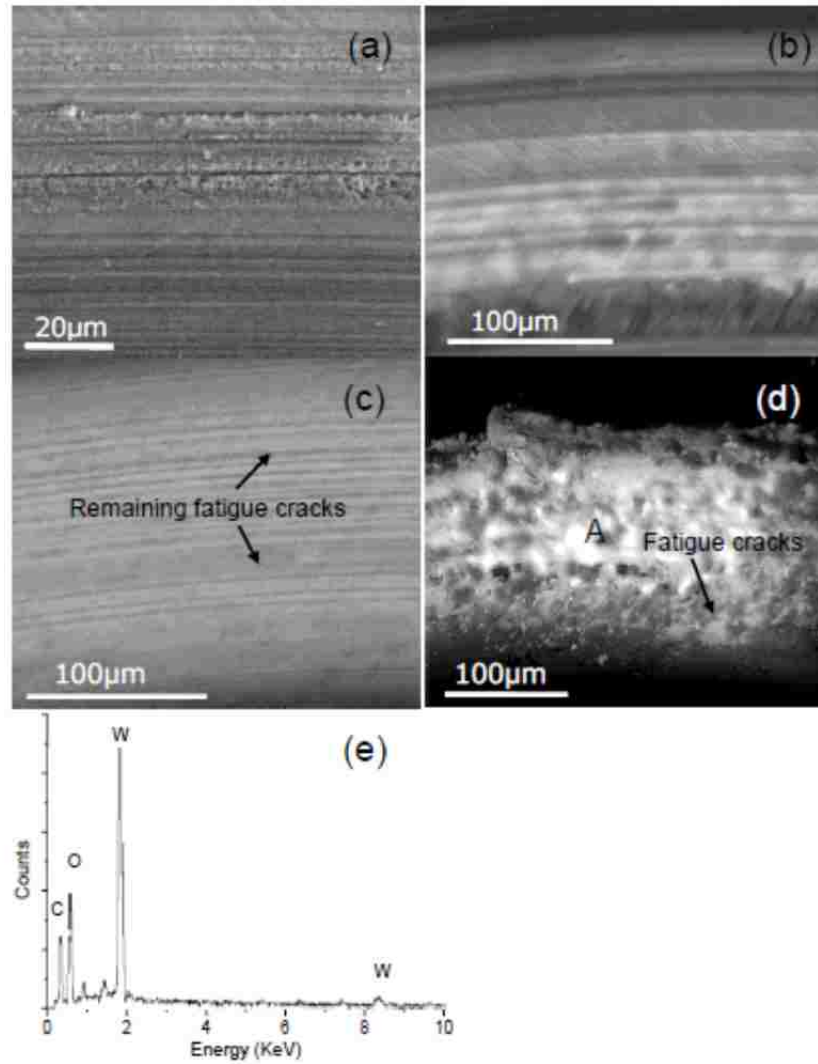
Figure 4- 3 Backscatter SEM observations of the pin-on-disc wear tracks on the DLC coating after (a) 5,000, (b) 30,000, (c) 60,000 and (d) 275,000 revolutions; (e) EDX spectrum taken inside the wear track (area A). The sliding direction was from right to left.
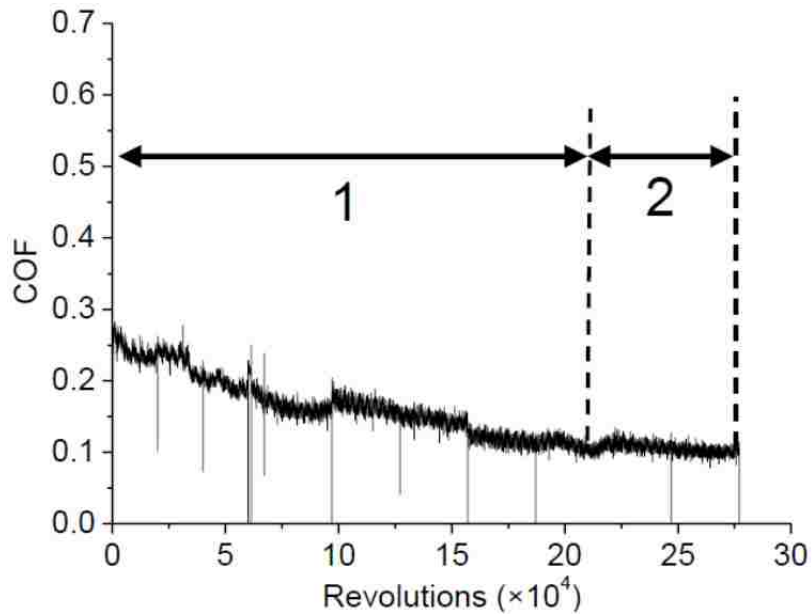
Figure 4- 4 Dynamic COF curves of the DLC coating after 275,000 revolutions of

the pin-on-disc wear test.

As-deposited DLC is thought to be a metastable structure and it tends to transform into stable graphite after an energy barrier is overcome. The present observations show that the process of sliding friction provides the energy required for the transformation of DLC $(111)_{DLC}$ (diamond cubic) to graphite $(0002)_{GR}$ (hexagonal) [15-17]. The transformation of DLC to graphite may also be facilitated by the shear stresses existing in the surface layer since the friction-induced shear forces cause strain parallel to the contacting surfaces and this strain energy produced by friction can be used to accomplish the necessary deformation for the transformation of DLC to graphite after the release of hydrogen atoms.

Instead of material transfer from the spherical counterface pin, previous experimental observations [15-17] show that during friction a carbon-rich transfer layer forms on the spherical counterface pin surface. Because the transfer layer is mainly composed of DLC, the tribological contact is modified from that of steel (material of the pin ball)/DLC to that of DLC/DLC and a significant rise in temperature rise may result at the point of contact due to the low thermal conductivity of DLC [15-17]. Therefore, the DLC coating provides a low friction coefficient, and the graphitization due to the force, strain and rising temperature results in even lower friction.

3.3. SEM observations on impact-sliding tracks

3.3.1. The evolution of fatigue cracks on the DLC coating

A. SEM observation of impact tracks under increasing test cycles.

SEM observations under low magnification of different cycles' impact-sliding tracks of the DLC coating are shown in Fig. 4-5. During the impact-sliding tests, a pre-set *Fi/Fp=200 N/400 N* combined force was used for different impact cycles. Only 10 impact cycles were used initially to study the initiation of fatigue cracks on the DLC coating, and then, the testing cycle was increased gradually to study the fatigue behavior of the coating and substrate as well as evolution of the fatigue cracks. From Fig. 4-5, it can be seen that the fatigue cracks on the DLC coating are mainly distributed in particular areas, namely: (A) the head edge, (B) the head/tail interface, (C) the tail center and (D) the tail edge. The degree of the fatigue cracks increased with the test cycles and more details of the evolution of these fatigue cracks are shown in Figs. 4-7 and 4-8 at higher magnifications.
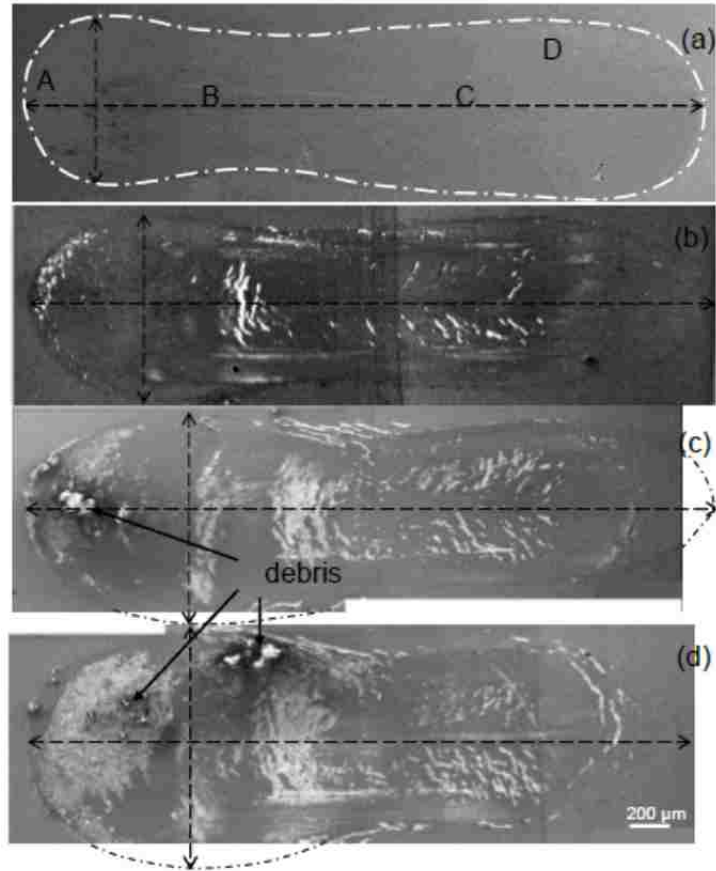
Figure 4- 5 Back scatter SEM observation of entire impact tracks on the DLC coating under a Fi/Fp=200 N/400 N impact-sliding force after (a) 10, (b) 500, (c) 1000 and (d) 1500 impact cycles.

Figure 4-5 clearly shows that the size of the head part becomes larger with the increase of impact cycles; however, the width and length of the tail part keep almost constant. Some debris was found in the head area in the 1000 and 1500 cycles' impact-sliding tracks (see Fig. 4-5 (c, d)), but because only DLC top layer materials (no Fe) could be detected by EDX on the debris the transferred materials were not from the pin ball, and so it is believed that the DLC top coating material was transferred to the ball and then returned back to the impact-sliding track.

B. Quantitative evaluation of impact tracks

With the increase of the number of test cycles, failure areas at the crater and along the sliding track became larger and connected to each other to form the shape illustrated in Fig. 4-5 (d). Based on SEM observations, the performance and degrees of failure of the DLC coating against the steel ball are summarized and evaluated in Table 4-1. This evaluation method was firstly introduced by J. Su etc. [18].

Table 4- 1 Evaluation of the degree of failure of the WC DLC coating vs. number of test cycles.

Test cycles	Head (area %) (impact)	Middle (area %) (sliding)	Tail (area %) (sliding)	Subtotal (area %) (sliding)	Total (area %) (failure)
10	1	1	1	1	1
100	3	10	3	6.5	5
500	10	30	5	17.5	15
1,000	40	60	10	35	36
1,500	60	80	15	47.5	52
10,000	90	90	20	55	67

From Table 4-1, the total failure was summed from three parts: the impact crater, the middle of the sliding track and near the tail of the sliding track. The percentages of these three different failure areas are presented using different shades in Fig. 4-6, where the trend of failure area percentage vs. the increasing test cycles can be read from the increasing of the shaded areas. The total impact-sliding-affected-area (A_t) is assumed to be 100% and the total coating failure percentages is the ratio of all the failed coating areas in the three locations (A_f) (including chipping, peeling and cracking) vs. the total impact-sliding scar surface area, A_t.
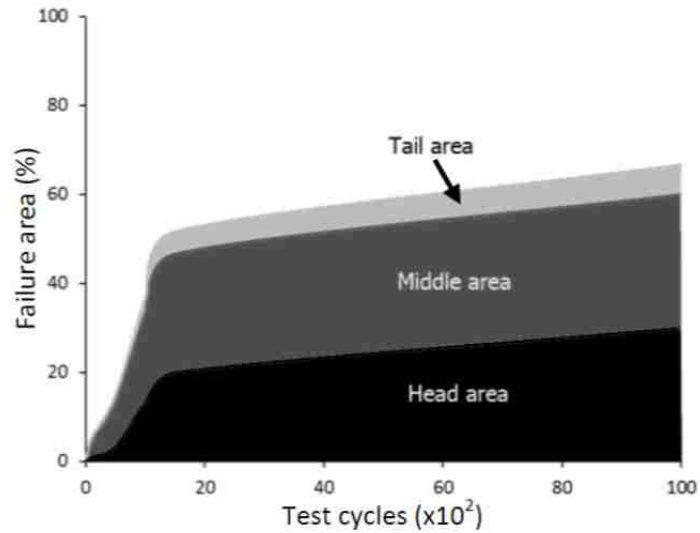
Figure 4- 6 The trend of changes of the failure area as a function of the impact-sliding test cycles. Total failure = the sum of failures at the head, in the middle and near the tail of the sliding track.

From Fig. 4-6, it can be seen that the total failure area increased rapidly in the first 1000~1500 test cycles to a degree of around 50% failure area. After that, the failure area kept increasing but at a much lower rate. Furthermore, the impact load, Fi, caused a higher degree of fatigue failure in head areas (chipping failure is predominated [18] as no substrate material was detected by EDX) on the WC DLC coating. The sliding caused great local deformation in the area (over 80% area) between the head and the tail part and a much slighter fatigue crack/failure was formed in the tail part. The large deformation was corresponding to the impact-sliding at a high inclination angle, $\theta = 20°$, and the tail end was corresponding to a low inclination angle, $\theta = 10°$. This situation was also found in our previous study on different types of coatings [20]. K.-D. Bouzaki et al. [5] published very detailed studies on different inclination angles, θ, and the corresponding value of stress in the impacted coating. They announced that in a certain range of θ the

occurring stress has a maximum value inside the coating area and tends to cause chipping failure in the coating; however, the sliding motion was not included in their research. At the end of the impact-sliding tests (after 10,000 cycles), the DLC coating was still adhered to the substrate and very little material transfer was found.

3.3.2. SEM observations of the details inside the impact-sliding tracks

The evolution of fatigue cracks on the DLC coating is shown in Fig. 4-7 and, as can be seen, after 10 impact cycles only a few short and discontinuous cracks were found near the head edge, head/tail interface and end of the tail, corresponding to Areas A, B and C in Fig. 4-5 (a) and Fig. 4-7 (A1, B1 and D1), respectively.
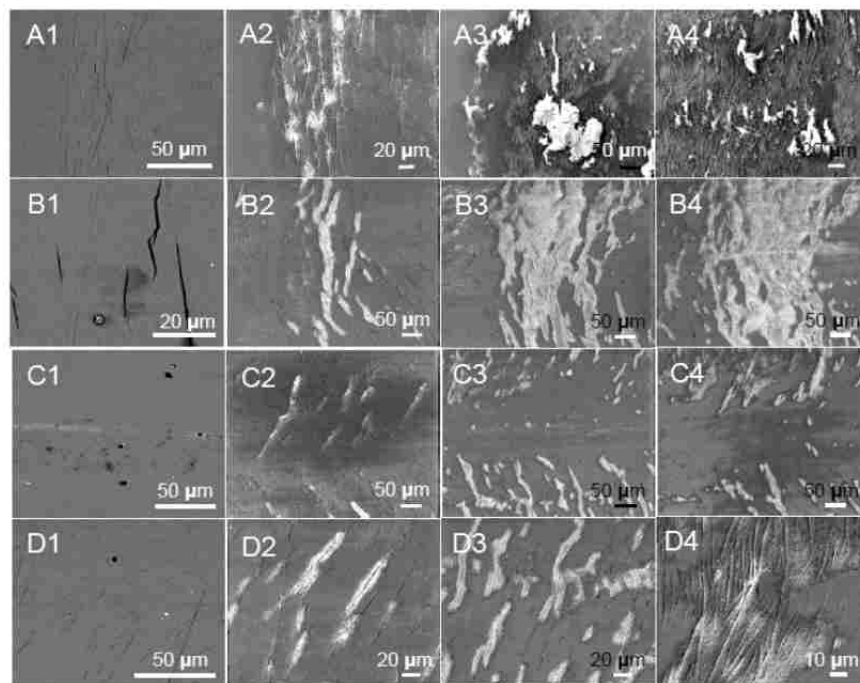
Figure 4- 7 Evolution of fatigue cracks in the (A) head edge, (B) head/tail interface area, (C) tail center, and (D) tail edge. Columns (1-4) show the test cycles numbering 10, 500, 1000 and 1500, respectively.

Those cracks were formed mainly by the bending of the coating due to plastic deformation of the relatively soft substrate under the high impact-sliding forces. One or two shallow sliding grooves could be seen in the center of the tail part (area C) and peripheral cracks which paralleled to each other could also be observed in the tail edge (area D) where the peripheral cracks appeared at a 45º tilt to the sliding direction. This type of fatigue crack was observed in our previous study[6] on TiN PVD coated M2 tool steel as well as the wear tracks in the pin-on-disc test shown in Fig. 4-3 (b, d), which was believed to be caused by the combination of compressive stresses in the coating at front of the counterface ball and tensile stresses in the coating behind the ball during the impact-sliding test. The bending of the coating due to the underling substrate deformation caused by the maximum 400 N pressing force at the end of tail resulted in low angle cracks, forming another group of parallel cracks in area D. The two kinds of parallel cracks cross each other and form a network (see Fig. 4-7 (D1) and Fig. 4-8 (e)) after a high number of test cycles. With the increase of impact cycles the discontinuous short cracks become longer and longer until the cracks meet and tangle with each other, forming a wavy network of fatigue cracks. Meanwhile, new fatigue cracks also form between previous ones until the density of the cracks reach a saturated value.
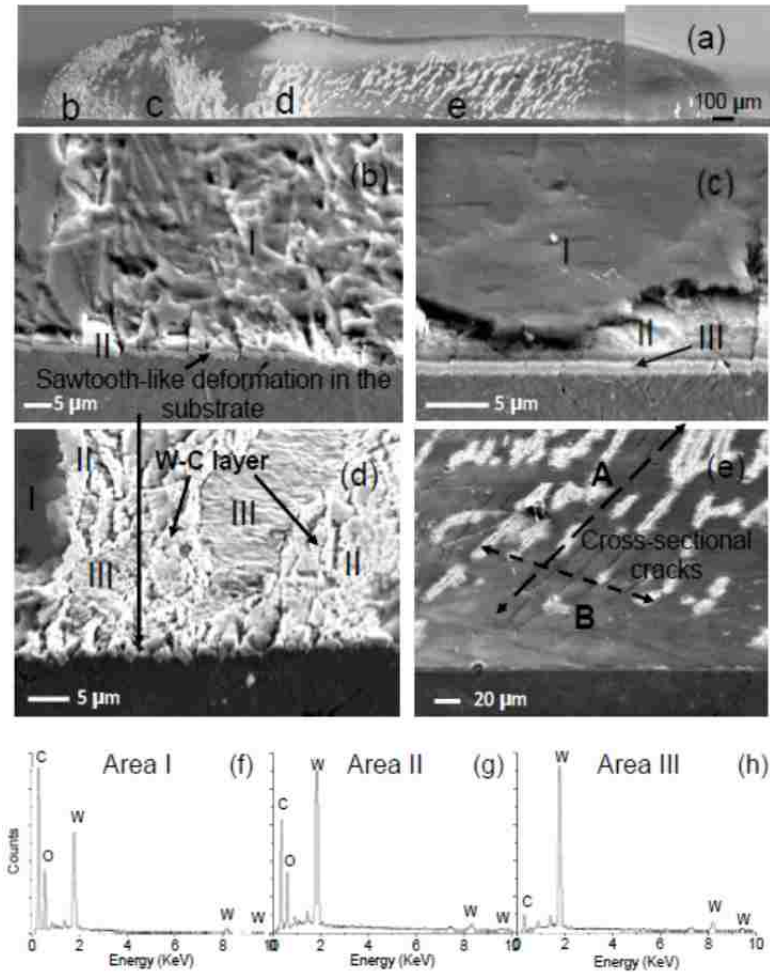
Figure 4- 8(a-e) 45º tilted SEM observations on the cut sample tested at Fi/Fp=200 N/400 N after 1000 cycles, and (f-h) EDX spectra taken on areas I, II and III, respectively.

In order to have a better view into the effects of coating fatigue cracks on the different layers of the DLC coating and substrate under the inclined impact-sliding test, the sample tested with 1000 cycles was divided by wire cutting into two parts along its axis in the direction of sliding. The cut surface of the half sample was polished and then observed by SEM at a 45º degree tilt, which is shown in Fig. 4-8 where Figs. 4-8 (b-e) illustrate the details of the impact-sliding track at high magnifications, corresponding to

the areas b, c, d and e marked in Fig. 4-8 (a). From Fig. 4-8, a two-layer coating structure with a dark grey DLC top layer and a light grey W-C transition layer is observed. There is a very thin W bonding layer in the coating/substrate boundary evidenced by a very high tungsten content detected by EDX (Fig. 4-8 (h)). The thickness of the DLC coating top layer is close to 2 μm and the underlying tungsten-carbide (W-C) transition layer has a thickness of around 1 μm, and this two-layer structure of the DLC coating is distributed evenly on the flat substrate/coating interface. The very thin (≈0.1 μm) W bonding layer serves as the adhesion improvement layer between the DLC coating and substrate together with the W-C transition layer [15]. The SEM micrographs clearly show that after the impact-sliding tests the DLC coating top layer is deformed after a certain number (100~150) of test cycles under the impact-sliding force of the counterface ball, causing the coating materials to be separated into long strips with the appearance of vertical cracks between them (Fig.4-8 (b)). These coating strips could be sunk into the substrate with one side (facing the crater center) being more significant than the other side, as shown in Fig. 4-8 (b) and Fig. 4-7 (A3 and A4). It is also believed that some coating materials transferred to the counterface ball which then helped to decrease the friction force in the contact area.

Due to the bending deformation in the head area and the tensile stress generated during the onset of the sliding motion at the beginning of the tail area [6], the cracks were formed in the head-tail interface zone (Fig. 4-7 (B1)) and quickly expanded with the exposure of the W-C transition layer (Fig. 4-8 (b-d (Area II))) and the W bonding layer (Fig. 4-8 (d (Area III))). The tilted SEM micrograph shows that the W-C layer was also broken into pieces and pressed into the substrate (Fig. 4-8 (d)) and in some areas the W-C

106

layer was torn apart and the W-rich bonding layer was squeezed upwards. In Fig.4-8 (e), two types (types A and B) of fatigue cracks can be more clearly observed which cross over each other (see arrows) at a certain angle. Type A cracks had a 45° angle with respect to the direction of sliding and were distributed asymmetrically on both sides of tail part, and the density of the cracks kept increasing with the increase in the number of test cycles. As mentioned above, these cracks were produced by the tensile stress due to the sliding motion of the ball [13, 14]. Type B cracks were not as distinct as Type A and could only be seen via the tilted SEM observation. This type of crack is due to the increased bending stress caused by the accumulation of the substrate deformation and the density of these cracks increased gradually as the track approached the end of the tail due to the increase of pressing force, Fp, during the sliding.

The EDX spectra show the different C/W ratios collected in different exposed layers in Figs. 4-8 (f-h). Almost no Fe could be detected, which means that even 1000 test cycles test the DLC coating still adheres well to the substrate, although the coating top layer is peeled off in some places, and that no material transfer of the steel ball to the DLC coating took place. There are several possible reasons for the great endurance of the DLC coating during such a high impact-sliding load. First of all, there is a great improvement of the adhesion property of coating and substrate due to the W-C transition layer and W bonding layer. Second, due to the high resilience of the DLC top layer, as indicated by recoverability during nanoindentation, the impact energy was greatly dispersed and absorbed by the peripheral coating/substrate during the impact-sliding. In this case, the actual stresses in the DLC coating was much lower than other ceramic coatings. Finally, the probable graphitization of the DLC coating (sp3 bonding to sp2

107

bonding [17]) during the sliding wear. This situation was well documented in the pin-on-disc wear test and it is very likely occurring in this inclined impact-sliding test as well. The graphitization would make the friction coefficient even lower due to the easy shear of the low-strength atomic carbon interlayer in the sp2-based graphite structure. This is demonstrated by the dynamic friction coefficient curve during the long sliding distance pin-on-disc test in section 3.2.

3.3.3. Impact test on the stainless steel substrate:

A 1000 cycles impact test under a *Fi/Fp=200 N/400 N* load was carried out on a 316L stainless steel substrate. The SEM micrographs of the impact-sliding tracks and an optical micrograph of the counterface ball are shown in Fig. 4-9.
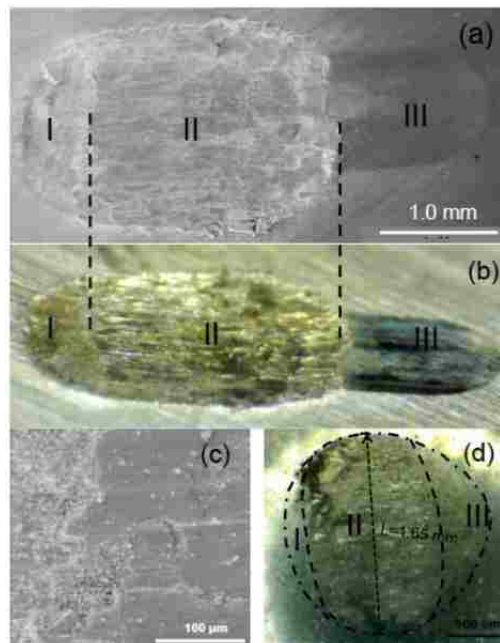
Figure 4- 9(a) SEM and (b) 45°tilted optical micrographs on impacted stainless steel, (c) sliding grooves and wear debris in the impact-sliding track and a (d) optical photo of the counterface steel ball.

As can be seen, a very wide (≈1700 μm) and deep track was formed on the stainless steel material and sliding grooves and wear debris can be observed both inside the wear track and on the counterface ball. Contrasted with the TiN and DLC coated samples the uncoated stainless steel was plastically deformed to a very large degree. From both the SEM and optical micrographs three distinct areas can be found on the impact-sliding track and counterface ball. Area I was formed mainly by the normal force, Fn, where sliding has not taken place. Area II was formed by the combination effect of Fn and Ft, where impact and sliding deformations caused wide and deep sliding grooves and a lot of wear debris inside the track. A relatively narrow and shallow tail part (Area III) was formed where a relatively slow sliding speed and a smaller Ft occurred due to the decease of the inclination angle, θ. During one whole impact-sliding cycle the contact area on the counterface ball was actually changed for a certain angle, the value of which equals to the decrease of the inclination angle θ of the sample holder. In this case, the impact-sliding test caused an egg-shaped wear scar on the counterface ball (Fig. 4-9 (d), which is much larger than those on the balls used for the DLC coating tests. The Areas I, II and III on the ball in Fig. 9 (d) correspond to the Areas I, II and III on the sample in Figs. 4-9 (a, b).

3.3.4. Discussion

As mentioned earlier, the interactive force between the ball and the coating surface can be divided into a normal force, Fn, and a tangential force, Ft. In one test cycle the ball first impacts and then pushes downward against the flat coating specimen, causing sliding between the ball and the flat specimen in the first half of each test cycle. The initial contact of the ball causes an impact crater (head) where Fn obtained its maximum value (full contact), which equals the impact force, Fi, measured by the load cell in Fig.

4-2 and no relative sliding movement (only a sliding tendency took place) between the ball and coating. Bending occurred in the peripheral and central areas of the impact crater which caused very high stresses in the coating. This bending stress was high enough to stretch the coating on its contact surface when the coating is adhered to the substrate, generating cracks in the coating at the location of maximum tensile stress. According to SEM observations, cohesive cracks were formed close to but not in the center of the head part due to the inclination angle, θ [4, 5]. Radical cracks, which were caused by cohesive and adhesive fatigue failures, formed mainly in the head edges (Fig. 4-8 b) simultaneously.

Subsequent to the initial impact, sliding occurred with a gradual increase of the normal component, Fn, from 200 N to its maximum value equal to the pressing force shown in the force curve $Fp=400\ N$ (see Fig. 4-1 (a)). During this period the counterface ball approaches to the end of the tail part, forming a long sliding track (see Fig. 4-5), the depth of which increases gradually due to the increasing Fn.

Analysis of the failure process with a ramping normal load on a ceramic coating can be divided into three stages; namely, full elastic recovery, plastic deformation and delamination of the coating [4, 5]. The sliding counterface ball deformed the coating surface both plastically and elastically where the principle of the sliding deformation was similar to the scratch test except that the initial force of sliding was not equal to zero but at a very high value ($\approx$ 200 N/cos20°=213 N) and the sample was not fixed horizontally but had a decreasing degree of angle to the vertical loading direction. After the spherical indent (head crater) was formed (full contact between the ball and coating surface), the plastic material flow pushed up material around the ball in a torus shape. As the ball

110

moved forward, a groove (tail part) was formed with increasing depth and width. The sliding spherical steel ball deformed the surface both plastically and elastically with the increase of the normal force, Fn, and the decrease of the inclination angle, θ.

After several test cycles the analysis of the sliding deformation became complicated due to the changing conditions of the contact area; a large number of fatigue cracks formed inside the impact-sliding track and the plastic deformation occurred in the coating/substrate and on the counterface ball. Graphitization also lowered the friction coefficient and, therefore, the value of the friction force during the long-period sliding wear before the failure of DLC coating. Furthermore, the top DLC layer in the track may also affect the impact-sliding behavior and material transfer from the top DLC layer to the counterface ball, which would modify the tribological contact from one of steel (material of pin ball)/DLC to that of DLC/DLC, and a significant temperature rise may result at the point of contact due to the low thermal conductivity of DLC.

In some areas of the impact-sliding track the DLC top layer coating was pushed forwards and downwards simultaneously and then piled up in the edge areas, most of which occurred in the head area. This debris, which appeared as bright agglomerates in Figs. 4-5 (c and d), was tested and found to be some oxide and amorphous carbon which had a certain amount of both sp2 and sp3 bondings [17]. Through this long-time testing, the WC DLC coating was proved to be durable under repetitive high loads.

It is important to note that the Young's modulus of this WC DLC (193 GPa) is much lower than most ceramic coatings, and even that of 316L stainless steel. According to Hertz's theory [17, 19], under an impact force equal to $Fi=200 N$, the maximum and

mean contact pressures during the initial contact of the first impact are calculated to be around *2.6 GPa* and *1.73 GPa*, respectively, which are much larger than the yield strength of 316L stainless steel. However, the relatively low Young's modulus of the DLC coating would lower the contact stress during dynamic impact because the DLC coating can absorb the energy of a shock or cushion an impact. In other words, the DLC coating has a higher resilience than other hard and tough ceramic coatings [6].

Compared with the uncoated stainless steel substrate, the mechanical and wear resistance properties of the DLC coating was significantly superior. The lubricous effect of the DLC coating is remarkable for its durability during the inclined impact-sliding tests.

4. CONCLUSIONS

A pin-on-disc test was used to study sliding wear and an inclined impact-sliding test was used to study the performance of a WC DLC coating under repetitive combined dynamic loads (impact and sliding). The nanoindentation test showed that the coating had a high hardness and a low elastic modulus with a high recoverability. The good coating-substrate combination and special characteristics of the DLC top layer provided a quite high impact-sliding wear resistance during the inclined impact-sliding tests. The observations and analysis can be concluded as follows:

1. The pin-on-disc wear test showed that the long-distance sliding between the steel counterface and DLC coating caused a decrease of the dynamic friction coefficient where the range of decrease was from 0.26 to close to 0.1. Parallel fatigue cracks first appeared in the top layer of the DLC coating and then were gradually removed by sliding

wear whereupon scratch grooves showed on the W-C transition layer. After a certain number (100~150) of sliding revolutions, fatigue cracks showed up again in the W-C transition layer. The worn top layer became debris and was pushed apart and piled up along the sides of wear track.

2. The adhesion/cohesion properties of different layers of the coating became very distinct during the inclined impact-sliding test. The top layer of the DLC coating made the sliding easier and caused less deformation and wear on the counterface ball. The W-C transition layer and the W bonding layer showed remarkably high adhesion to the substrate under such a high impact-sliding force.

3. The impact-sliding track was composed of two parts—the head part, which was mainly created by the normal component of the impact force, Fn; the tail part, which was formed by the combined effects of Fn and Ft as well as the friction force, Ff. The width of the head part was influenced by the number of impacts and the impact force, Fi, and the length of the whole sliding track was determined by the pressing force, Fp, and friction coefficient between the two contact surfaces of the coating and the ball.

The impact force, Fi, caused severe sample deformation and coating chipping in the head area of the tracks. The severity of the failure due to sliding was relatively low for the WC DLC coating due to its low friction coefficient, though it also highly depended on the degree of the inclination angle, θ.

4. The high impact force, Fi, caused bend stresses in both peripheral and central areas of the impact crater (head). The stresses were too high to be absorbed and released by the coating and consequently caused circular cracks which penetrated the whole

113

coating and also caused sawtooth-like deformation into the substrate. During the sliding after the full contact of the ball upon the coating surface, compressive and bending stresses were formed in front of the ball and tensile stress behind the ball. Two types of fatigue cracks were observed in the sliding track (tail part) which crossed over each other. In the boundary zone between the head and tail part, the DLC coating suffered greatly from the bend deformations at the head and tail areas caused by the impact-sliding. An amount of the coating material was removed and chipping and peeling of the top layer and the W-C transition layer could be observed and, in addition, W bonding layer was squeezed up and exposed (Area III in Fig. 4-8). In this case, the interface area appeared as a "white" area in SEM observations, the area of which kept increasing with the number of test cycles.

5. Chipping and peeling could be observed inside the impact area after a certain number (100~150) of impacts on the DLC coating. The crack density increased with the number of test cycles until it reached a saturated density, whereupon, failure occurred in some spots. However, no ball material transfer could be detected by EDX on the DLC impact-sliding track after up to 10,000 impact cycles. This amazing result is believed to be due to the following reasons:

(1) The low friction coefficient of the DLC top layer;

(2) The absorption and release of the impact energy by the DLC coating;

(3) Graphitization of the coating which took place during the impact and sliding;

(4) The transfer of the DLC material to the counterface ball surface, which changed the DLC/stainless steel sliding system into a DLC/DLC sliding system.

6. A very large and deep impact-sliding track was formed on the uncoated stainless steel substrate after the same test conditions, In contrast to the coated substrate. Deep sliding grooves and a large amount of wear debris and material transfer from the steel ball were observed in the track. The counterface ball was also worn to a high degree and great amount of material transfer was observed.

ACKNOWLEDGEMENTS

REFERENCES

[1]   Knotek, B. Bosserhoff, A. Schrey, T. Leyendecker, O. Lemmer, and S. Esser, Surf. & Coat. Technol. 54-55 (1992) 102.

[2]   Knotek, E.Lugscheider, F. Loffler, A. Schrey, and B. Bosserhoff, Surf. & Coat. Technol. 68-69 (1994) 253.

[3]   R. Bantle, and A. Matthews, Surf. & Coat. Technol. 74-75 (1995) 857.

[4]   K.-D. Bouzakis, A. Asimakopoulos, G. Skordaris, E. Pavlidou, and G. Erkens. Wear. 262 (2007) 1471.

[5]   K.-D. Bouzakis, A. Asimakopoulos, N. Michailidis, S. Kompogiannis, G. Maliaris, G. Giannopoulos, E. Pavlidou, and G. Erkens. Thin Solid Films. 469–470 (2004) 254.

[6]   Y. Chen, and X. Nie. Surf. & Coat. Technol. 206 (2011) 1977.

[7]   L. Wang, J.F. Su, and X. Nie. Surf. & Coat. Technol. 205 (2010) 1599.

[8]   J.F. Su, D. Yu, X. Nie, and H. Hu. Surf. & Coat. Technol., 206 (2011) 1998.

[9]   J.C. Avelar-Batista, E. Spain, G.G. Fuentes, A. Sola, R. Rodriguez, and J. Housden, Surf. & Coat. Technol. 201 (2006) 4335.

[10] S.D.A. Lawes, M.E. Fitzpatrick, and S.V. Hainsworth, J. Phys. D-Appl. Phys. 40 (2007) 5427.

[11] B. Bhushan. Handbook of micro/nanotribology, 2nd ed. (CRC Press, Boca Raton, US, 1999), pp. 250.

[12] K.W. Lee, Y.W. Chung, C.Y. Chan, I. Bello, S.T. Lee, A. Karimi, J. Patscheider, M.P. Delplankcke-Ogletree, D.H. Yang, B. Boyce, and T. Buchheit. Surf. & Coat. Technol., 168 (2003) 57.

[13] K. Holmberg, H. Ronkainen, A. Laukkanen, K. Wallin, S. Hogmark, S. Jacobson, U. Wiklund, R. M. Souza, and P. Stahle, Wear 267 (2009) 2142.

[14] G. Berg, C. Friedrich, E. Broszeit,and C. Berger, Fresenius J. Anal, Chem. 358 (1997) 281.

[15] W. Ni, Y. Cheng, A.M. Weiner, and T. A. Perry, Surf. & Coat. Technol. 201 (2006) 3229.

[16] Y. Liu, A. Erdemir, and E.I. Meletis, Surf. & Coat. Technol. 82 (1996) 48.

[17] Y. Liu, and E.I. Meletis, J. Mater. Sci. 32 (1997) 3491.

[18] http://www.a-sp.org/database/custom/Coating%20Impact%20Fatigue%20Test%20-%20Phase%20II.PDF. (14 April, 2012).

[19] http://www.tribology-abc.com/calculators/e2_1.htm, (12 December, 2011).

[20] http://www.a-sp.org/database/custom/Impact-Sliding%20Wear%20Tests%20on%20Duplex-Treated%20Die%20Materials%20-%20Final%20Report.pdf.(15 April, 2012).

CHAPTER 5 SUBSTRTE AND BONDING LAYER EFFECTS ON

PERFORMANCE OF DLC AND TIN BIOMEDICAL COATINGS IN HANK'S

SOLUTIONS UNDER CYCLIC IMPACT-SLIDING LOADS

1. INTRODUCTION

Premature mechanical failure of metallic biomaterials is often related to cyclic dynamic stresses. The complicated interaction between fatigue and corrosion in the physiological environment has been the subject of many investigations [1-6]. Degradation may lead to the failure of an implant device in two ways: first, metal ions may cause inflammatory reactions in the surrounding tissues and second, localized corrosion process may contribute to the nucleation of fatigue cracks and corrosion fatigue is often the main reason for the mechanical failure of the metallic implants [7-9]. The selection of a metallic biomaterial as a load-bearing orthopedic device should be based on a reliable analysis of relevant material properties. Contact failure wear behavior is also one of the most important issues to be addressed in this case. In addition to mechanical loads, implants are exposed to the physiological fluid that consists of a saline solution [10] including Na^+, Mg^{2+}, Cl^-, SO_4^{2-} and HCO_3^{2-}. Corrosion resistant metallic implants should ideally form a stable, compact and continuous passive oxide that prevents the underlying bare metal from coming into contact with the aggressive environment. However, there is a risk that the passive film will locally dissolve (especially in the presence of Cl^- ions), causing pits that quickly penetrate the passive film. Furthermore, cracks initiated by cyclic loading have been demonstrated to be related to the presence of pits [8]. Under aqueous conditions, small flaws initiated by corrosion propagate and form surface cracks. When cyclic loads are involved, this failure process is accelerated and

causes combined attacks due to corrosion and contact stress simultaneously, and thus the service life is reduced dramatically.

It is widely accepted that wear resistance of a surface can be largely increased by applying hard coatings such as nitrides, carbides and carbonitrides, as well as diamond-like-carbon (DLC) [11]. PVD (physical vapor deposition) and CVD (chemical vapor deposition) have been used to deposit wear- and corrosion-resistant coatings on the metallic biomaterial surfaces to improve their performance [12-14]. Currently, TiN and DLC coatings are still considered as promising coatings used for protection of load-bearing biomaterials and have been used in orthopedic prostheses, cardiac valves and dental prostheses [15, 16]. Both TiN and a-H:C DLC are found to be biocompatible and have been reported to achieve corrosion protection under most of the biomedical environments [17, 18], owing to their superior tribological and mechanical properties with corrosion resistance, biocompatibility, and hemocompatibility. Pin-on-disc tribometer and hip or knee simulator [19, 20] have been used as laboratory instruments to evaluate the coated biomaterials. However, few works were conducted to investigate the contact fatigue behavior of coatings under a load condition where impact and sliding forces can be involved in, for instance, simulating some special activities such as sport contact, jumping and trampoline game. When fatigue cracks and chipping are formed in the coatings, the interlayer and the underlying substrate would be locally exposed to the body fluid environment. The adhesion-promoting interlayer of around 100 nm thickness between the metallic substrates and the coatings is Ti- and Si- based for TiN and DLC, respectively. There is a lack of understanding about the response of coating/substrate interfaces in such stress-corrosion conditions.

As reported by R. Hauert, etc. [11], it is not adequate to measure the adhesion of hard coatings in air, which will usually result in the interface toughness, because corrosion may effect or even govern the failure processes after medical implantation. As for regular in vitro fatigue tests [20-23], e.g. hip and knee simulator, a relatively low pressure of ~20 MPa is applied, which takes long time for each test. In this paper, accelerated failure behaviors of the DLC and TiN biomedical coatings under an extremely high level of cyclic combined impact-sliding loads were investigated in both ambient and a HBSS environment. Since it is difficult to observe the corrosion behaviors during the process of impact-sliding tests, the corrosion property is studied on partially damaged coated samples after the progressive tests with different numbers of cycle. The testing contact stress was much higher than the normally applied contact pressure on biomedical implants The inclined impact and sliding motions (the inclined angle was around 20° [24]) also introduced a high shear force to the bonding layer of the coatings. Coating deterioration under the test was initiated from the fatigue cracks followed by chipping and peeling of the coating.. The local chipping and peeling of the coating result in partial exposure of the coating's bonding layer or even the substrate [24], which enabled this study to investigate their progressive corrosion responses to a simulated body fluid environment. The lubricating effect of HBSS on enhanced coating performance was also discussed.

2. EXPERIMENTAL DETAILS

2.1 Sample preparations and hardness measurement:

A recently developed cyclic inclined impact-sliding test method [24] was used for at least three times on one testing sample to limit experimental errors.

TiN and DLC coatings were prepared by electron-beam Plasma-Assisted Physical Vapour Deposition (PAPVD) and Plasma Enhanced Chemical Vapour Deposition (PECVD), respectively, using a standard commercial process at Tecvac Ltd. [12, 13]. Metallic titanium for TiN and amorphous silicon for DLC were used as the bonding layer, before deposition of the coatings. Ti-6Al-4V and hardened tool steel AISI M2 were used as substrate materials. M2 has high hardness and wear resistance [25, 26]. However, it has inferior corrosion resistance in the presence of salt water [25]. On the other hand, Ti-6Al-4V has an excellent corrosion resistance but relatively low hardness [27]. Thus, M2 and Ti-6Al-4V were utilized as two typical substrate materials to study the coating failure behaviors under inclined impact-sliding tests in ambient dry (25°C, 50~60% humidity) and HBSS solution environments. The hardness of the M2 and Ti-6Al-4V used are 8.0 GPa and 3.4 GPa, respectively [28, 29]. The elastic modulus and hardness of coatings were measured by Hysitron® nano-indentation tester are shown in Table 5-1. The indentation load was 1000 μN to make less than 30nm depth of indents on both TiN and DLC coatings to avoid substrate effects. Up to 9 points on each sample surface were measured to obtain an average value of reduced Modulus of Elasticity (E_r) and Hardness (H).

Table 5- 1 Properties of TiN and DLC coatings

Coating type	Thickness (μm)	Bonding layer material	Elastic modulus of coating (GPa)	Hardness of coating (GPa)
TiN	2.3	Ti	345.0	30.0
DLC	2.7	Si	220.2	24.7

2.2 Testing methods

2.2.1 Cyclic inclined impact-/sliding tests

A recently-developed testing method, cyclic inclined impact-sliding wear test [24, 30] was used to study coating resistance to combined dynamic impact and sliding loadings as well as the effect of substrate materials on coating performances. In each impact-sliding cycle, the forces comprise an initial dynamic impact load, Fi, and an increasing "pressing" load during the sliding motion, Fp. The "pressing" load (normal to sample surface) reaches the maximum value at the end of the sliding wear track. Fig. 5-1(a) shows the force curve of one test cycle collected by PCD30A signal collector with a 10,000 Hz sampling rate. The illustration of the setup of the inclined impact-sliding wear tester is shown in Fig. 5-1(b).
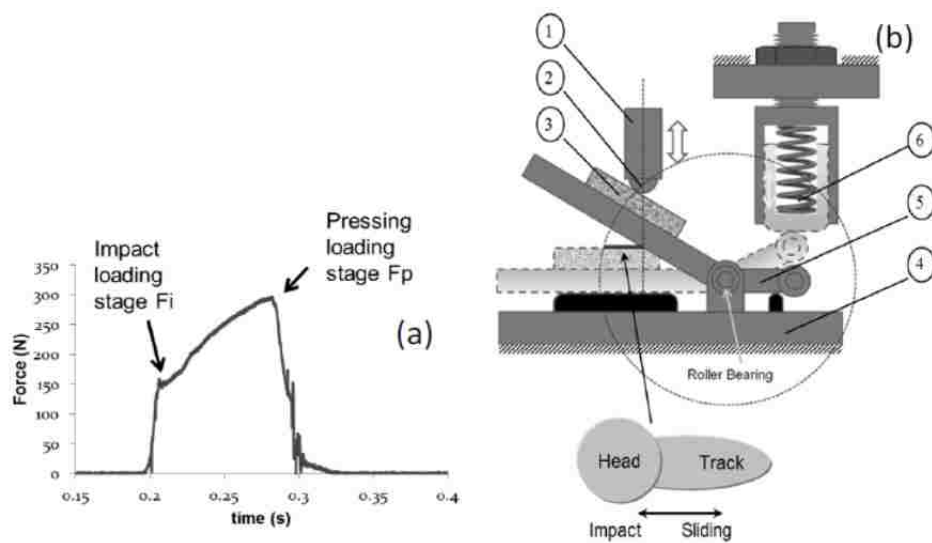

Figure 5- 1. (a) load curve in one impact–sliding wear test cycle showing dynamic impact force Fi and increasing pressing force Fp. (b) Setup illustration of inclined impact–sliding tester with a tested track, in which, 1—ball specimen drive (e.g., air

121

cylinder), 2—ball specimen, 3—flat specimen (i.e., coating), 4—rigid frame, 5—

rotatable rocker, and 6—return drive (e.g., spring).

During the test, the sample was fixed on an inclined sample holder. The sample

holder functions as a rocker which can rotate around a fixed roller bearing due to the

pressing of the counterface ball when the piston in an air cylinder moves up and down. In

each test cycle, the ball first impacts and then pushes downward against the flat coating

sample, causing a sliding track on the sample surface. A spring, which acts as a drive

device for reversing movement, is fixed on the other end of rocker arm. It can rotate the

rocker back to its initial position when the piston moves upward. The loads applied

through a ball(in this case, steel ball,10 mm in diameter, AISI 52100 steel, hardness:

HRC 58-62) could be pre-set before the actual test. In this work, the loads used in each

impact-sliding cycle were 140 N for the dynamic impact and 300 N for the maximum

pressing force, i.e., F_i = 140 N, Fp_{max} = 300 N. The F_i caused a near-circular crater

(head) which was partially overlapped by the following sliding track (tail) caused by Fp

(see Fig. 5-1(b)). Endurance of the tested coating/substrate systems depends on its

resistance to the debonding of the coating from the substrate (adhesive failure or peeling),

fracture of the coating (cohesive failure or chipping) or substrate plastic deformation

[30]. The typical failure modes including fatigue cracking, chipping, peeling and material

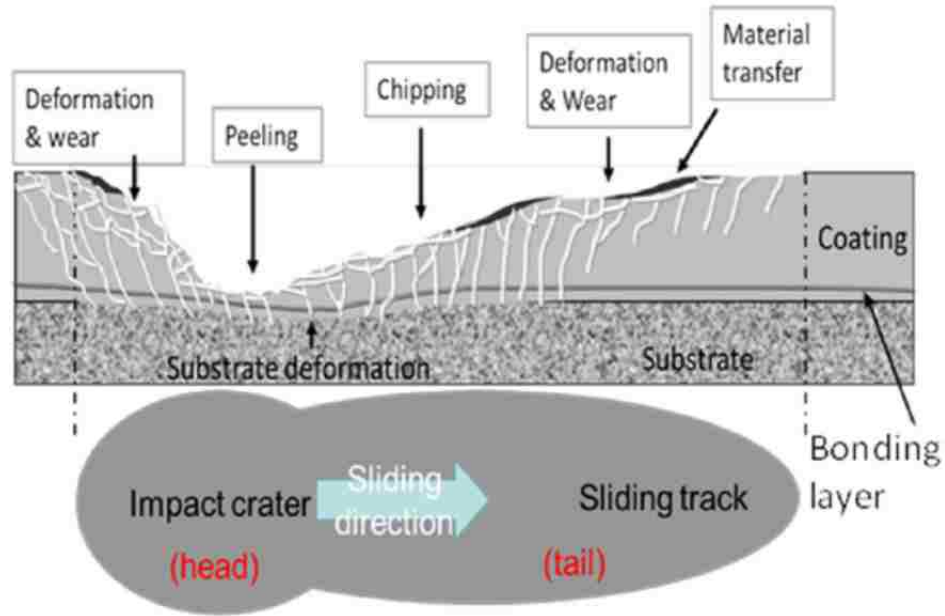transfer were illustrated in Fig. 5-2.

Figure 5- 2 Schematic illustration of typical failure modes (chipping, peeling and material transfer) on damaged coating.

In this study, we defined the failed coating area as the top coating layer was peeled off with the exposure of bonding layer or substrate. Before the top layer peeled off, fatigue cracks and chipping could have already formed inside coating area, but coating is still adherent and protecting the substrate. The impact-sliding wear tests were conducted at dry air condition (25°C, 50~60% humidity) and in a HBSS (Hank's Body Simulated Solution) solution. The salt solution can work as a lubricant to decrease the friction coefficient under sliding loads but may also negatively cause corrosion issues to the materials. After cyclic testing in a range of 50 to 5000 cycles (the number of test cycles were decided by some trial tests to obtain certain degrees of coating failure under certain test conditions), the degree of failure was evaluated based on an approximate evaluation of failure area percentage as well as the corrosion resistance properties of the damaged coating, bonding layer and substrate system

123

2.2.2 Pin-on-disc tests

Since the tribological property of the coatings and potential lubricating effect of the HBSS were believed to be responsible for the difference in coating failure behaviors in the impact-sliding tests. It was necessary to study the effect of coefficient of friction on the coating failure behavior under a sliding motion. In this case, pin-on-disc tribotests were carried out using 5N normal load applied by a 5.5 mm AISI 52100 steel pin ball under both dry and HBSS lubricated conditions. The sliding velocity was 0.075m/s. The coefficient of friction was recorded vs. revolution number of the rotation.

2.2.3 Corrosion tests

Potentiodynamic polarization tests were carried out on partially damaged coatings in the HBSS solution at 37°C and on undamaged DLC coating for comparison. An Ag/AgCl electrode in saturated KCl solution was used as a reference electrode and platinum as a counter electrode. The corrosion tests were carried out without plunging any gas into the solution. The obtained corrosion curves were analyzed for investigation into the electrochemical response of coatings that had been tested with a certain number of impact-sliding testing cycles. A circular area of 1cm^2 was the exposed area of tested sample surface to the corrosive media in the potentiodynamic polarization test. For a damaged coating, the damaged areas in the tested track after the impact-sliding tests were totally included in that 1cm^2 exposed area; in this case, the damaged areas was believed to be dominant in corrosion behavior of the circular coating tested area.

2.2.4 Observations

Optical microscopy (OM) and scanning electron microscopy (SEM) with Energy-Dispersive X-ray (EDX) (SEM JOEL 2100, using 15 kV operating voltage) analysis were used to make observations and evaluation of the tested coating surfaces.

3. RESULTS AND ANALYSIS
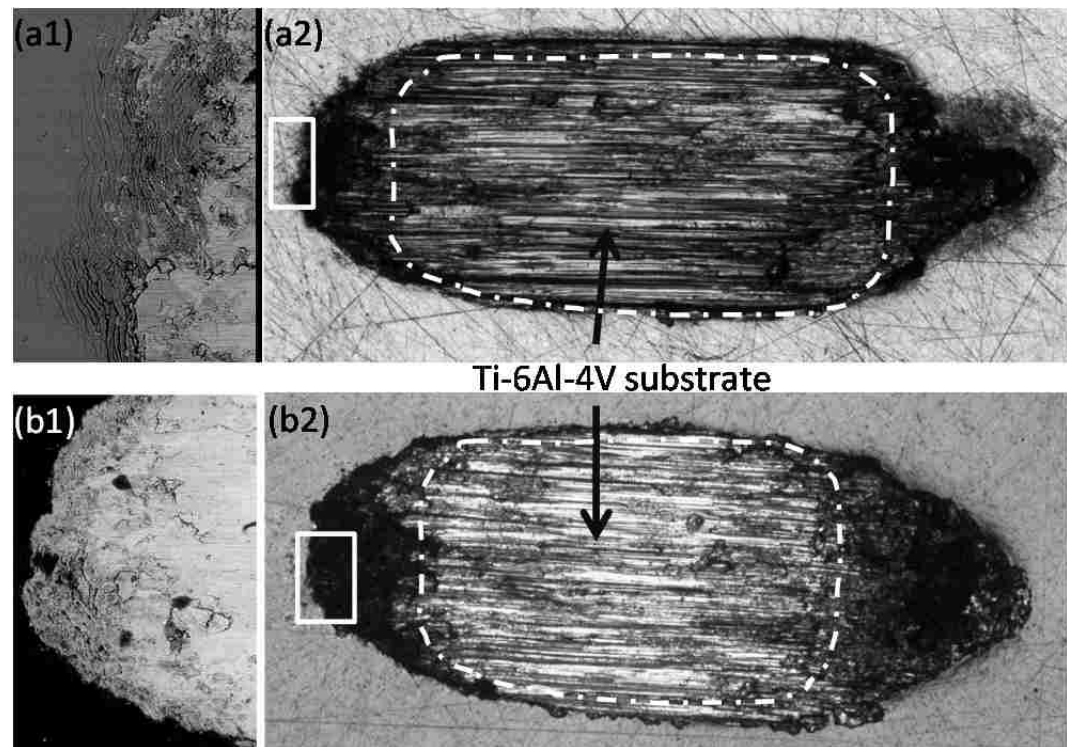
3.1 Impact-sliding tests on coated Ti-6A-4V

Figure 5- 3 Optical and SEM micrographs of (a) TiN coating and (b) DLC coating on Ti–6Al–4V alloy under Fi = 140 N, Fp = 300 N,50 cycle test in a dry condition. (i and ii) Fatigue cracks near the edge area of the track.

Fig. 5-3 shows the 50 cycles' test results on (a) TiN and (b) DLC coated Ti-6Al-4V samples under a $F_i = 140\ N$, $F_p = 300\ N$ testing load in dry air condition. In this paper, all the head areas of the tested track are shown in the left side of the images, and

the sliding direction was from left to right. It can be observed from Fig. 5-3 that after 50 cycles' test, the failure areas of both DLC and TiN coatings on Ti-6Al-4V exceeded 90%, the substrate was considerably deformed, and wide and deep wear tracks appeared. Significant amounts of material transfer from the steel pin ball could be revealed by EDX analysis. Fatigue cracks, similar to those reported in a previous publication [24], formed at the early stage of the test (see the insertion of i and ii in Fig. 5-3). The low substrate hardness should be responsible for the large degree of coating failure and considerable plastic deformation of the substrate under the extremely high loads in the dry testing condition. However, the tests were carried out under contact stresses that largely exceeded a normal operation stress of bio-implants. The contact stress (Hertzian stress) of the first impact load can be calculated based on the mechanical properties of steel (pin ball) and coating materials. The maximum Hertzian contact stresses on TiN and DLC under the impact force F_i=140 N were around 2700 MPa and 2400 MPa, respectively [31]. The coatings on relatively soft Ti alloy substrate could not sustain such high impact stresses and failed quickly. Failure modes such as chipping and peeling [30] took place in the head area of the track and resulted in the increase of the surface roughness and thus friction. Finally, the wear debris generated from the damaged contact area could accelerate the coating failure during the following sliding motions in the tail part of the track.
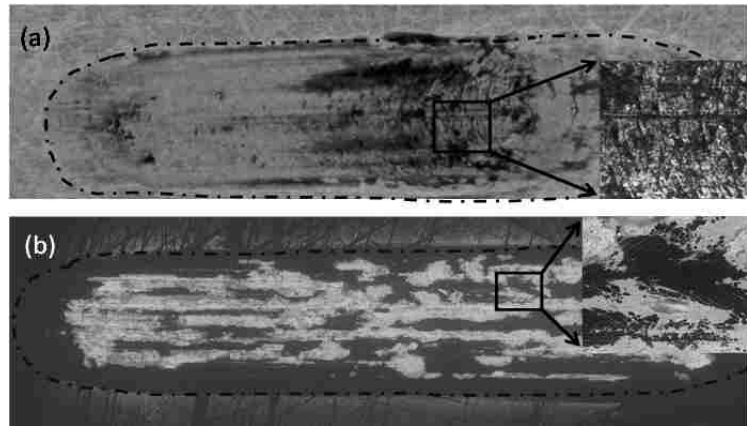
Figure 5- 4 Optical and SEM micrographs of (a) 5000 cycles' tested track of TiN coating and (b) 2000 cycles' tested track of DLC coating on Ti–6Al–4V alloy under Fi = 140 N, Fp = 300 N, in a HBSS lubricated condition.

Fig. 5-4 shows results of TiN and DLC coated Ti-6Al-4V samples tested in HBSS wet environments under the same loading condition (F_i = 140 N, F_p = 300 N). After a 5000 cycles test, less than 10% of the tested area was failed on TiN coating while more than 25% failure area was observed on DLC coating after 2000 cycles test. For TiN coating, the cracks and failed areas were not distributed evenly on the impact-sliding track. Few cracks were formed at the center of head area. Parallel fatigue cracks [24] were generated, due to the sliding motion of the steel pin ball in the tail area (see insert in Fig. 5-4(a)). The density of fatigue cracks increased along the sliding track (tail) from left to right due to the increasing of the pressing force Fp to its maximum. However, due to the excellent bonding strength, the top TiN coating was remained to be protective in most of areas of tested track after the 5000 cycles' test although a high density of cracks could be found at the end the track (see Fig. 5-4(a)).

On the DLC coating, chipping and peeling took place all around track area especially along the sliding grooves (Fig. 5-4(b)). From a higher magnification image

127

inserted in Fig. 5-4(b), it can be observed that the coating was peeled-off from the areas where the fatigue cracks intersected. High Si content together with chemical composition of Ti-6Al-4V could be was detected from these damaged areas, such as area A in the insert of Fig. 5-4(b). Material was transferred from the steel pin ball and filled in some exposed areas, which showed a high Fe content, for instance, area B in the insert.

In order to have better understanding of HBSS effect on the impact-sliding test in terms of the sliding friction, pin-on-disc tribotest was carried out using a steel pin ball under a 5N normal load in both dry and HBSS conditions. The coefficient of friction (COF) vs. the rotating revolutions of all tested samples were recorded and shown in Fig. 5-5.
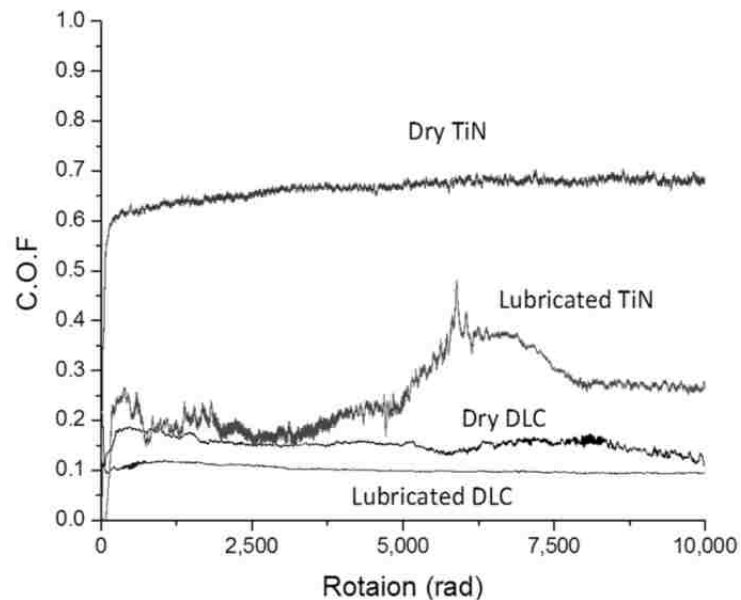

Figure 5- 5 COF vs. sliding revolutions of pin-on-disc tests on DLC and TiN coatings under dry and HBSS lubricated conditions.

From the COF curves vs. revolution of rotation, it was obviously that the HBSS solution did have a positive effect on coated Ti-6Al-4V during the sliding, especially on

TiN coating. The COF of TiN coating decreased from 0.65 to around 0.2; the HBSS showed a lubricating effect. The large fluctuation in the curve of TiN under the HBSS condition (at around 6000 revolution) was caused by addition of HBSS solution, at that time, which may flush away the wearing debris from the sliding track. After that, the COF was stabilized at a value around 0.25, which was still much lower than the COF measured in the dry sliding test condition.

For the DLC coating, HBSS decreased the COF from around 0.15 (in dry) to less than 0.1. However, when the sliding distance was long enough, the COF differences became less significant. The decreased COF at the dry test condition would be due to graphitization which took place on the amorphous carbon coating, the near-graphite structure benefited in decreasing COF under the sliding motion at the dry condition.

The lower COF due to the HBSS was believed beneficial to the improved coating performance as shown in Fig. 5-4(b), compared to the dry test result in Fig. 5-3(b2).

3.2 Impact-sliding tests on coated M2 substrate

The same loadings were applied to the TiN and DLC coated M2 in both dry and HBSS lubricated conditions. Fig. 5-6 shows the micrographs of the samples tested in the dry environment after 1000 test cycles. In contract to the test results of coated Ti-6Al-4V (Fig. 5-4), coated M2 can sustain much longer test cycle in the dry condition. Although cracks were formed in the whole contact area, a lower percentage of failure area (i.e. coating peeling), was found on both coatings. The hard M2 substrate provided a loading supported to coatings better than the Ti alloy substrate against high dynamic loads. Dark dashed lines in the Fig. 5-6 indicate the tested zones on the sample surfaces where the

substrate was exposed after coatings were peeled-off. The failed areas were distributed mainly on the head/tail boundary regions where the combined impact and sliding motions (normal and tangential loads) caused a greater damage to the coatings, compared to almost the pure impact in the center of the head area and pure sliding in the tail part. However, with the increase of test cycle (>1000), the failed areas gradually enlarged and extended to the end of the tail area. Fig. 5-6 shows that after 1000 test cycles, the failure percentage of the two coatings was almost the same, at a value around 25%. Cracking, chipping, peeling and material transfer could be found in local areas of the tested track. The insert images in Fig. 5-6 (i and ii) are the fatigue cracking formed in the damaged area.
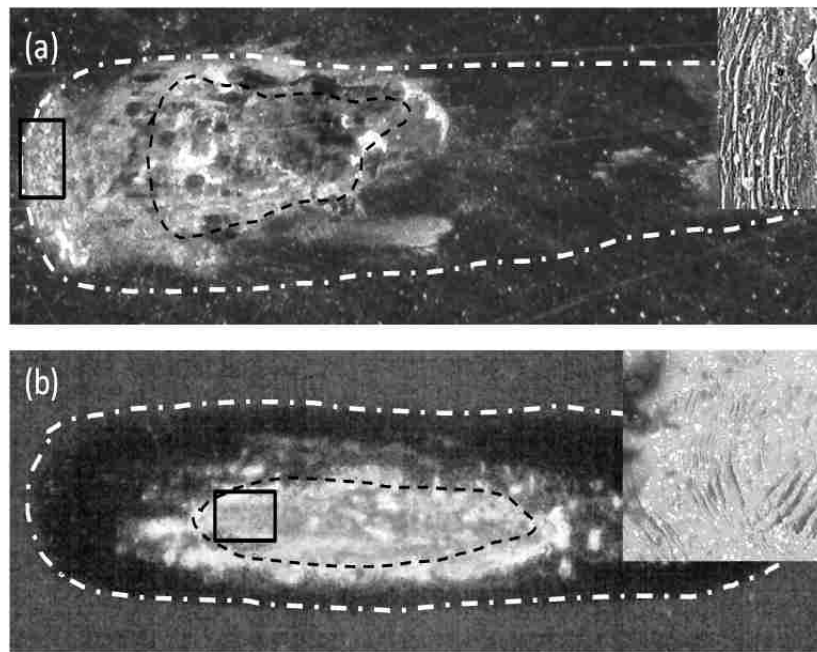

Figure 5- 6 Optical and SEM micrographs on (a) TiN coating and (b)DLC coating onM2 substrate under Fi = 140 N, Fpmax = 300 N,1000 cycle test in a dry condition. Inserts i and ii are the framed areas at high magnifications.
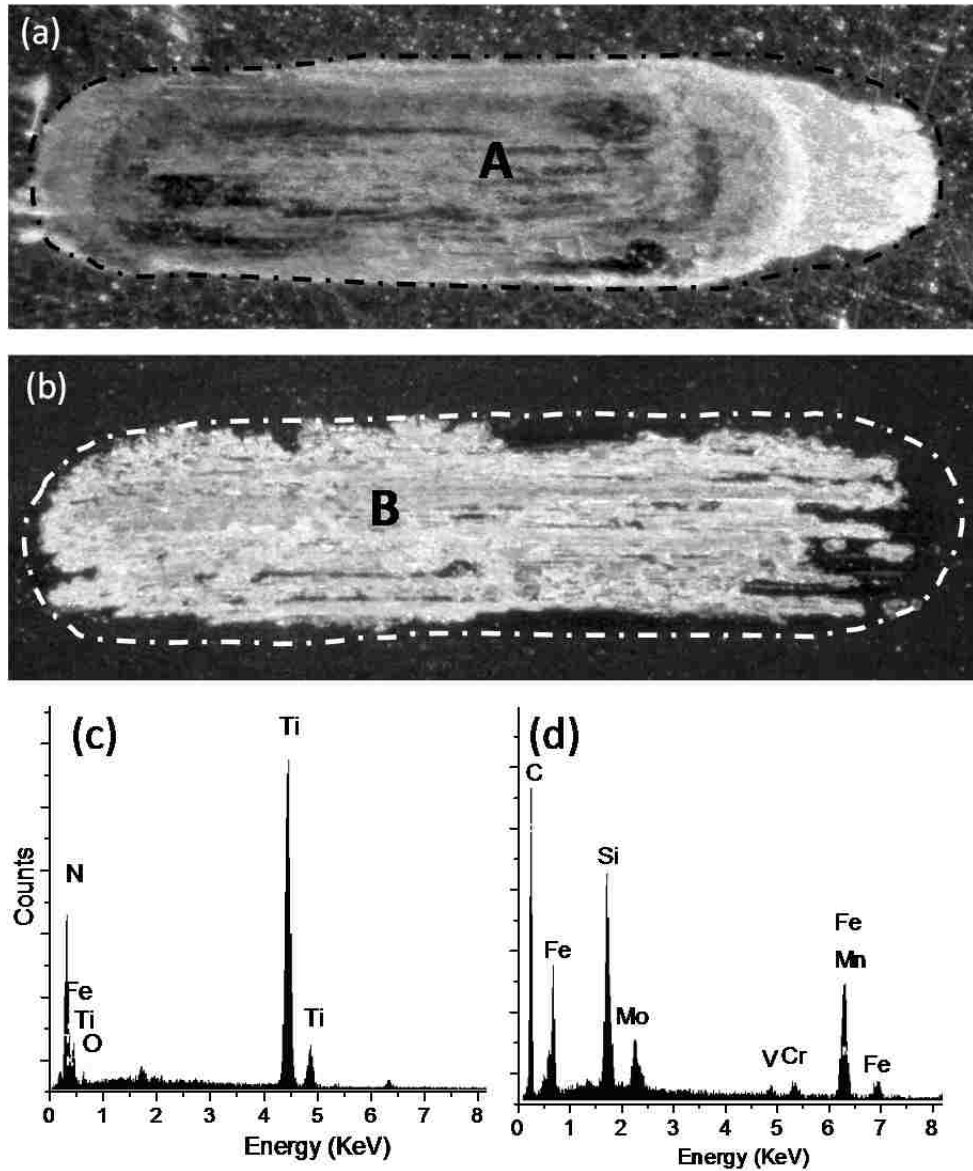
Figure 5- 7 Optical micrographs of (a) 5000 cycles' tested track of TiN coating and (b)1000 cycles' tested track of DLC coating onM2 under Fi = 140 N, Fp = 300 N, in a HBSS lubricated condition. (c, d) EDX spectra on point A of (a) and point B of (b), respectively.

Fig. 5-7 is the observation of impact-sliding tracks tested under the HBSS lubricated conditions. A 5000 cycle test was carried out on TiN coated M2 while only

1000 cycles were applied on DLC coated M2 (Figs. 5-7(a, b)). On one hand for TiN coating case, the relatively soft alloy Ti-6Al-4V was more likely to yield under cyclic high loading conditions. Parallel cracks were formed on the TiN coating surface due to the plastic deformation of the substrate (Fig. 5-4(a)). On the other hand, M2 had a much higher hardness and provided better support to the TiN coating, thus very limited damage could be observed on TiN coated M2 and local chipping and peeling were not obvious after the test. The EDX spectrum (Figs. 5-7(c, d)) collected from the inside of the impact-sliding track (area A in Fig. 5-7(a)) shows the TiN coating inside the track area was still in good condition. The light amount of iron and oxygen (Fig. 5-7(c)) was due to material transfer from the steel pin ball which was likely corroded and formed FeO_x in the HBSS environment.

For the DLC coating case, over 90% coating area failed after only 1000 cycles of the test in the HBSS solution (see Fig. 5-7(b)). The degraded coating performance (Fig. 5-7(b)), compared to the test result from a dry condition (Fig. 5-6(b)), would be attributed to the low corrosion resistance of the M2 substrate. After the DLC coating had fatigue cracks during the test, the cracks would penetrate the Si bonding layer and the HBSS reached to the substrate. The M2 was corroded with formation of corrosion products which caused corrosion-induced stress underneath the coating layer and thus weakened the bonding strength. The applied stresses during the test would accelerate the corrosion. This stress-corrosion interaction caused the large degree of coating failure. EDX spectra were collected in the area B of Fig. 5-7(b) and shown in Fig. 5-7(d). Large amount of Mo, V, Cr and Mn were found from the exposed substrate.

132

The test results above are likely related to the characteristics of the bonding layers of TiN and DLC coatings. As a standard coating deposition process, there is a thin bonding interlayer (Ti for the case of TiN and Si for DLC) with a thickness in a range of 100-200 nm that was first deposited and followed by 2.7 μm thick TiN and 2.3 μm thick DLC coatings on the top. The Ti bonding layer is metal-based, which may be able to impede extension of the coating cracks into the substrate. When the bonding layer is Ti, it may also help in some degree to insulate the substrate for the corrosion media since Ti has a good corrosion resistance in a HBSS environment. When the bonding layer is Si-based, the brittle bonding layer may allow coating cracks to pass through, which would cause a quick degradation when the substrate is a corrodible M2 steel as described in section 3.2. Bearing this assumption in mind, the corrosion tests in the following section were performed on partially damaged coatings which exposed the bonding layers to certain degree. The role of the bonding layers in coating performances during tests in the HBSS corrosion environment was thus studied.

3.3 Effect of the bonding layers

In order to better understand the corrosion response of the bonding layer/substrate system to the HBSS under the impact-sliding forces, potentiodynamic polarization tests were introduced and applied to both undamaged coatings and damaged coatings with different degrees of failure. Before the potentiodynamic polarization tests, impact-sliding tests with different testing cycles were carried out to observe coating progressive failures in a step by step way. For the case of M2 substrate, the selected test cycles were in a range of 500 to 800. Fig. 5-8 shows the gradually increased coating failure on the DLC

coated M2 after the tests in the HBSS. The dashed lines circled the tested areas on the coating surface.
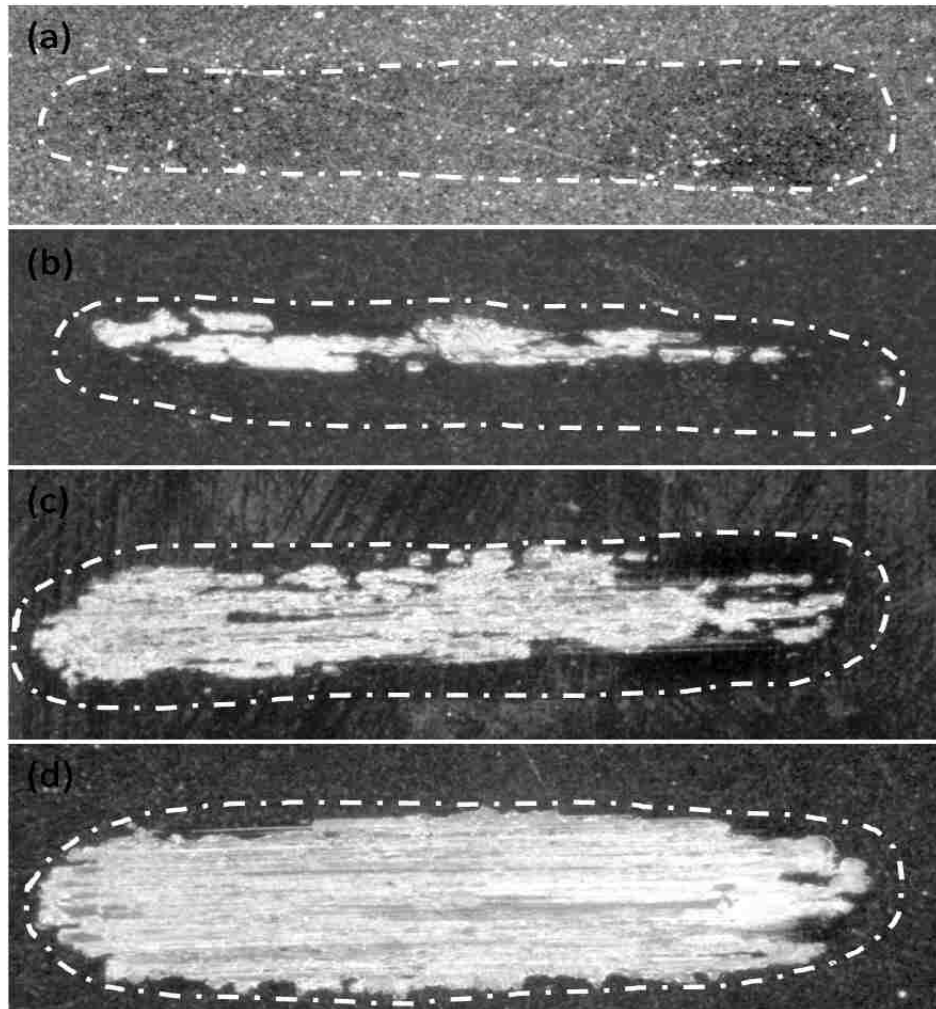

Figure 5- 8 Optical micrographs of DLC coated M2 tested with the increasing cycles of (a) 500, (b) 600, (c) 650 and (d) 800 cycles.

From the optical micrographs, it can be seen that the coating remained in good condition up to 500 testing cycles (Fig. 5-8(a)) under the combined impact-sliding loads. After 600 cycles (Fig. 5-8(b)), the localized coating failure was initiated, and the fatigue cracks quickly propagated and extended in the track area when another 50 cycles was

added (Fig. 5-8(c)). After 800 cycles, around 90% DLC coating was peeled-off. A further increase in test cycles was just to widen and deepen the track onto the M2 substrate. This observation indicated that there was a critical test cycle number under a certain loading condition for the DLC coated M2 in the HBSS environment. After this critical number of cycles (in the range of 600-650 in this test) was reached, the coating failed abruptly, likely due to the cracks that started to penetrated the bonding layer and caused corrosion to be occurred underneath (i.e., M2 substrate in this case). Compared to a much better performance of DLC coated M2 at the ambient dry test condition, the degraded coating in the wet testing condition might be caused by the HBSS which led to corrosion and greatly weakened the interface strength resulting in the accelerated coating failure process. When the HBSS touched down to the substrate, the corrosion behavior of the substrate would show up during the following corrosion tests.

Fig. 5-9 shows the corrosion polarization curves of damaged and undamaged DLC coatings as well as two substrate materials as references. Table 5-2 summarizes corrosion density (I_{corr}), corrosion potential (E_{corr}) and passive current density (I_{pass}) of the tested samples. The data would be corresponding to the electrochemical corrosion behavior of the material that had contacted with the HBSS solution. If more than one material was involved, the less corrosion resistant material would dominate the corrosion results shown in the table. Particular attention can be placed on the values of E_{corr} and I_{pass} since that information can be used as an indicator of which material had a significant interaction with the corrosion medium HBSS during the progress of the impact-sliding tests. The coating damage during the tests included coating fatigue cracking, top coating

135

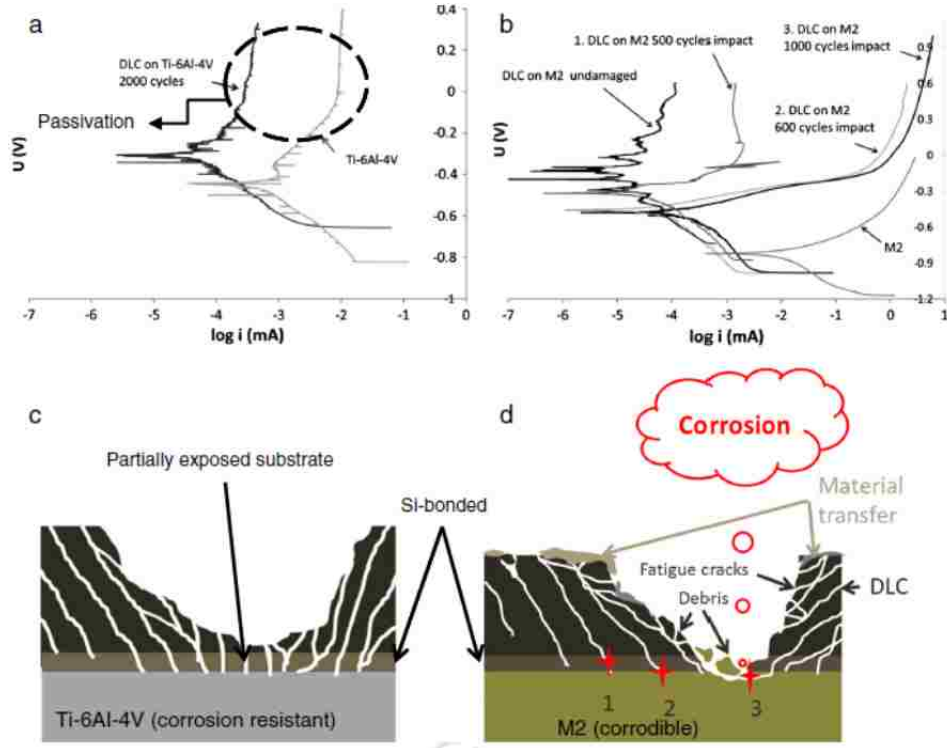layer chipping (to expose the bonding layer), and coating peeling at the substrate interface [30].

Figure 5- 9(a, b) Potentiodynamic polarization curves of DLC coated Ti–6Al–4V andM2 (coated and uncoated) tested in a HBSS solution at 37 °C; (c, d) schematic illustration of partially failed DLC from cross-sectional way.

Generally speaking, when the fatigue cracks formed, the corrosion medium could penetrate the top coating layer and contact the bonding layer. When the top coating layer was chipped after the fatigue cracks formed a network [30, 33], the bonding layer was exposed to the corrosion medium. After the coating peeling occurred, the substrate would be uncovered. Therefore, when the corrosion resistant ceramic coating was damaged gradually from fatigue cracking to chipping and peeling, the I_{pass} values would increase and E_{corr} would decrease to the level of degree which was similar to corrosion property of

the bonding layer or substrate. This was also true even if the coating cracking was the only failure mode but the cracks were deep and expended to the bonding layer and substrate.

Table 5- 2 Results of electrochemical corrosion tests in a HBSS solution at 37 ℃.

Test samples	Substrate/test cycles	I_{corr} ($\mu A/cm^2$)	E_{corr} (V)	I_{pass} ($\mu A/cm^2$)
Si bonded DLC coating	Undamaged DLC (M2 substrate)	0.00316	-0.118	0.057
	M2 substrate, 500 cycles (Fig. 5-6 (a))	0.0079	-0.316	1.698
	M2 substrate, 600 cycles (Fig. 5-6 (b))	0.016	-0.436	334
	M2 substrate, 1000 cycles (Fig. 5-5 (b))	0.083	-0.469	1349
	Ti-6Al-4V substrate, 2000 cycles (Fig. 5-2 (b))	0.023	-0.313	0.253
Ti bonded TiN coating	Undamaged TiN (M2 substrate)	0.037	-0.347	2.042
	M2 substrate, 4000 cycles (similar to Fig. 5-5 (a))	0.058	-0.235	0.589
	Ti-6Al-4V substrate, 5000 cycles (Fig. 5-2 (a))	0.135	-0.236	0.589
Substrate materials	M2	2.82	-8.17	2805
	Ti-6Al-4V	1.104	-0.45	8.51

In Fig. 5-9(a), Ti-6Al-4V and DLC coating on Ti substrate (see dashed line circled area in Fig. 5-9(a)) showed good corrosion resistance and passivation property. As mentioned in section 2.2.3, the test area in the corrosion test was 1cm^2, which included the test wear track. The appeared corrosion data would reflect two parts: the undamaged coating and the substrate where the top coating layer was damaged. This should explain why the partially damaged coating after 2000 cycles' test was still better than the substrate shown in corrosion curves.

From Fig.5-9(b) and Table 5-2, the undamaged DLC coating (on M2) showed the lowest corrosion current 0.0032 $\mu A/cm^2$ since a DLC based coating usually has a high corrosion resistance in HBSS [32]. After the coating was damaged, the corrosion behavior significantly changed. Schematic illustrations in Figs. 5-9(b) and (d) indicate that corrosion can occur at three possible areas inside a damaged coating: 1) when cracks only reach to the bonding layer, the bonding layer may still protect the substrate from corrosion; 2) when cracks had penetrated the bonding layer and caused the corrosive media touched the substrate in some localized areas, the substrate corrosion behavior became obvious ; and 3) after the coating in the impact-sliding wear track was peeled off, the totally exposed M2 substrate had a poor corrosion resistance, similar to that of an uncoated M2 material. The corrosion curves 1-3 in Fig. 5-9(b) were corresponding to the above three situations. After 500 cycles' test on DLC-coated M2 (curve 1), the I_{corr} increased by 2.5 times, indicating the coating started to initiate fatigue cracks. The E_{corr} decreased toward the corrosion potential of a steel (see M2 curve in Fig. 5-9 (b)). I_{pass} was also significantly increased, however, the fatigue cracks exhibit small features (in sub-micron scales) which allowed accumulation of corrosion product in the cracks for passivation. The corrosion product, on the other hand, started to weaken the interface strength. As a result, an additional 100 cycles' test (i.e., 600 cycles -curve 2, after corrosion) led to considerably decrease of the E_{corr} (-0.436V) and an increase of the I_{pass} (334 $\mu A/cm^2$), which means that the M2 substrate was largely exposed to the corrosion medium. The substrate explosion could be observed from Fig.5-11 (a) with an EDX spectrum (Fig. 5-11 (c) obtained inside the test track-area A of Fig. 5-11(a). After 1000 cycles of tests (curve 3) on DLC-coated M2, the I_{pass} reached to a very large number

(1349 $\mu A/cm^2$), suggesting that the substrate was lack of protection due to a severe coating failure. Referred back to Fig. 5-8, the tested coating samples were shown with a progressive coating failure process. The Si bonding layer was corrosion-resistant but brittle, which could not act as a barrier layer to corrosion and cracking. For such a case, the corrosion property of the substrate became critical. The M2 substrate was inferior in corrosion property; the corrosion medium was detrimental to the coated sample performance after the fatigue cracks were formed. To overcome this problem, it is necessary to select a corrosion resistant substrate as the case of Ti alloy. The HBSS corrosion effect would not be significant when the substrate had a good anti-corrosion property.

To verify the effect of the Ti bonding layer, TiN-coated M2 and Ti-6Al-4V samples were also tested in the HBSS after 4000-5000 cycles of impact-sliding tests (see Fig. 5-10 and Table 5-2). Both cases had almost the same E_{corr} (-0.235 V) and I_{pass}(0.59 $\mu A/cm^2$) and are very similar to the corrosion behaviors of undamaged TiN coating in Fig. 5-10 (c), although the Ti bonding layer may also affect the corrosion behaviors of partially damaged TiN coatings. This suggests that up to the 5000-6000 cycles' tests, the M2 substrate was not yet obviously exposed to the corrosion medium as indicted in Fig.5-11 (d) with the EDX spectrum obtained inside test track at area B of Fig. 5-11(b). The Ti bonding layer had functioned as an impeding layer which provided a barrier to corrosion attack and cracking propagation for the corrodible M2 substrate. The ductile and corrosion resistant adhesive bonding layer was beneficial to the less corrosion resistant M2 substrate.
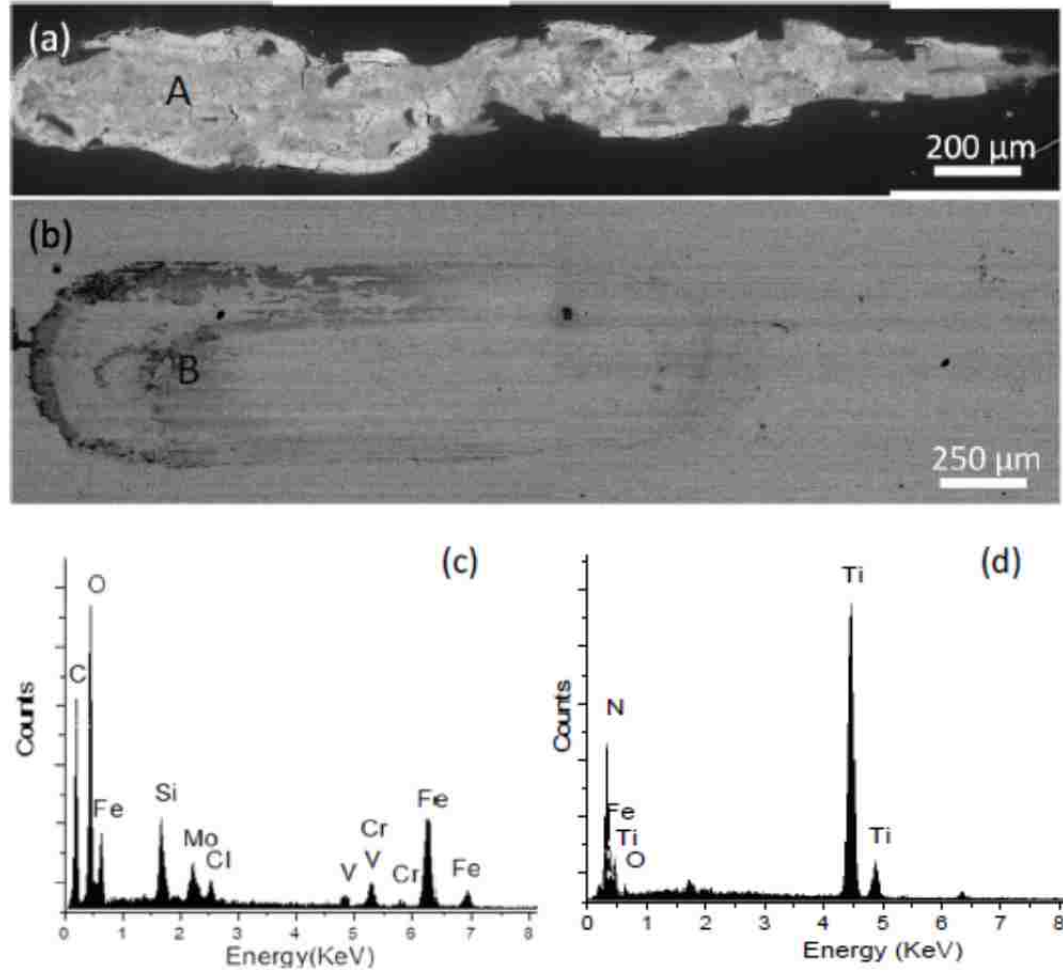
Figure 5- 10 SEM observations on corroded tracks after being tested under (a)

600 cycles on DLC coatedM2 and (b) 4000 cycles on TiN coatedM2. (c, d) EDX spectra

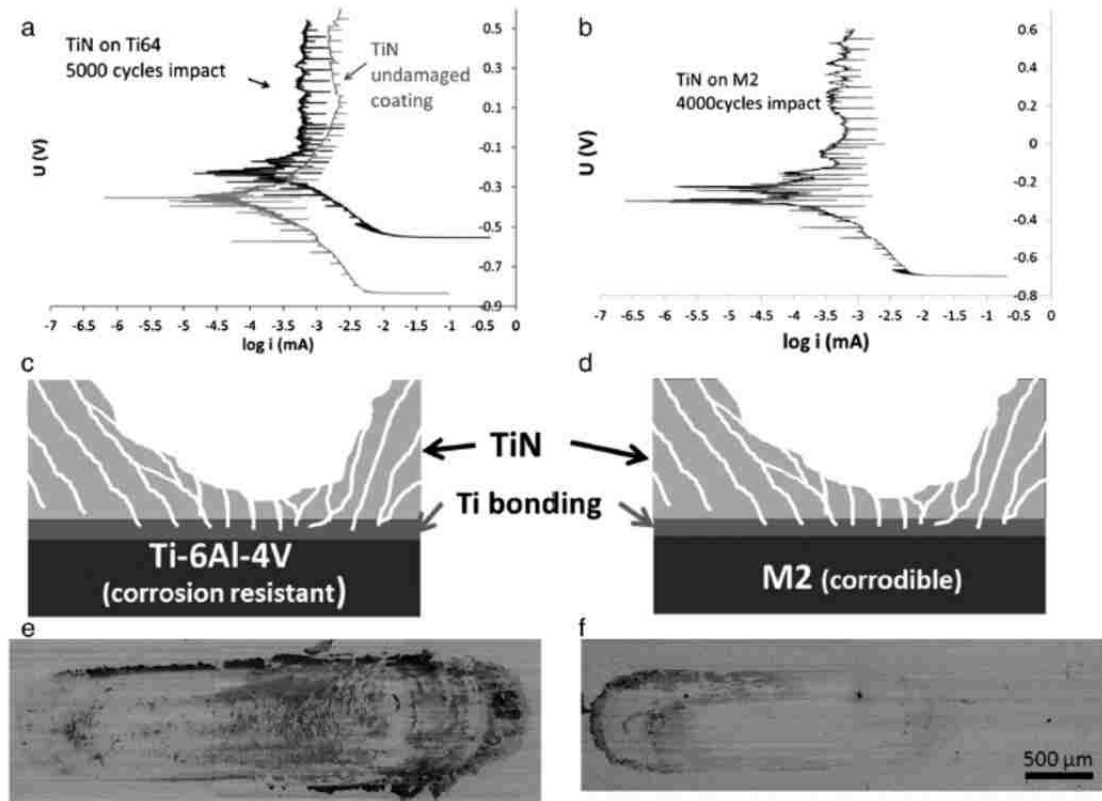on point A of (a) and point B of (b), respectively.

Figure 5- 11(a, b) Potentiodynamic polarization curves of TiN coated Ti–6Al–4V (damaged and undamaged) and tested in a HBSS solution at 37 °C; (c, d) schematic illustration of partially failed DLC from cross-sectional way. (e, f) SEM observations on tested tracks on TiN coated (e) Ti–6Al–4V and (f) M2.

However, it is necessary to notice that the cyclic impact-sliding test is carried out using a very high contact stress, making the coated sample failed in a relatively short time, comparing to the real biomedical implantation or even a hip and knee simulator tests. R. Hauert [11] reported that the promising in vitro results of DLC cannot transfer these results to in vivo applications because the long term performance of these articulating joint replacements could be largely shortened by crevice corrosion of the

141

adhesion-promoting interlayer. In this case, delamination can then occur by a slowly advancing crack in this thin layer, which cannot to be seen in short-term testing methods.

4. CONCLUSIONS

The cyclic inclined impact-sliding test was successfully utilized in evaluating fatigue wear behaviors of DLC and TiN biomedical coatings under extremely high contact stresses in ambient dry air and Hank's balanced salt solution (HBSS) conditions. Progressive amounts of damage were made on testing samples and the degree of failure was evaluated based on the percentage of coating failed area and the corrosion behaviors of the damaged areas after impact-sliding tests. When tested under dry condition, both coatings were mechanically more durable on hard M2 substrate than Ti alloy substrate. In the wet solution testing condition, the HBSS didn't cause obvious corrosion degradations to the coated samples when either the bonding layers or substrates were Ti-based (Ti bonding layer or Ti-6Al-4V substrate) within 5000 testing cycles. Instead, the solution provided a lubricating effect and enhanced coating durability. The Si-based bonding layer in the DLC coating, although the layer was corrosion resistant, couldn't block the cracking propagation into the substrate after a certain number of testing cycles; the crack opening allowed the HBSS solution to contact the substrates, which would only cause minor problem when the substrate was a corrosion-resistant Ti alloy. However, when the substrate, i.e. M2, did not have a good anti-corrosion property, a severe corrosion-induced weakening of the interface would occur. On the other hand, when a corrosion-resistant Ti bonding layer (within the TiN coating) existed, the Ti layer could function as a corrosion and cracking barrier to protect the M2 steel from corrosion, thus, no obvious corrosion-induced interface degradation appeared. Therefore, a corrosion-resistant

142

bonding layer and its ability to block the extension of cracking under cyclic dynamic loads can have a critical influence on the coating failure behaviors in a corrosive environment when the substrate has an inferior anti-corrosion property. However, for evaluation of a long-term durability of the coatings under a normal operating condition, different testing methods should be used.

Acknowledgement

REFERENCES

[1]   E.A. Magnissalis, S. Zinelis, T. Karachalios and G. Hartofilakidis. J. Biomed. Mater. Res., 66(B) (2003) 299.

[2]   G.S. Rao, V. Singh and L.K. Singhal. Materials Science and Engineering, A 538 (2012) 224.

[3]   R.A. Antunes and M.C. L. de Oliveira. Acta Biomaterialia, 8 (2012) 937.

[4]   S. Suresh. Fatigue of materials. 2nd ed. Cambridge: Cambridge University Press; 2004.

[5]   C.R.F. Azevedo. Eng. Fail. Anal., 10(2003)153.

[6]   E.J. Giordani, V.A. Guimarães, T.B. Pinto and I. Ferreira. Int. J. Fatigue,26 (2004) 1129

[7]   R.A. Anutunes, M.C. de Oliveira Crit. Rev. Biomed. Eng., 37 (6) (2009) 425.

[8]   T.S. Sudarshan, T.S., Srivatsan and D.P. Harvey II. Eng. Fract. Mech., 36(1990) 827.

[9]   M.A. Arenas, T.J. Tate, A. Conde and J.D. Damborenea. British Corrosion Journal, 35(3) (2000) 1.

[10]   D.R. Bloyer, J.M. McNaney, R.M. Cannon, E. Saiz, A.P. Tomsia and R.O. Ritchie. Biomaterials, 28 (2007) 4901.

[11] R. HAUERT, K. Thorwarth, G. Thorwarth. Surface & Coatings Technology (2013), http://dx.doi.org/10.1016/j.surfcoat.2013.04.015.

[12] M. Bin-Sudin, A. Leyland, A.S. James, A. Matthews, J. Housden and B. Garside. Surface & Coatings Technology, 81 (1996) 215.

[13] J.C. Avelar-Batista, E. Spain, G.G. Fuentes, A. Sola, R. Rodriguez and J. Housden. Surface & Coatings Technology, 201 (2006) 4335.

[14] K.J. Clay, S.P. Speakman, N.A. Morrison, N. Tomozeiu, W.I. Milne and A. Kapoor. Diamond and Related Materials, 7 (1998) 1100.

[15] S. Piscanec, L. C. Ciacchi, E. Vesselli, G. Comelli, O. Sbaizero, S. Meriani and A. De Vita. Acta Materialia 52 (2004) 1237.

[16] P.A. Dearnley. Proc. Inst. Mech. Eng., H, 213 (1999) 107.

[17] R.K. Roy and K.R. Lee. J. Biomed. Mater. Res. B Appl. Biomater., 83(1) (2007)72.

[18] S. Piscanec, L. C. Ciacchi, E. Vesselli, G. Comelli, O. Sbaizero, S. Meriani and A. De Vita. Acta Materialia, 52 (2004) 1237.

[19] W. Zhu, L. Puppulin, A.Leto, Y. Takahashi, N. Suganoa and G. Pezzottib. Journal of the Mechanical Behavior of Biomedical Materials (2013), http://dx.doi.org/10.1016/j.jmbbm.2013.01.018.

[20] S. Affatato, M. Spinelli, M. Zavalloni, C. Mazzega-Fabbro and M. Viceconti. Medical Engineering & Physics, 30 (2008) 1305.

[21] A. Vadiraj and M. Kamaraj, Surface & Coating Technology, 200 (2006) 4538.

[22] C.J. Boehlert, C.J. Cowen, J.P. Quast, T. Akahori and M. Niinomi. Materials Science and Engineering, C 28 (2008) 323.

[23] S.H. Teoh. International Journal of Fatigue, 22 (2000) 825.

[24] Y. Chen and X. Nie. Surface & Coatings Technology, 206 (2011) 1977.

[25] A. M. Bayer, B. A. Becherer and T. Vasco, ASM Handbook, Volume 16, p 51-59.

[26] A.S. Chaus and M. Hudáková. Wear, 267 (2009) 1051.

[27] E.H. Mirza, S.F.A. Ali, M. Asif, W.M. Azhar, S. N. Hassan. Biomedical Engineering (ICoBE), (2012) 117.

[28] G. Cassar, S. Banfield, J.C. Avelar-Batista Wilson, J. Housden, A. Matthews and A. Leyland, Surface & Coatings Technology, 206 (2012) 2645.

[29] J.C. Avelar-Batista, E. Spain, J. Housden, G.G. Fuentes, R. Rebolz, R. Rodriguez, F. Montala, L.J. Carreras and T.J. Tate. Thin Solid Films, 491 (2005) 177.

[30] J.F. Su, D. Yu, X. Nie and H. Hu, Surface & Coatings Technology, 206 (2011) 1998.

[31] http://www.tribology-abc.com/calculators/ (20 March, 2012)

[32] L. Wang, J.F. Su and X. Nie. Surface & Coatings Technology, 205 (2010) 1599.

CHAPTER 6 FAILURE MECHANISM OF DLC COATED Ti-6Al-4V AND COCR BIOMATERIALS UNDER CYCLID HIGH COMBINED CONTACT STRESSES

1. INTRODCUTION

Materials used in total joint replacements have received significant development over past decades. Metal-on-Metal (MoM) pairings are a viable choice because of their comparatively fine machinability, guaranteeing very smooth and precisely assembling contact surfaces [1-3]. However, such surfaces, which are typically composed of Ti based alloys and Co–Cr–Mo alloys, are highly susceptible to mechanical damage when the metal ball and the metal cup rub against each other during walking or running, or even jumping and striking. In hip and knee implants, wear occurs mainly on bearing surfaces leading to adverse metallic ions and particulate debris generation. Some of the metal ions (e.g. aluminum, vanadium and chromium) from the metal implant or from the metal particles will cause tissue blacken and enter the bloodstream. All these drawbacks of MoM implants giving rise to the demand for a more wear-resistant modification or coating against human body environment. Diamond-like carbon (DLC, amorphous hydrogenated carbon a-C:H) is a candidate for coatings of biomedical implants as shown by its success in mechanical applications and its proven bio-inertness [4, 5]. DLC can be deposited on most substrate materials by a variety of plasma processes and has been the focus of intense research over the past decades (e.g. [4–7]). However, peculiarities encountered in the in vivo environment have thus far barred widespread implant application; examples include increased wear against polyethylene in synovial fluid [8-10] and unpredicted adhesion failure [8-10]. However, the biological lubricant can act

like a shock-absorber and enable hip joint to transmit high dynamic loads (7-8 times the body weight) and accommodate a wide range of movements.

For better understanding of the failure mechanism that governs the performances of DLC-coated implants, it is thus necessary to carry out tests under conditions resembling the in a simulating situation, in which, dynamic contact stresses including cyclic impact and sliding wear are often involved. This paper used an effective test method—cyclic inclined impact-sliding wear test method to study the mechanism that governs roughening of sample surface and subsequent damage nucleation and wear at the bearing interfaces on coated and uncoated metallic biomaterials. Hanks' balanced salt solution was used as biological lubricant in the tribotests and corrosion tests on those coatings and substrate materials.

2. EXPERIMENTAL DETAILS

2.1 Test samples

In this study, a-C:H DLC coated high carbon/high nitrogen cobalt chromium and Ti-6Al-4V biomedical alloy discs were applied to be tested under a simulating environment, in which, an biological lubricant and cyclic dynamic forces were involved.

As per ASTM F-75, with the addition of Carbon and Nitrogen having lower limits specified, the chemical compositions of those two substrate materials are listed in Table 6-1 as follows:

Table6- 1 Chemical compositions of ASTM F-75 CoCr alloy and Ti-6Al-4V [11-13]

ASTM F-75	Composition (wt.%)	Ti-6Al-4V	Composition (wt.%)
Chromium (Cr)	27.0% to 30.0%	Carbon (C)	0.1% max
Molybdenum (Mo)	5.0% to 7.0%	Iron (Fe)	0.3% max
Nickel (Ni)	0.50% max	Nitrogen (N)	0.05% max
Iron (Fe)	0.75% max	Oxygen (O)	0.2% max
Carbon (C)	0.20% to 0.35%	Aluminium (Al)	5.5-6.76%
Silicon (Si)	1.00% max	Vanadium (V)	3.5-4.5%
Manganese (Mn)	1.00% max	Hydrogen (H)	0.015% max
Tungsten (W)	0.20% max	Titanium (Ti)	Balance
Phosphorous (P)	0.020% max		
Sulphur (S)	0.010% max		
Nitrogen (N)	0.125% to 0.250%		
Aluminium (Al)	0.10% max		
Titanium (Ti)	0.10% max		
Boron (B)	0.010% max		
Cobalt (Co)	Balance		

The hardness (H) of ASTM F-75 CoCr alloy and Ti-6Al-4V alloy is very similar, at a value of around 35 HRc. The elastic moduli (E) of the two alloys are 240 GPa for CoCr and 115 GPa for Ti-6Al-4V, respectively, provided by coating supplier.

DLC coating was made by Plasma Enhanced Chemical Vapour Deposition (PECVD), using a standard commercial process, in Tecvac. Ltd. The DLC coatings have a thickness of around 2.7 μm with a thin interlayer (≈ 300 nm) of Si based carbide to increase the coating adhesion. The H of this a-C:H DLC is around 18 GPa and the E is in a range of 170-200 GPa). The surface roughness (Ra) of DLC coated Ti6Al4V is measured to be around 0.046 μm and DLC coated CoCr is around 0.226.

Based on previous researches, under such high contact stress, the interface layer—Si based bonding, and mechanical properties (e.g., wear resistance, strength) of the substrate highly affect the coating performances. Therefore, it is necessary to study the support of the substrate separately under loading condition. In this case, a nano-indentation test was used to measure the change of hardness and elastic modulus of the uncoated substrates under certain numbers of impact-sliding wear tests.

2.2 Potentiodynamic polarization test

A freshly made H1387 HBSS provided by SIGMA-ALORICH was used as the electrolyte in the potentiodynamic polarization corrosion tests. Both coated and uncoated samples were tested in a scan range of -0.5-1.0V and by a 0.1mV/s scan speed.

2.3 Pin-on-disc test

Pure sliding study was carried out on both uncoated and coated F-75 Co-Cr and Ti-6Al-4V materials using pin-on-disc testing method. 2N normal load was used on uncoated materials while 10N was applied on DLC coated ones. The contact stresses of tested couples were calculated by Hertz equation and summarized in the row 2 and 3 in Table 6-2. An AISI 52100 steel ball (60-65HRc) was used as counter-face pin. Rotating sliding mode was used at a 0.075 m/s linear velocity. Wear rate K (mm3/Nm) was calculated based on the mass loss in the sliding track, which was measured by Mitutoyo SJ-201P surface profiler scan across the track, according to the following expression:

$$\text{wear rate} = \text{volume loss}/(\text{sliding distance} \times \text{normal load})$$

The test was first carried out in dry air (room temperature, $\approx$25% humidity), then, the HBSS was used to simulating wet sliding condition (body fluid environment). The

presence of a liquid between two bodies inhibits direct contact, and replaces dry friction by fluid friction. The body fluid was replenished at a constant rate by a dropper and made the wet environment refreshed progressively.

Table6- 2 Hertz contact stresses of the testing couples in POD and impact-sliding tests.

Normal Load (N)		CoCr (MPa)	Ti-6Al-4V (MPa)	DLC (MPa)
POD (Fn)	2N	1025	765	$\times$
	10N	$\times$	$\times$	1605
Impact-sliding wear (Fi)	140N	2576	1950	2300

2.4 Nano-indentation test

An Ubi 1^{TM} nano-mechanical testing system was used to measure the elastic modulus (E) and hardness (H) on both undamaged and damaged substrate, before and after certain cycle of impact-sliding test. A 500 µN indentation loading was chosen to make less than 30 nm deep indentations to avoid substrate effect. Due to the shape of indenter, a near-flat testing surface is necessary. So the nano-indentation test is not suitable for measuring excessively deformed tested tracks (with a lot of abrasive wear) on which worn parts have to be replaced (e.g., deep grooves, material transfer etc.). Three points, which located in the head, the middle and the end of the impact-sliding wear tested tracks (less than 100 cycles test for CoCr substrate and less than 10 cycles for Ti-6Al-4V), were measured and the average data was used to study the change of E and H during the test.

2.5 Cyclic impact-sliding wear test

Cyclic impact-sliding wear test method is a new reference to the prediction of load-bearing coatings under combined impact and sliding forces. During the test the flat coating was fixed on an inclined surface on the longer side of a ' √ ' shape sample holder with its transition point fixed by a roller bearing. The other side of the sample holder was

pressed downward (preloading) by a high stiffness copper spring. During the test, a Φ10-mm AISI 52100 steel ball moves up and down, driven by an air-pressed piston, applies impacting forces on the inclined coating surface. When the coated sample was impacted, the sample holder will rotate around the fixed roller bearing like a seesaw. In this case, instead of rigid impact, the steel ball will slide a certain distance on the coating (pressing force was applied on coating during sliding wear) before it moves upside and make a sliding wear track. This impact (F_i) and the maximum value of pressing (F_{pmax}) forces were determined by the air pressure in the piston and the initial gap between the ball and the undamaged coating surface, the value of which can be adjusted before each round of the test. In this study, the F_i and F_{pmax} were pre-set to be 140N and 300N. Based on Hertz contact stress calculation, the maximum contact stresses between the steel ball and uncoated and DLC coated sample surfaces were shown in the fourth raw of Table 6-3. From the calculation results, it can be understood that the contact stress during the impact-sliding tests was far beyond the yield stress of either coated or uncoated materials. This test method is to study the failure behaviors of metallic biomaterials by observing partially failed testing tracks using an accelerating mode. Details of the tests can be found in Table 6-3 as following:

Table6- 3 Testing cycles of both coated and uncoated CoCr and Ti-6Al-4V in the impact-sliding wear test.

Test load F_i =140N F_{pmax} =300N	CoCr substrate		DLC coated CoCr		Ti-6Al-4V substrate		DLC coated Ti-6Al-4V	
Test condition	dry	wet	dry	wet	dry	wet	dry	wet
Test cycles	10~100	5000	100	5000	10~100	100~1000	100	2000

3. OBSERVATIONS AND ANALYSIS

3.1 Pin-on-disc (POD) test on bare and DLC coated CoCr and Ti6Al4V

3.1.1 POD tests on substrates

During the rotating POD tests, the coefficient of friction (COF) was recorded and is shown in Figs 6-1a for dry test condition, and b for wet test condition. Around 25000-revolution-test was used in dry test while 60000-revolution test was used in wet test for both tested substrates. After the tests, optical microscopy was taken on tested tracks, which can be found in Figs. 6-1 (b-e). Cross-width surface profile was measured on the tracks in the directions indicated in Figs. 6-1 (b-e) and the curves expressed by depth (µm) vs. width (mm) are exhibited in Figs. 6-1 (b'-e'). The depth and width of each track was measured and indicated on the surface profile curves using the same length unit as the x- and y-axis.

In the dry test, a large scale of vibrations of COF (in a range of 0.4) was observed for both CoCr and Ti-6Al-4V (Fig. 6-1a). Tested under same distance, a 0.5 mm wide, 3.6 µm deep track was formed on CoCr, while a 0.8 mm wide, 27 µm deep one was formed on Ti-6Al-4V.

Most material mechanical properties influence on the wear response such as elastic modulus, yield strength, hardness or fracture toughness. In low stress conditions, it is commonly accepted that the hardness of materials is a dominating parameter controlling wear.

Figs. 6-1A-D show SEM images using a much higher magnification of the areas insert in the points A-D in Figs 6-1 b-e, respectively. In dry test, some wear debris was formed and accumulated inside the wear track of CoCr which might represent the peaks

measured in the cross-width surface profile (Fig 6-1 d'). Noticeable plows that parallel to the sliding direction, fine particles, and material pile-up and transfer occurred on the worn Ti-6Al-4V, which shows that the dominant wear mode is adhesive wear for Ti-6Al-4V alloy.

In wet tests, a 0.52 mm wide, 2.75 μm deep track was formed on CoCr and a 1.2 mm wide, 64 μm deep track was observed on Ti6Al4V. COF was measured to be decreased to 0.3 for both tested materials. EDX analysis within the sliding tracks showed that there was a very thin layer of iron oxides coated on the track surface. That was supposed to be material transfer from the counterface steel ball due to the inferior corrosion resistance in body fluid of steel comparing to tested biomaterials. A squamose morphology and tearing evidence could be found on worn Ti6Al4V surface. This result has a good agreement with the analysis of the wear scar profile and coefficient of friction. It is attributed to the fact that Ti-6Al-4V alloy has a poor abrasive and adhesive wear tendency and is easily plastically deformed even at low applied loads.
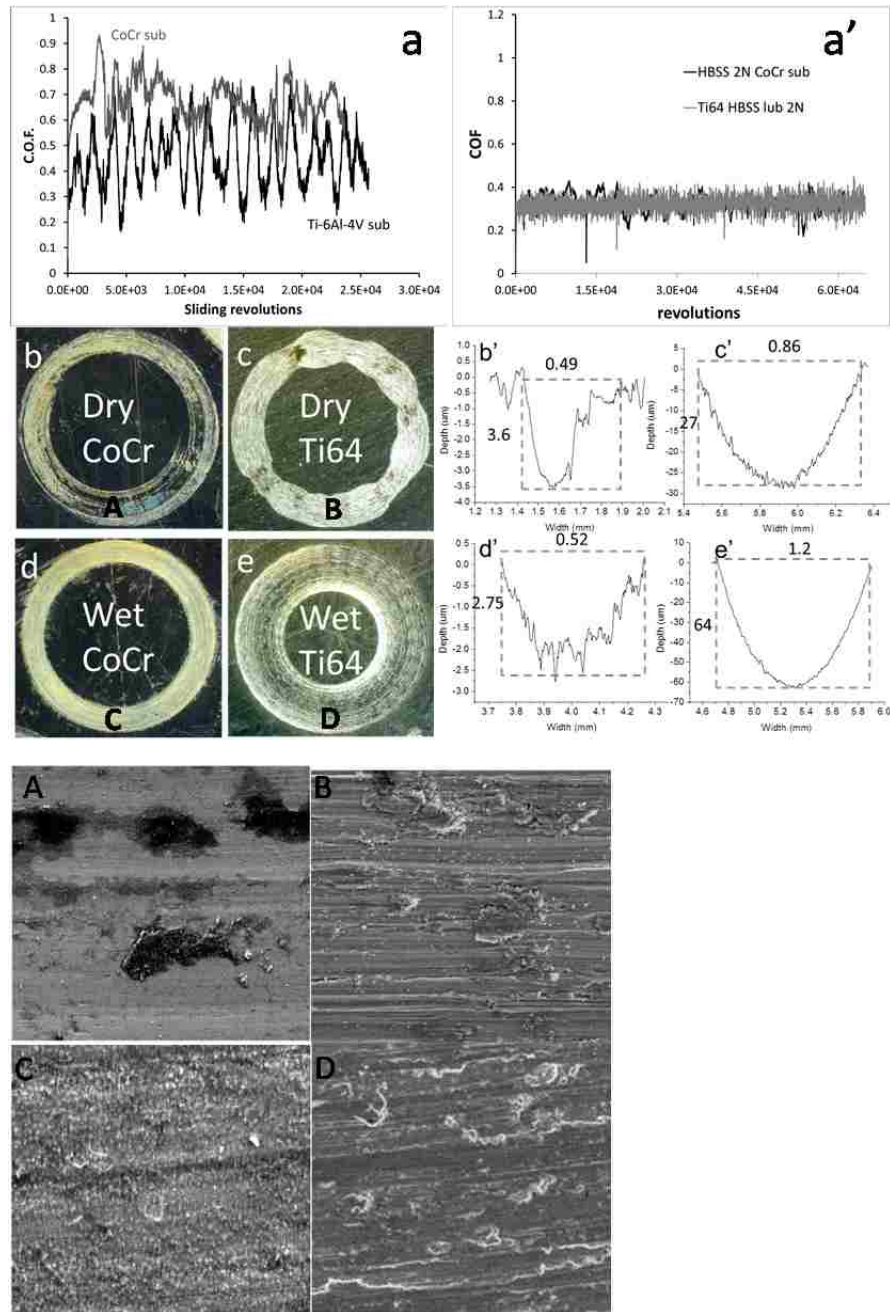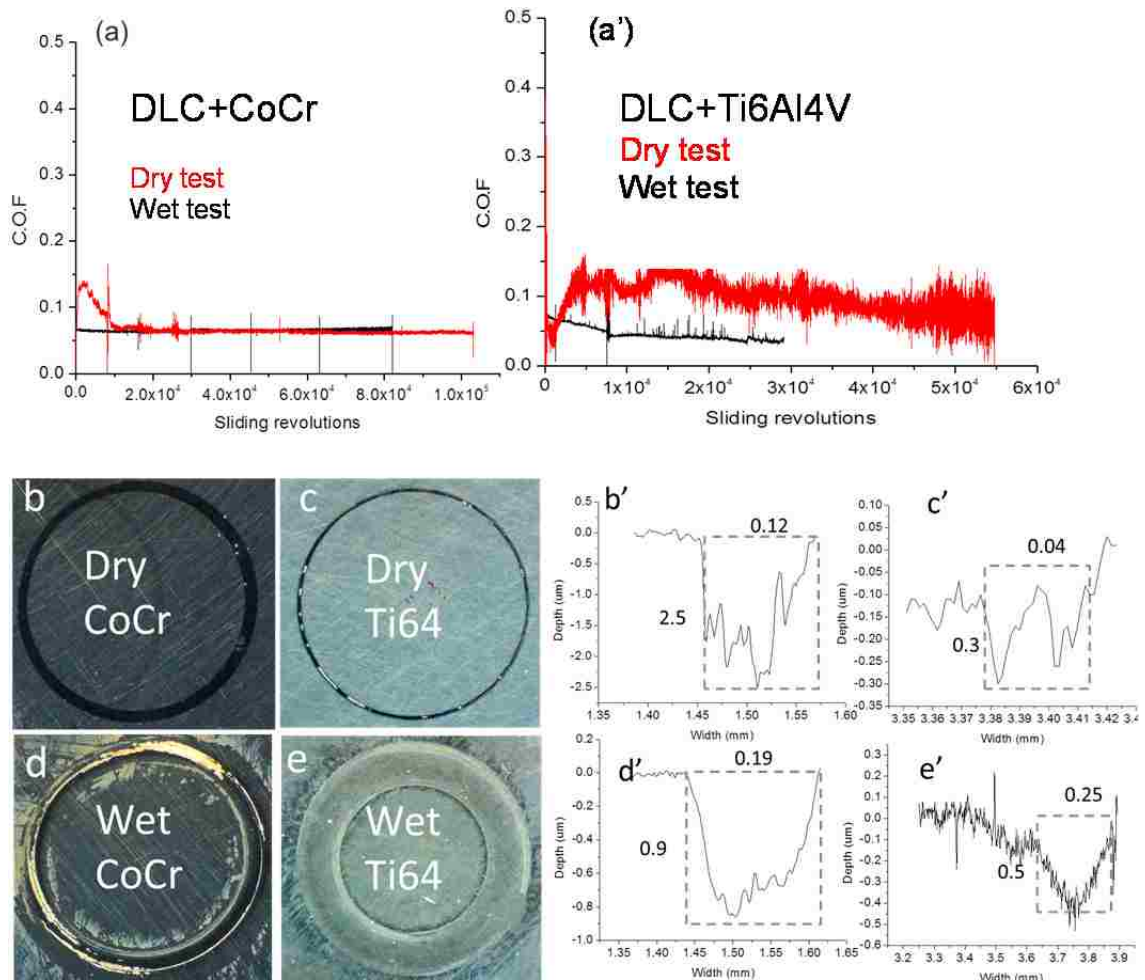
Figure 6- 1 Pin-on-disc test results of uncoated CoCr and Ti-6Al-4V alloys, where (a and a'), COF vs. sliding revolutions; (b-d) Optical observations on sliding tracks; (b'-d') Cross-width surface profile on the wear tracks in b-e; and (A-D) SEM observations inside sliding tracks of the insert area A-D B insert in d-e.

On one hand, viscous HBSS can slightly enhance the wear performance on CoCr comparing to the dry test. CoCr didn't corrode in a HBSS environment in a short period testing time. The result of potentiodynamic polarization test (Fig. 6-2) also showed that the CoCr has the highest corrosion resistance property in this HBSS solution comparing to other metallic biomaterials (the result of 316L is even lower than that of Ti6Al4V and is not shown in the image). On the other hand, HBSS didn't show much lubricant effect on Ti6Al4V but a negative effect with corrosion involved. The friction and wear in Hanks' solution are complex processes. It is related to wear and corrosion. During pure wear, weight changes can be related to loss of material worn away or adsorption of material from the environment. During corrosion processes weight changes can be associated with material lost via dissolution or buildup of material due to repassivation incorporating material from the environment. The passive film of Ti6Al4V formed in a HBSS solution is not stable, reported by Reis [14]. Furthermore, under repetitive damage from sliding motion of the steel ball, it has insufficient time to regenerate the passive film. In this case, the surface inside the testing track always remains active and on reaction with moisture in the solution and large amount of mass was lost after the POD test.

However, the velocity and frequency of the sliding for the real usage of a joint connection cannot be that high. Potentiodynamic polarization test in HBSS solution shows the passivation film formed on Ti6Al4V surface has good corrosion resistance and repassivation property when it is uniform.
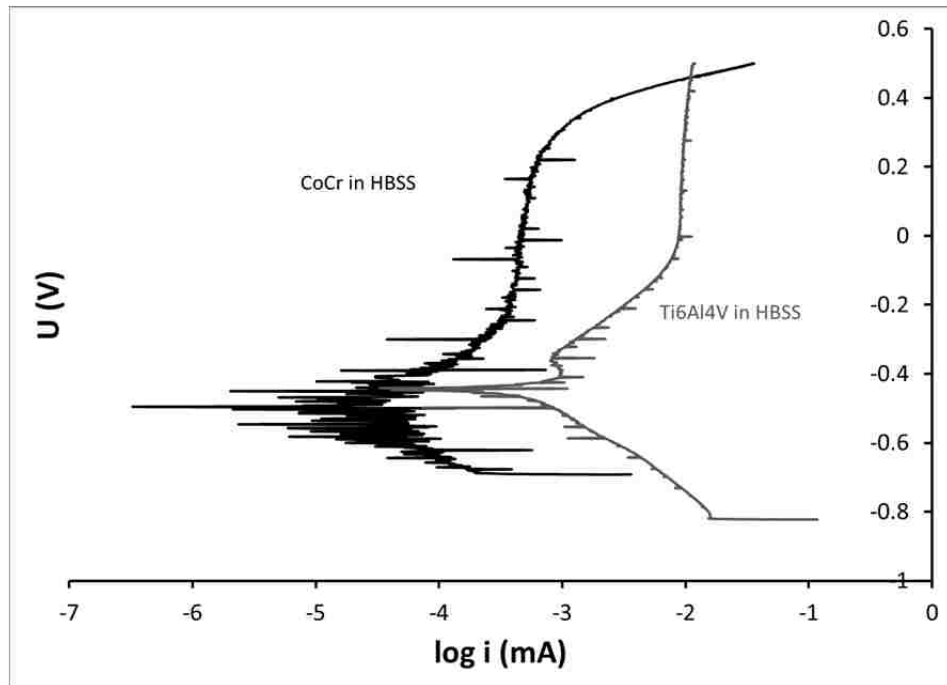
Figure 6- 2 Results of corrosion tests of CoCr and Ti6Al4V bulk

materials in HBSS environment.

3.1.2 POD tests on DLC coatings

10N normal load was applied on a:H-DLC coated CoCr and Ti6Al4V with a SiC interface layer under both dry and HBSS wet conditions. After a certain unstable COF, 'run-in' period on both coated samples, DLC showed an excellent wear resistance by exhibiting a low COF that equals to around 0.06 in dry test conditions. Comparing to the COF measured in our previous work [15], in which a value of 0.1 was measured on the same DLC coated Ti6Al4V, it is because a higher normal load was used in this paper.

156

Figure 6- 3 Pin-on-disc test results of DLC coated CoCr and Ti-6Al-4V, where (a

and a'), COF vs. sliding revolutions; (b-e) Optical observations on sliding tracks; and (b'-

d') Cross-width surface profile on the wear tracks in b-e.

DLC coatings largely enhanced the wear performance of both CoCr and Ti-6Al-4V,

especially on Ti-6Al-4V sample, under wet or dry conditions. Very tiny mass was lost on

all four slide tracks. The cross-width examination showed that the depth of all the tracks

did not exceed the thickness of DLC coating (2.7 μm + 0.3 μm SiC). That indicates the

DLC coating is still protective after the POD tests. The width of the tracks are larger in

wet tests than that in dry tests might be explained by the change of friction mechanisms between the DLC coating and steel ball surfaces.

The improvement of wear performance of tested samples are summarized and shown in Table 6-4 and the Wear rate of each POD test was exhibited in Table 6-5.

Table6- 4 The COF measured in dry and wet tests for coated and uncoated samples

POD tested samples		Dry	Wet
Uncoated	CoCr alloy	0.58-0.7	0.25-0.37
	Ti-6Al-4V alloy	0.3-0.7	0.28-0.38
DLC coated	CoCr alloy	0.15↘0.06	0.07
	Ti-6Al-4V alloy	0.12↘.0.08	0.048

Table6- 5 Wear rate in dry and wet tests for coated and uncoated samples

Test sample	Normal load (N)	Wear rate ($10^{-8} \times mm^{-3}$/N mm)	Range of error
CoCr substrate (dry)	2	2.26	0.47
CoCr substrate (wet)	2	0.60	0.17
Ti64 (dry)	2	49.54	6.73
Ti64 (wet)	2	46.21	5.15
DLC coated CoCr (dry)	10	0.154	0.03
DLC coated CoCr (wet)	10	0.065	0.03
DLC coated Ti64 (dry)	10	0.01	0.01
DLC coated Ti64 (wet)	10	0.04	0.02

Based on the wear rate calculation, the highest wear rate in the POD test is on bare Ti6Al4V under dry test condition and the lowest wear rate is on DLC coated Ti6Al4V under dry test condition. HBSS did benefit the wear performance when DLC coating is utilized in this test condition.

Generally speaking, the lubricating effect of HBSS was more distinct on bare metals than on DLC coatings. The corrosion of HBSS may be one of the reasons to cause the large mass loss on Ti6Al4V substrate.

3.2 Inclined cyclic impact-sliding wear test results

3.2.1 Study on substrates that tested under dry and wet conditions

Figs 6-3 and 6-4 show the optical images on impact-sliding wear tracks tested in both dry and wet conditions. The cross-width surface profile was measured in a line that perpendicular to the sliding wear direction and in the middle area of the tested tracks (along the direction of dashed arrow in Fig. 6-3). On CoCr substrate, 100 cycles dry test made a 0.41 mm wide, 2.3 μm deep track. SEM observation shows fine particles are formed together some sliding grooves in the tested tracks, especially in the head area (mainly subjected to impact loading). Some iron oxide is detected in the material pile-up area at the end of tail part (see Fig. 6-3 B). Fatigue cracking in very fine scale is observed on the worn surface of CoCr. However, the result of CoCr substrate tested in dry condition overwhelms that of Ti6Al4V, on which the same test condition was carried out and the results are given in Figs. 6-4a and b. Deep plough due to adhesive wear occurred on Ti6Al4V surface after only 3 cycles test and extended to the whole contact area quickly. The result showed a very wide and deep track after 100 cycles dry test.

When tested under wet conditions, HBSS showed an overwhelming lubricating effect to the CoCr surface. Up to 5000 cycles test resulted in an only 0.41 mm wide, 2.5 μm deep track. Little failure behaviors could be found inside the track except for some corrosion products from the counterface ball was slightly coated on some areas of the track. On the contrary, HBSS showed little improvement on Ti6Al4V substrate after testing under same cycles (100) as in dry condition (see Fig. 6-4 c). It is hard to figure the effect of corrosion during the impact-sliding test due to the extreme high contact loadings

which can fully deform the structure of near-surface-layers. The lubricating film could not formed and stabilized on Ti6Al4V, comparing to that on CoCr.
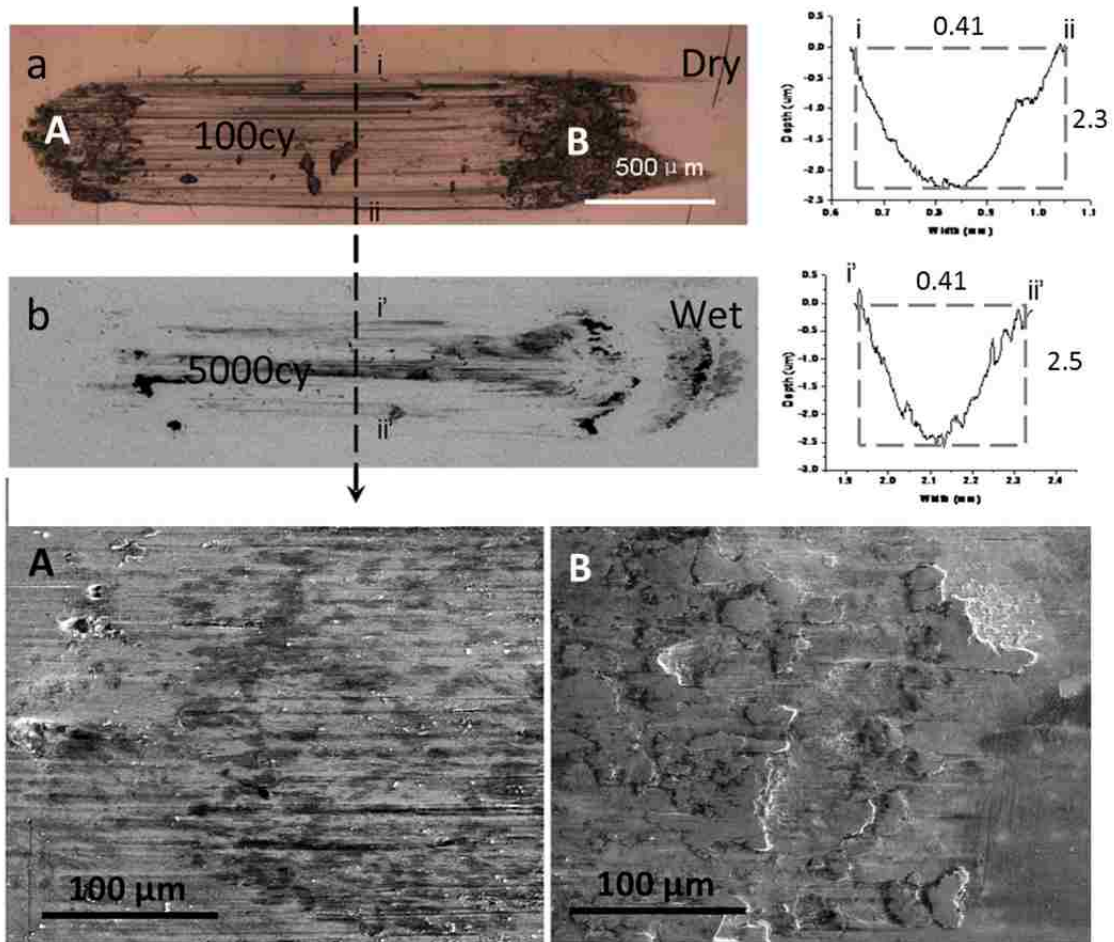
Figure 6- 4 Optical observations and cross-width measurement on tested tracks of CoCr substrate in dry and wet test conditions, where (a) 100 cycles dry test and (b) 5000 cycles wet test; (A and B)SEM microscopy on area A and B insert in a.
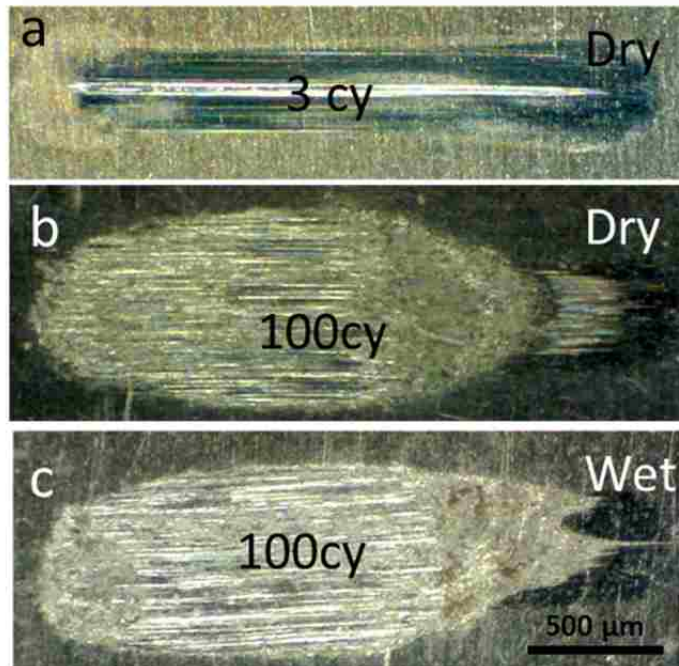
Figure 6- 5 Optical observations on tested tracks of Ti6Al4V substrate in dry and wet test conditions. (a) 3 cycles dry tests, (b) 100 cycles dry test and (c) 100 cycles wet test .

Undamaged surface together with wear tracks tested after 10 and 50 cycles test in dry condition on both CoCr and Ti6Al4V substrate were used for mechanical evaluation by a nano-indentation test. Three measurements were taken on each track in its head, middle and end areas and the average value was calculated. The Hardness (H) and Elastic modulus (E) are measured and shown in Table 6-6 as following:

Table6- 6 Hardness and elastic modulus on damaged CoCr and Ti6Al4V substrates

Test samples	Uncoated CoCr			Uncoated Ti6Al4V		
	Undamaged	10-cy test	50-cy test	Undamaged	10-cy test	50-cy test
E (GPa)	244.68	245.65	363.28	113.8	119.12	81.51
H (GPa)	3.48	4.09	4.41	3.43	3.46	2.76

The H increased gradually with a 26% during the 50 cycles impact-sliding wear test on CoCr in dry test under room temperature. This is believed to be one of the reasons for

the good resistance of CoCr alloy to the impact and sliding forces in both dry and wet (without much effect of corrosion) conditions. However, the H decreased by 19% after 50 cycles test, which is due to the loosen material tranferred from counterface and the uneven topograph caused by the impact and sliding forces. From the results of 10 and 50 cycles on Ti6Al4V, it can be found the deformation was accelerated after 10 cycles test.

3.2.2 Study on DLC coatings that tested under dry and wet conditions

100 cycles tests were carried out on both DLC coated CoCr and Ti6Al4V in dry condition, while 5000 and 2000 cycles test were used on CoCr and Ti6Al4V, respectively, in wet condition. The results are illustrated in Figs. 6-5 and 6-6 for dry tests and wet tests, respectively.
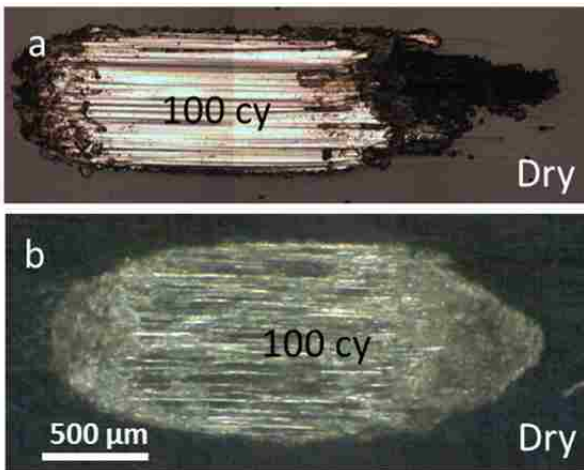
Figure 6- 6 Optical observations on tested tracks of CoCr and Ti6Al4V

substrate in dry condition .
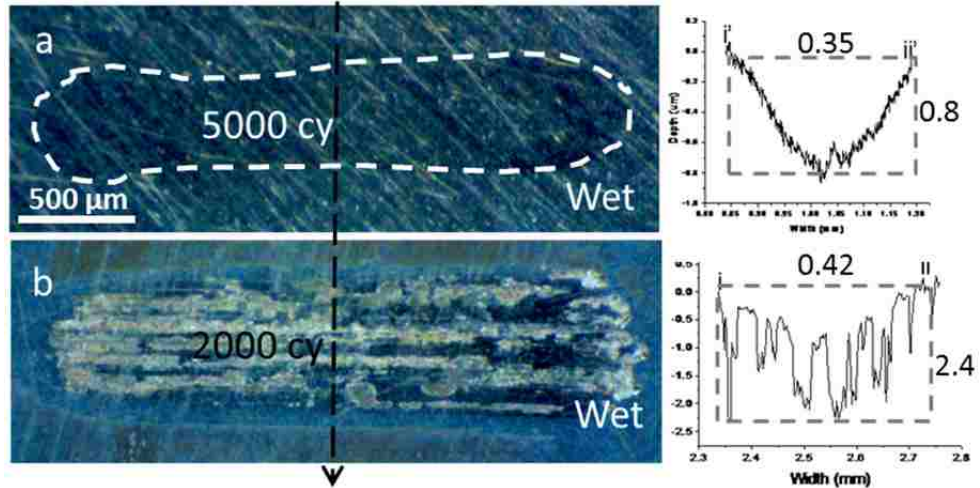
Figure 6- 7 Optical observations and cross-width surface profile measurement on tested tracks of CoCr and Ti6Al4V substrate in wet condition .

Large percentage of failed coating area are observed on both CoCr alloy and Ti6Al4V after 100 cycles dry test. DLC coating showed little protection in the dry impact-sliding weart test to the substrates. DLC coated CoCr showed an even worse result with a much severe deformed worn surface of the substrate (refer to Fig 6-3 a). it was because the DLC coating could not sustain such a high contact stress (refer to Table 6-2) and failed quickly during the test. The hard and irrigular-shaped wear debris particles were invovled in the sliding wear and caused micro-cutting to the underneath CoCr substrate (three-body abrasive wear) that accelerate the failure of coated sample. DLC coating remains on some local areas in the latter half of the sliding wear track (tail). However, with the increase of test cycles, the remained coating will progressively chippedoff and then, peeled off. The same thing happed on DLC coated Ti6Al4V. Due to the insufficient wear performance, the DLC coating was fully peeled off from the substrate.

Under wet test condition, DLC coating showed an outstanding protection to CoCr and an improved performance on Ti6Al4V, comparing to that of dry tests on coatings and wet tests on uncoated materials. A slight deformance was detected with its width to be 0.35 mm and depth to be 0.8 μm. Failure mechanisms could hardly be observed in the tested area. For coated Ti6Al4V, a similar result (around 25% failure area) was found as reported in our previous study [15], fatigue cracking with local chipping and peeling were formed along with the sliding grooves inside tested area. Crack propagation in sliding wear is due to a combined loading of compression and shear on the crack—compressive stress on the crack and shear deformation at the crack tip and cause local chipping and peeling. The cross-width surface profile curve shows the DLC coating is mainly adherent to the substrate. However, the roughness of the coating is pretty high after 2000 cycles test and further test in not necessary.

4. CONCLUSION

In this study, a new commonly used metallic biomaterial, CoCr alloy, was studied by using inclined cyclic impact-sliding wear test. Ti6Al4V, as a comparison, was also used to do further studies beyond the previous research progress.

Due to the excellent corrosion resistance of CoCr alloy and Ti6Al4V, the corrosive HBSS showed very little influence to cause corrosion problem, instead, it behaved as a lubricant for both coated and uncoated alloys in the POD tests. The coefficient of friction (COF) decreased more than a half on uncoated surfaces than coated ones in wet environment for both substrates. After a certain period of high COF 'run-in' period, both coated samples showed a close value of COF for either dry or wet test conditions.

In the impact-sliding wear tests, large scale of work hardening was observed on CoCr alloy under repetitive high dynamic loadings, which promoted the durability of both bulk material and DLC coating up to over 5000 cycles test. Hardness measured by nano-indentation tests in the tested track on the CoCr bulk material showed the work hardening occurred at very early stage during the test. The value of hardness increased 26% in the first 50 cycles test. Ti6Al4V, on the contrary, showed great amount of abrasive wear and resulted in deep and wide test tracks for either coated or uncoated ones. DLC coating started failing within first 5-cycle-test and the hard, small particles, which deprived from DLC coating, were entangled in the following tests and caused three-body-abrasive wear. Great scale of damage was formed on both tested surface and the couterface surface. The existence of HBSS could improve the wear behavior of Ti6Al4V to some extent. Surface profile measured across the tested tracks showed both chipping and peeling were formed inside the damaged DLC coated Ti6Al4V.

REFERENCES

[1]   F. Godlee, BMJ 344(2012) e1539.

[2]   S. Bauer, P. Schmuki, K. Mark, J. Park, Progress in Materials Science 58 (2013) 261.

[3]   K.J. Bozic, J. Browne, C.J. Dangles, P.A. Manner, A.J. Jr Yates, K.L. Weber, K.M. Boyer, P. Zemaitis, A. Woznica, C.M.Turkelson, J.L. Wies, J Am Acad Orthop Surg. 20(6) (2012) 402.

[4]   J.C. Avelar-Batista, E. Spain, G.G. Fuentes, A. Sola, R. Rodriguez, J. Housden, Surface & Coatings Technology 201 (2006) 4335.

[5]   G. Cassar, S. Banfield, J.C.A. Wilson, J. Housden, A. Matthews, A. Leyland, Surface & Coatings Technology 206 (2012) 2645.

[6]   A.M. Ladwig, R.D. Koch, E.G. Wenski, R.F. Hicks, Diamond Relat. Mater. (2009), doi:10.1016/j.diamond.2009.02.026.

[7]   C. Rattanasatien, N. Tonanon, W. Bhanthumnavin, B. Paosawatyanyong, J Nanosci Nanotechnol. 12(1) (2012) 642.

[8]   R. Hauert, Diamond and Related Materials 12 (2003) 583.

[9]   G. Thorwarth, U. Müller, C.V. Falub, B. Weisse, C. Voisard, M. Tobler, R. Hauert, European Cells and Materials 17. Suppl. (1) (2009) 25

[10]   G. Thorwarth, U. Müller, C.V. Falub, B. Weisse, C. Voisard, M. Tobler, R. Hauert, Acta Biomaterialia 6 (2010) 2335.

[11]   H. Hermawan, D. Ramdan, J.R.P. Djuansjahy (2011), Metals for Biomedical Applications, Biomedical Engineering - From Theory to Applications, Prof. Reza Fazel (Ed.), ISBN: 978-953-307-637-9.

[12]   A. Srivastav, An Overview of Metallic Biomaterials for Bone Support and Replacement, 307-513-6, Published: January 8, 2011 under CC BY-NC-SA 3.0 license, DOI: 10.5772/13488.

[13]   R. Narayan (ed.) Biomedical Materials, DOI 10.1007/948-0-387-84872-3_2. pp. 41

[14]   R.L. Reis, F.J. Monteiro, Journal of Materials Science: Materials in Medicine, 5 (1994) 457.

[15]   Y. Chen, X. Nie, A. Leyland, J. Housden , A.Matthews, Surface & Coatings Technology 237 (2013) 219.

CHAPTER 7 SUMMARY

In this dissertation, totally six chapters were presented with a logical relationship of a continuous study on the failure mechanisms of coated metallic biomaterials using an effective testing method—cyclic inclined impact-sliding test method. Chapter 1 gives some background of information on some of the challenging and critical problems of metallic biomaterials and the some commercial improvement techniques. The testing and evaluating methods used in this study were then introduced. Several initiatory trial tests for the mechanical studies were firstly carried out on some non-biomedical-utilized coatings and substrates (TiN on M2 and W-DLC) and reported in Chapters 2, 4, 5. Another type of coating—PEO coating were also include to study the effects of coating thickness, surface morphology and chemical composition on the coating failure behaviors under high dynamic contact stresses, which was presented in Chapter 3. After that, all the three commercially used biomaterials were studied comprehensively based on previous experiences obtained in those trial tests. The results were concluded in Chapter 6 and, some of which, in this chapter. Several critical parameters, which were found to affect greatly on the failure mechanisms of coated metallic biomaterials were studied individually or comprehensively in each chapter and could be concluded as following. The study of those parameters can provide some useful references of choosing the proper material or substrate/bonding/coating combination to the clinical usage.

1. CRITICAL PARAMETERS TO THE FAILURE OF THE COATINGS

1.1 Substrate effects (Chap. 2, 4, 5, 6).

Hardness of the substrate—higher hardness substrate supported better to the coatings against high dynamic loadings when the contact stress is beyond the yield stress of the coating.

Corrosion resistance of the substrate—insufficient corrosion resistant substrate can cause corrosion-induced stresses into the coating-substrate interface and weaken the bonding strength of the coating, and thus, create early failure of the protective coating when dynamic loadings are applied.

1.2 Bonding layer effects (Chap. 2, 4, 5).

Bonding strength—the bonding layer with higher bonding strength can largely increase the coating attachment to the substrate, even after the formation of the fatigue cracks inside the coating. The ductile bonding layer material has higher bonding strength than that of brittle ones, for example, the metallic based bonding layer such as Ti and W had higher bonding strength than that of ceramic based ones, such as SiC, under the condition of cyclic inclined impact-sliding tests.

The corrosion resistance—the bonding layer with higher corrosion resistance helped preventing corrosive media from getting in touch with the less corrosion resistant metallic substrates. For example, the W-DLC had a less corrosion resistance than Si-DLC due to the corrodible bonding layer—W.

1.3 Coating wear-resistance effects (Chap. 4-6).

DLC coatings had a much higher wear resistance property than TiN and PEO coatings. This helped to improve the survival of the coating against pure sliding and the sliding motion during the impact-sliding tests (the tail part of tested tracks)

1.4 Coating surface morphology & roughness (Ra & Rsk) effects (Chap. 3).

DLC and TiN coatings had very smooth coating surface than PEO coatings. In this case, the surface roughness and morphology did not show a very distinct difference on the former two coatings. However, the surface morphology and roughness showed great effect on porous PEO coatings during the cyclic impact-sliding tests. The PEO coatings with longer deposition time, which led to larger pore size on average on its surface showed a worse result in the impact-sliding tests (with an increasing failure area percentage on tested tracks under the same test conditions).

1.5 Coating thickness effects (Chap. 3).

PEO coatings with a thickness of 30 μm were found to have a greatest wear resistance under pure sliding motion, comparing to the other PEO coatings with the thickness in the range of 9-20 μm. It could be explained by the higher composition of magneli phase, which was reported to have a lubricant property, on the thicker coating surfaces during the PEO coating deposition processes. However, due to the relatively low toughness property of the PEO coatings (porous ceramic coating layer), none of the coating could survive under the high contact stresses applied by the testing instrument in this study, even under low testing cycles. To conclude, other surface treatment methods are required for this type of coating to be used under such a loading condition, for

example, multilayer coating deposition and selective laser melting surface treatment on the PEO coatings to provide a high loading resistance.
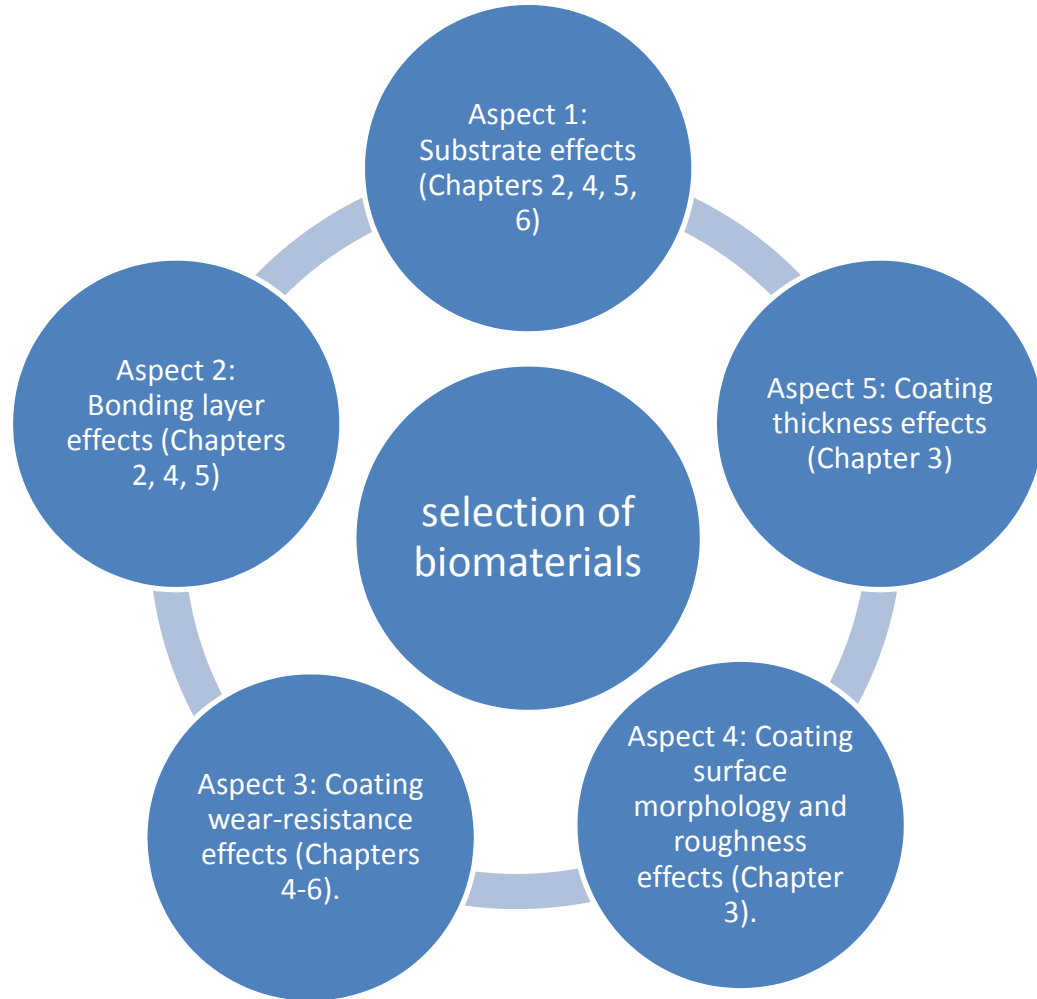
Figure 7- 1 Critical parameters expressed in the dissertation.

2. SUMMARY OF THE TESTING RESULTS

A conclusive summary is made on all the tested coatings and substrates and shown in Tables 7-1—7-3. Optical micro-observations were made on all tested tracks and listed in the increasing of testing cycles and loads. The damage on tested coatings were evaluated by four increasing degrees from little damage to severe under each optical

image. Head (H), middle (M) and tail (T) were evaluated separately for each tested track for the individual study of coating resistance to impact and sliding. An overall evaluation was also made for each tested track and a ranking was made based on the results.

Table 7- 1 Summary of tested tracks on DLC and TiN coatings

COATING	BONDING	SUBSTRATE	OPTICAL IMAGES (H/M/T)*1 –(head→tail)						RANK
			140-300N / 20 cy	140-300N / 50 cy	140-300N / 500 cy	140-300N / 3000 cy	140-300N / 5000 cy	200-400N / 5000 cy	
DLC	Si	CoCr	0/0/0*2	XX/XXX/XX	XXX/XXX/XXX				5
DLC	Si	M2			0/0/X	X/X/XX	XX/X/XX		3
DLC	W	M2			0/0/0	X/XX/XX	X/XX/XX		2
DLC	W	316 L SS			0/0/0	X/0/0	X/0/0	X/0/X	1
DLC	Si	Ti6Al4V	XX/XXX/XX	XX/XXX/XX	XXX/XXX/X				6
TiN	Ti	M2			XX/XXX/X	XX/XXX/X	XXX/XXX/XX		4
TiN	Ti	Ti6Al4V	XX/XX/XX	XX/XX/XX	XXX/XXX/XXX				6

*1 Note-H/M/T indicates Head/Middle/Tail of the impact-sliding wear track locations

*2 Note- 0-litttle damage, X-mild, XX-moderate, XXX-severe.

172

Table 7- 2 Summary of tested tracks on PEO coated Ti6Al4V

PEO on Ti6Al4V-Coating deposition time (min)	Coating thickness (μm)-as-deposited\polished	80-200N/ 100cy	140-300N/ 50cy	140-300N/ 100cy	200-400N/ 100cy	Rank
PEO 5 min	10.8↘8.8	(a2) 0/0/0		(a) 0/0/X	(a1) X/XX/X	1
PEO 10 min	17.8↘9.7	(b2) X/0/0		(b) X/X/X	(b1) XX/XXX/XX	2
PEO 15min	27↘10.6	(c2) X/0/0		(c) XX/XXX/XX	(c1) XX/XXX/XX	3
PEO 25min	45↘20		XX/XX/X			4
PEO 25min	45↘30		XX/XX/X			4
PEO 45min	65↘20		XX/XXX/XX			6
PEO 45min	65↘30		XXX/XXX/XXX			7

173

CHAPTER 8 GENERAL CONCLUSIONS AND FUTURE WORK

1. CONCLUSIONS OF EACH CHAPTER

Fatigue wear and failure mechanisms on coated and uncoated biomaterials under high dynamic contact stresses were studied by a progressive experimental research. Results and analysis are concluded with the organization of chapters as the following:

I. Contact fatigue behaviors on TiN coated unhardened M2 under inclined cyclic impact-sliding wear tests can be concluded as follows:

1.   There were four types of fatigue cracks were observed inside the impact-sliding scars, which were: radical cracks, cohesive cracks, intersectional cracks and peripheral crack.

2.   The radial cracks occurred in the impact craters, the density of which increased greatly with the increase of impact cycles and expanded both inward—around the area exerted by the greatest impact force, and outward—increased the size of impact crater.

3.   The cross-linked cracks were formed due to the bending deformations from axial and normal-to-axial directions. Coating failure always takes place in the center area of this type of crack, where the highest crack density was observed after a critical number of impact cycle. The peripheral cracks formed along the edges of tail part were very similar to the ones in the scratch testing. Its length and density increased with the increase of impact cycles.

4.   The test results indicated that a relative soft substrate allowed quick formation of fatigue cracking and failure under high load condition. Thus, it is necessary to increase the hardness of the substrate for the parts working in the operating environment involved

in impact and sliding forces. Using a hard substrate or a very thick coating may likely reduce the degree of the pressing-in deformation and reduce the cracking formation as a result.

II. Pin-on-disc (POD) tests and inclined cyclic impact-sliding wear tests carried out on another type of biomedical coating—PEO coatings on Ti6Al4V alloy lead to the following observations.

1)   The surface roughness of the PEO coatings (i.e., Ti-based oxide coatings) had a very significant effect to the sliding behaviors of the contacting couples. Thick coatings may result in no advantage due to their high surface roughness. All of the coatings had a relatively high but constant COF comparing to the substrate. The COF of the polished coatings decreased greatly.

2)   For the coatings having similar coating thickness and surface roughness Ra, the coating surface profile characteristics such as skewness Rsk seemly played a significant role in the transferring and wear mechanism of the counterface material. Close-to-zero value of Rsk caused less counterface material transferring to the thin (10 μm) coating , which exhibited a decreased COF after the running-in process. The reduced COF would lead to a less shear stress in the coating during the impact-sliding test. As a result, S1 had the best performance among the three coatings. The sub-stoichiometric Ti oxide in S2 showed a high lubricity and less intendancy of picking up materials from a counterface steel pin ball. As a result, the material transferred from the steel ball was less for S2 than for S3, Figs. 3-4 (d and f). However, with the increase of the sliding distance, more amount of patchy Fe oxide covered the wear track, causing the COF increase. At the final stage of the tests, S2 and S3 had the same high COF values. The Fe oxides show no

lubricity in this test, although some Fe (FeO, known as Wuestite [42], or Fe2O3 and Fe3O4 [43]) oxides may exhibit a low COF.

3)   The results of POD tests agreed well with the failure behaviors of coatings during the inclined impact-sliding tests. S1 had the lowest COF value after the steady stage was reached and it also showed the best performance during the impact-sliding test.

4)   For a thin and relatively smooth coating, the porous structure may help in resilience of the impact force compared to the exposed dense inner layer of the thick coatings that were ground to have a similar surface finish. Therefore, the wear failure behavior can be altered by changing surface profiles and by doping different chemical elements, the latter can change wear mechanisms by changing surface affinity behavior and stoichiometry.

5)   Beside the effects of the coating thickness and pores as previously discussed for the polished coating, the lubricant sub-oxide in the coating was supposed to facilitate the decreasing of COF but the benefit may exist only at the beginning of the test of S2. With the increase in impact-sliding test cycles, a large amount of counterface material transfer occurred and the COF of S2 would increase significantly, like that in the late stage of its POD test. On the contrast, S1 had less counterface material transfer and its COF reduced due to the polishing running-in effect. A low COF would introduce a less shearing force in the coating, which is very critical for the performance of a coating during the impact-sliding tests. Therefore, the thin coating showed a better result than the mid-thick coating. The thickest (27 µm) coating in this section of study had a high COF from the beginning. As a result, the thickest one had the worst performance in both POD and impact-sliding

tests. The low cohesive strength of the coatings due to pores within the coating may be the reason of the early failure under the impact and pressing forces.

The test result showed that a standalone PEO coating with a thickness thinner than 30 μm may not be strong enough to withstand the high contact stresses.

III. PVD/CVD coatings were necessarily reconsidered to form different combinations of coatings and substrates. When DLC coated 316L was chosen, the good coating-substrate combination and special characteristics of the DLC top layer indeed provided a quite high impact-sliding wear resistance during the inclined impact-sliding tests. The detailed findings can be described as follows:

1) The pin-on-disc wear test showed that the long-distance sliding between the steel counterface and DLC coating caused a decrease of the dynamic friction coefficient where the range of decrease was from 0.26 to close to 0.1. Parallel fatigue cracks first appeared in the top layer of the DLC coating and then were gradually removed by sliding wear whereupon scratch grooves showed on the W-C transition layer. After a certain number (100~150) of sliding revolutions, fatigue cracks showed up again in the W-C transition layer. The worn top layer became debris and was pushed apart and piled up along the sides of wear track.

2) The adhesion/cohesion properties of different layers of the coating became very distinct during the inclined impact-sliding test. The top layer of the DLC coating made the sliding easier and caused less deformation and wear on the counterface ball. The W-C transition layer and the W bonding layer showed remarkably high adhesion to the substrate under such a high impact-sliding force.

177

3) The width of the head part was influenced by the number of impacts and the impact force, Fi, and the length of the whole sliding track was determined by the pressing force, Fp, and friction coefficient between the two contact surfaces of the coating and the ball. The impact force, Fi, caused severe sample deformation and coating chipping in the head area of the tracks. The severity of the failure due to sliding was relatively low for the WC DLC coating due to its low friction coefficient, though it also highly depended on the degree of the inclination angle, θ.

4) The high impact force, Fi, caused bend stresses in both peripheral and central areas of the impact crater (head). The stresses were too high to be absorbed and released by the coating and consequently caused circular cracks which penetrated the whole coating and also caused sawtooth-like deformation into the substrate. During the sliding after the full contact of the ball upon the coating surface, compressive and bending stresses were formed in front of the ball and tensile stress behind the ball. Two types of fatigue cracks were observed in the sliding track (tail part) which crossed over each other. In the boundary zone between the head and tail part, the DLC coating suffered greatly from the bend deformations at the head and tail areas caused by the impact-sliding. An amount of the coating material was removed and chipping and peeling of the top layer and the W-C transition layer could be observed and, in addition, W bonding layer was squeezed up and exposed. The area of which kept increasing with the number of test cycles.

5) Chipping and peeling could be observed inside the impact area after a certain number (100~150) of impacts on the DLC coating. The crack density increased with the number of test cycles until it reached a saturated density, whereupon, failure occurred in

some spots. However, no ball material transfer could be detected by EDX on the DLC impact-sliding track after up to 10,000 impact cycles. This amazing result is believed to be due to the following reasons:

(1) The low friction coefficient of the DLC top layer;

(2) The absorption and release of the impact energy by the DLC coating;

(3) Graphitization of the coating which took place during the impact and sliding;

(4) The transfer of the DLC material to the counterface ball surface, which changed the DLC/stainless steel sliding system into a DLC/DLC sliding system.

6). A very large and deep impact-sliding track was formed on the uncoated stainless steel substrate after the same test conditions, In contrast to the coated substrate. Deep sliding grooves and a large amount of wear debris and material transfer from the steel ball were observed in the track. The counterface ball was also worn to a high degree and great amount of material transfer was observed.

From mechanical evaluation direction, W-DLC showed good performance under such a loading condition. However, tungsten is not a proper interface material for biomedical application because of it is inferior biocompatibility issues.

IV. Another type of inert DLC coating should be considered using SiC as its interface material, which is now widely accepted by many medical services. TiN, as another biomedical implant coating, was included. Both dry and wet (in a Hank's balanced salt solution) test conditions were put into consideration as both mechanical and practical evaluation is necessary in this research.

In the test, progressive amounts of damage were made on testing samples and the degree of failure was evaluated based on the percentage of coating failed area and the corrosion behaviors of the damaged areas after impact-sliding tests. When tested under dry condition, both coatings were mechanically more durable on hard M2 substrate than Ti alloy substrate. In the wet solution testing condition, the HBSS didn't cause obvious corrosion degradations to the coated samples when either the bonding layers or substrates were Ti-based (Ti bonding layer or Ti-6Al-4V substrate) within 5000 testing cycles. Instead, the solution provided a lubricating effect and enhanced coating durability. The Si-based bonding layer in the DLC coating, although the layer was corrosion resistant, couldn't block the cracking propagation into the substrate after a certain number of testing cycles; the crack opening allowed the HBSS solution to contact the substrates, which would only cause minor problem when the substrate was a corrosion-resistant Ti alloy. However, when the substrate, i.e. M2, did not have a good anti-corrosion property, a severe corrosion-induced weakening of the interface would occur. On the other hand, when a corrosion-resistant Ti bonding layer (within the TiN coating) existed, the Ti layer could function as a corrosion and cracking barrier to protect the M2 steel from corrosion, thus, no obvious corrosion-induced interface degradation appeared. Therefore, a corrosion-resistant bonding layer and its ability to block the extension of cracking under cyclic dynamic loads can have a critical influence on the coating failure behaviors in a corrosive environment when the substrate has an inferior anti-corrosion property. However, for evaluation of a long-term durability of the coatings under a normal operating condition, different testing methods should be used.

V. Another type of commonly used metallic biomaterial, CoCr alloy, was studied at the last stage of this research. Ti6Al4V, as a comparison, was also used to do further studies beyond the previous research progress.

Due to the excellent corrosion resistance of CoCr alloy and Ti6Al4V, the corrosive HBSS showed very little influence to cause corrosion problem, instead, it behaved as a lubricant for both coated and uncoated alloys in the POD tests. The coefficient of friction (COF) decreased more than a half on uncoated surfaces than coated ones in wet environment for both substrates. After a certain period of high COF 'run-in' period, both coated samples showed a close value of COF for either dry or wet test conditions.

In the impact-sliding wear tests, large scale of work hardening was observed on CoCr alloy under repetitive high dynamic loadings, which promoted the durability of both bulk material and DLC coating up to over 5000 cycles test. Hardness measured by nano-indentation tests in the tested track on the CoCr bulk material showed the work hardening occurred at very early stage during the test. The value of hardness increased 26% in the first 50 cycles test. Ti6Al4V, on the contrary, showed great amount of abrasive wear and resulted in deep and wide test tracks for either coated or uncoated ones. DLC coating started failing within first 5-cycle-test and the hard, small particles, which deprived from DLC coating, were entangled in the following tests and caused three-body-abrasive wear. Great scale of damage was formed on both tested surface and the couterface surface. The existence of HBSS could improve the wear behavior of Ti6Al4V to some extent. Surface profile measured across the tested tracks showed both chipping and peeling were formed inside the damaged DLC coated Ti6Al4V.

As general conclusions, both TiN and DLC coatings can be used to withstand impact-sliding contact stresses. A strong substrate with work hardening characteristics (e.g., CoCr alloy) is a better choice of substrate for a load bearing biomedical implant due to its stronger load bearing capability. A corrosion and ductile metallic interface layer between coating and substrate would be beneficial. Compared to Si or SiC, Ti may be a better candidate as an interface layer. A PEO coating can be used as a biomedical hard coating for protection of Ti against a pure sliding. However, the PEO coating itself may not be good enough to withstand high impacting and pressing forces due to pore-induced low cohesion strength of the coating. On the other hand, the polished PEO coating may be used as an intermediate layer of a PVD/CVD coating for better load supporting.

2. SUGGESTION FOR FUTURE WORK

1. More comprehensive studies, for instance, the stress field distribution, are required inside the coating area and interface layer.

2. Mathematic model should be built to simulating the failure behavior under different required conditions and to optimizing the test. At least the model of single-layer-coating should be built.

3. Real-time measurement of the multi-axial loadings will be necessary to understand the complex failure behaviors.

4. Other type of counterface contact material (beside steel ball) is required to simulate different contact conditions.

CHAPTER 9 STATEMENT OF ORIGINALITY

The following aspects of this study, in the author's opinion, are novel and distinct contributions to original knowledge:

- A new testing method was developed for successful use in simulating the complex failure behaviors of load-bearing biomaterial surfaces. In this method, combined impact and sliding forces can be simultaneously applied on testing surfaces analogue to human kinetic activities.

- A systematic evaluation of performances of metallic biomedical materials under high dynamic contact loadings is built based on the study of failure mechanisms within the damaged area.

- The combination of coating, interface and substrate system under repetitive contact stresses is investigated and a basic conception of choosing property material is built.

APPENDICES

Appendix A

<u>CHAPTER 2</u>

License Number	3360821144413
License date	Apr 02, 2014
Licensed content publisher	Elsevier
Licensed content publication	Surface and Coatings Technology
Licensed content title	Study on fatigue and wear behaviors of a TiN coating using an inclined impact-sliding test
Licensed content author	Ying Chen,Xueyuan Nie
Licensed content date	25 December 2011
Licensed content volume number	206
Licensed content issue number	7
Number of pages	6
Type of Use	reuse in a thesis/dissertation
Portion	full article
Format	both print and electronic
Are you the author of this Elsevier article?	Yes
Will you be translating?	No
Title of your thesis/dissertation	Failure mechanism of coated biomaterials under high impact-sliding contact stresses
Expected completion date	May 2014
Estimated size (number of pages)	120
Elsevier VAT number	GB 494 6272 12
Permissions price	0.00 USD
VAT/Local Sales Tax	0.00 USD / 0.00 GBP
Total	0.00 USD

Dear Ms. Ying Chen,

Thank you for placing your order through Copyright Clearance Center's RightsLink service. Elsevier has partnered with RightsLink to license its content. This notice is a confirmation that your order was successful.

Your order details and publisher terms and conditions are available by clicking the link below: http://s100.copyright.com/CustomerAdmin/PLF.jsp?ref=c8e4955e-1ada-4fbe-a568-fd547b7bd9ca

Order Details

Licensee: Ying Chen
License Date: Apr 2, 2014
License Number: 3360821144413
Publication: Surface and Coatings Technology
Title: Study on fatigue and wear behaviors of a TiN coating using an inclined impact-sliding test
Type Of Use: reuse in a thesis/dissertation
Total: 0.00 USD

To access your account, please visit https://myaccount.copyright.com.

Please note: Online payments are charged immediately after order confirmation; invoices are issued daily and are payable immediately upon receipt.

To ensure that we are continuously improving our services, please take a moment to complete our customer satisfaction survey.

CHAPTER 3

License Details

Thank you very much for your order.

This is a License Agreement between Ying Chen ("You") and Elsevier ("Elsevier"). The license consists of your order details, the terms and conditions provided by Elsevier, and the payment terms and conditions.

Get the printable license.

License Number	3356551431837
License date	Mar 26, 2014
Licensed content publisher	Elsevier
Licensed content publication	Journal of Alloys and Compounds
Licensed content title	Wear failure behaviour of titanium-based oxide coatings on a titanium alloy under impact and sliding forces
Licensed content author	Y. Chen, T. Cheng, X. Nie
Licensed content date	25 November 2013
Licensed content volume number	578
Number of pages	9
Type of Use	reuse in a thesis/dissertation
Portion	figures/tables/illustrations
Number of figures/tables/illustrations	7
Format	electronic
Are you the author of this Elsevier article?	Yes
Will you be translating?	No
Title of your thesis/dissertation	Failure mechanism of coated biomaterials under high impact-sliding contact stresses
Expected completion date	May 2014
Estimated size (number of pages)	120
Elsevier VAT number	GB 494 6272 12
Permissions price	0.00 USD
VAT/Local Sales Tax	0.00 USD / 0.00 GBP
Total	0.00 USD

- Yes, sure. Go ahead.

Regards,

Joe

2014-04-01 14:33 GMT-07:00 Ying Chen <chen111w@uwindsor.ca>:

186

Dear Dr. Cheng

Can I use paper **Ying Chen**, Tse Cheng and Xueyuan Nie, Wear failure behavior of titanium-based oxide coatings on a titanium alloy under impact and sliding forces Journal of Alloys and Compounds 578（2013）336. as one chapter in my thesis?

Thanks

Regards

Sophia

CHAPTER 4

Portion	Excerpt (> 800 words)
Will you be translating?	No
Title of your thesis / dissertation	Failure mechanism of coated biomaterials under high impact-sliding contact stresses
Expected completion date	May 2014
Estimated size (number of pages)	120
Total	0.00 USD

Terms and Conditions

American Vacuum Society -- Terms and Conditions: Permissions Uses

American Vacuum Society ("AVS") hereby grants to you the non-exclusive right and license to use and/or distribute the Material according to the use specified in your order, on a one-time basis, for the specified term, with a maximum distribution equal to the number that you have ordered. Any links or other content accompanying the Material are not the subject of this license.

1. You agree to include the following copyright and permission notice with the reproduction of the Material:"Reprinted with permission from [FULL CITATION]. Copyright [PUBLICATION YEAR], American Vacuum Society." For an article, the copyright and permission notice must be printed on the first page of the article or book chapter. For photographs, covers, or tables, the copyright and permission notice may appear with the Material, in a footnote, or in the reference list.
2. If you have licensed reuse of a figure, photograph, cover, or table, it is your responsibility to ensure that the material is original to AVS and does not contain the copyright of another entity, and that the copyright notice of the figure, photograph, cover, or table does not indicate that it was reprinted by AVS, with permission, from another source. Under no circumstances does AVS, purport or intend to grant permission to reuse material to which it does not hold copyright.
3. You may not alter or modify the Material in any manner. You may translate the Material into another language only if you have licensed translation rights. You may not use the Material for promotional purposes. AVS reserves all rights not specifically granted herein.
4. The foregoing license shall not take effect unless and until AVS or its agent, Copyright Clearance Center, receives the Payment in accordance with Copyright Clearance Center Billing and Payment Terms and Conditions, which are incorporated herein by reference.
5. AVS or the Copyright Clearance Center may, within two business days of granting this license, revoke the license for any reason whatsoever, with a full refund payable to you. Should you violate the terms of this license at any time, AVS, American Vacuum Society, or Copyright Clearance Center may revoke the license with no

refund to you. Notice of such revocation will be made using the contact information provided by you. Failure to receive such notice will not nullify the revocation.

6. AVS makes no representations or warranties with respect to the Material. You agree to indemnify and hold harmless AVS, American Vacuum Society, and their officers, directors, employees or agents from and against any and all claims arising out of your use of the Material other than as specifically authorized herein.

7. The permission granted herein is personal to you and is not transferable or assignable without the prior written permission of AVS. This license may not be amended except in a writing signed by the party to be charged.

8. If purchase orders, acknowledgments or check endorsements are issued on any forms containing terms and conditions which are inconsistent with these provisions, such inconsistent terms and conditions shall be of no force and effect. This document, including the CCC Billing and Payment Terms and Conditions, shall be the entire agreement between the parties relating to the subject matter hereof.

This Agreement shall be governed by and construed in accordance with the laws of

the State of New York. Both parties hereby submit to the jurisdiction of the courts of New

York County for purposes of resolving any disputes that may arise hereunder.

Dear Ms. Ying Chen,

Thank you for placing your order through Copyright Clearance Center's RightsLink service. AIP Publishing LLC has partnered with RightsLink to license its content. This notice is a confirmation that your order was successful.

Your order details and publisher terms and conditions are available by clicking the link below: http://s100.copyright.com/CustomerAdmin/PLF.jsp?ref=18adbced-deed-4bb0-a79e-086451fa240f

Order **Details**
Licensee: Ying Chen
License Date: Apr 4, 2014
License Number: 3362060228632
Publication: Journal of Vacuum Science & Technology A
Title: Study of the fatigue wear behaviors of a tungsten carbide diamond-like carbon coating on 316L stainless steel
Type Of Use: Thesis/Dissertation
Total: 0.00 USD

To access your account, please visit https://myaccount.copyright.com.

Please note: Online payments are charged immediately after order confirmation; invoices are issued daily and are payable immediately upon receipt.

To ensure that we are continuously improving our services, please take a moment to complete our customer satisfaction survey.

CHAPTER 5

License Number	3360821274495
License date	Apr 02, 2014
Licensed content publisher	Elsevier
Licensed content publication	Surface and Coatings Technology
Licensed content title	Substrate and bonding layer effects on performance of DLC and TiN biomedical coatings in Hank's solution under cyclic impact–sliding loads
Licensed content author	Ying Chen,Xueyuan Nie,Adrian Leyland,Jonathan Housden,Allan Matthews
Licensed content date	25 December 2013
Licensed content volume number	237
Number of pages	11
Type of Use	reuse in a thesis/dissertation
Portion	full article
Format	both print and electronic
Are you the author of this Elsevier article?	Yes
Will you be translating?	No
Title of your thesis/dissertation	Failure mechanism of coated biomaterials under high impact-sliding contact stresses
Expected completion date	May 2014
Estimated size (number of pages)	120
Elsevier VAT number	GB 494 6272 12
Permissions price	0.00 USD
VAT/Local Sales Tax	0.00 USD / 0.00 GBP
Total	0.00 USD

Dear Ms. Ying Chen,

Thank you for placing your order through Copyright Clearance Center's RightsLink service. Elsevier has partnered with RightsLink to license its content. This notice is a confirmation that your order was successful.

Your order details and publisher terms and conditions are available by clicking the link below: http://s100.copyright.com/CustomerAdmin/PLF.jsp?ref=a0939cb4-ad49-43ee-8729-aa58a891d3e3

Order   **Details**
Licensee: Ying   Chen
License   Date: Apr   2,   2014
License   Number: 3360821274495
Publication: Surface   and   Coatings   Technology
Title: Substrate and bonding layer effects on performance of DLC and TiN biomedical coatings   in   Hank's   solution   under   cyclic   impact-sliding   loads

Type   Of   Use: reuse   in   a   thesis/dissertation
Total: 0.00 USD

To access your account, please visit https://myaccount.copyright.com.

Please note: Online payments are charged immediately after order confirmation; invoices are issued daily and are payable immediately upon receipt.

To ensure that we are continuously improving our services, please take a moment to complete our customer satisfaction survey.

- Re: Request for permission to include the paper in my dissertation from Dr. Allen Matthews

Yes, of course Ying. No problem.

Regards,

Allan

- Re: Request for permission to include the paper in my dissertation from Dr. Adrian Leyland

That   is   fine   Ying   Chen   -   no   problem   for   you   to   do   this.

Kind   regards,

Adrian.

- Re: Request for permission to include the paper in my dissertation from

Dr. Jonathan Housden

Dear Ying

I'm very well thank you and hope you are too.

I'm pleased to give my permission for you to include the paper "Substrate and bonding layer effects on performance of DLC and TiN biomedical coatings in Hank's solution under cyclic impact–sliding loads" (2013) Vol. 237, pp. 219-229."

in your dissertation. Thank you for asking.

The arrangements for your thesis meet with my approval.

I wish you success in completing your dissertation and your doctorate.

Kind regards,

Jonathan Housden.

Tecvac Ltd.

REFEREED JOURNAL PUBLICATIONS

1. **Ying Chen** and Xueyuan Nie, "Study on Fatigue and Wear Behaviors of a TiN Coating using an Inclined Impact-sliding Test", SURFACE & COATINGS TECHNOLOGY 206（2011）1977

2. **Ying Chen**, Tse Cheng and Xueyuan Nie, Wear failure behavior of titanium-based oxide coatings on a titanium alloy under impact and sliding forces Journal of Alloys and Compounds 578（2013） 336

3. **Ying Chen** and Xueyuan Nie, Study of the fatigue wear behaviors of a WC DLC coating on 316L stainless steel Journal of Vacuum Science and Technology A, 30 (2012) 051506

4. **Ying Chen,** Xueyuan Nie, Jonathan Housden, Adrian Leyland and Allan Matthews, Substrate and bonding layer effects on performance of DLC and TiN biomedical coatings in Hank's solutions under cyclic impact-sliding loads SURFACE & COATINGS TECHNOLOGY 237（2013）219

5. **Ying Chen** and Xueyuan Nie, Failure mechanisms of DLC coated Ti-6Al-4V and CoCr biomedical materials under cyclic high combined contact stresses

REFEREED CONFERENCE FULL PAPERS AND PRESENTATIONS

1. **Ying Chen** and Xueyuan Nie, "Study on Fatigue and Wear Behaviors of a TiN Coating using an Inclined Impact-sliding Test", Proceedings of 38th International Conference on Metallurgical Coatings and Thin Films (ICMCTF), San Diego, US, May 2nd –May 6th, 2011.

2. **Ying Chen** and Xueyuan Nie, "Study of the fatigue wear behaviors of a WC DLC coating on 316L stainless steel", Proceeding of American Vacuum Society 58th International Symposium & Exhibition, Nashville, US, Oct. 30th –Nov. 4th, 2011.

3. **Ying Chen,** Xueyuan Nie, Jonathan Housden, Adrian Leyland and Allan Matthews, "Substrate and bonding layer effects on performance of DLC and TiN biomedical coatings in Hank's solutions under cyclic impact-sliding loads", Proceeding of 40th International Conference on Metallurgical Coatings and Thin Films (ICMCTF), San Diego, US, April 29th –May 3rd, 2013.

4. **Ying Chen** and Xueyuan Nie, "Study on Fatigue and Wear Behaviors of a TiN Coating using an Inclined Impact-sliding Test", Proceedings of 41th International Conference on Metallurgical Coatings and Thin Films (ICMCTF), San Diego, US, May 28th –May 2nd, 2014.

VITA AUCTORIS

NAME: Ying Chen

PLACE OF BIRTH: Wuhan, China

YEAR OF BIRTH: 1984

EDUCATION: Huazhong University of Science and Technology, B.Sc., China, 2006

University of Windsor, M. Sc., Windsor, ON, 2010

University of Windsor, Ph.D., Windsor, ON, 2014